Trinity College Dublin
Coláiste na Tríonóide, Baile Átha Cliath
The University of Dublin

Stefan Scheurer, B.Sc., M.Sc.

3D Bioprinting of anatomically accurate Implants for Meniscus Tissue Engineering

Trinity College Dublin, 2020

A thesis submitted to the University of Dublin in partial fulfilment
of the requirements for the degree of

Doctor in Philosophy

Supervisors: Prof. Cathal J. Moran, Prof. Daniel J. Kelly

Internal examiner: Mr. Johnny McKenna

External examiner: Dr. Riccardo Levato

DECLARATION

I declare that this thesis has not been submitted as an exercise for a degree at this or any other university and is entirely my own work. I agree to deposit this thesis in the University's open access institutional repository or allow the library to do so on my behalf, subject to Irish Copyright Legislation and Trinity College Library conditions of use and acknowledgement.

Stefan Scheurer, Dublin, 2020

SUMMARY

Meniscus deficiencies through trauma or degeneration are common in all age groups and are associated with a loss in function, joint degeneration and osteoarthritis (OA). Meniscectomy surgery is widely performed to remove dislocated fragments of tears associated with accute pain or locking of the joint but the treatment is still associated with a 14-fold increase in the risk of developing OA compared to healthy patients. Commercially available implants to replace the removed meniscus tissue still do not fully regenerate the tissue and allograft transplants suffer from donor shortage. This has motivated increased interest in meniscus tissue engineering strategies via 3D bioprinting in order to create more advanced cell-based implants for joint regeneration. However, the majority of such constructs still do not mimic the internal matrix architecture of the tissue, which is essential for its function. The overall objective of this thesis was therefore to 3D bioprint a cell-laden tissue engineered construct which mimics the anatomy, anisotropy and heterogeneity of the human meniscus.

A 3D printed construct for meniscus tissue engineering has to fulfil the load carrying functions of the native tissue it replaces, whilst simultaneously supporting the regeneration of lost meniscus and integrating into the surrounding host tissue. Printed implants therefore have to show compressive and tensile properties similar to the native tissue to withstand the forces of the knee environment. Furthermore, the ‘bioinks’ used to print such regenerative scaffolds should also be supportive of a meniscal cell phenotype to allow matrix regeneration and tissue integration. In addition, since the meniscus is highly heterogenous, bioinks are needed that replicate the composition of both the inner and outer zones of the tissue. Finally, in order to increase contact areas with the joint and protect the underlying articular cartilage, implants are required to mimic the anatomical size and shape of the native tissue.

The thesis began by attempting to engineer materials with compressive and tensile properties similar to the native human meniscus tissue by 3D printing composite constructs consisting of interpenetrating network (IPN) hydrogels (alginate and gelatin methacryloyl (GelMA)) reinforced with networks of polycaprolactone (PCL) fibres. After systematically comparing the influence of PCL fibre diameter and spacing on the mechanical properties of the printed scaffolds, it was found that a fibre diameter of 120 μm and a fibre spacing of 2 mm best mimicked the axial compressive properties and radial tensile properties of the native tissue. Next the influence of the fibre print pattern was explored by 3D printing consecutive parallel layers 'offset' to the underlying parallel layer, which reduced the compressive modulus of 3D printed samples more than its tensile modulus, thereby increasing the ratio of the tensile to the compressive modulus, resulting in the development of constructs with mechanical properties more representative of the native meniscus. These PCL networks were then used to mechanically reinforce the IPN hydrogels, producing composites with soft tissue-like biomechanical behavior.

Chapter 4 of the thesis explored the potential of the IPN to support chondrogenesis of mesenchymal/marrow stem/stromal cells (MSCs) and further investigated the bi-phasic mechanical properties of such constructs. First a rheological characterization of the IPN was undertaken to assess its suitability for biofabrication, which demonstrated the shear thinning properties of this hydrogel. A histological, immunohistological, biochemical and biomechanical analysis of *in vitro* engineered tissues generated by MSCs encapsulated with such fibre reinforced IPNs and stimulated with TGF-β3 was then undertaken. MSCs generated a cartilage-like extracellular matrix (ECM) within these composites with time in culture, which further improved the bi-phasic compressive properties of the fibre reinforced IPNs.

Chapter 5 of this thesis sought to enhance the capacity of the developed bioinks to support meniscus-specific differentiation of MSCs by functionalizing them

with solubilized ECM isolated from the inner and outer region of porcine menisci. First, a solubilization protocol reduced the DNA content of the inner and outer meniscus ECM fractions to below a threshold which would cause an immune responses upon implantation, while keeping the collagen/sulfated glycosaminoglycan (sGAG) ratio comparable to that of the native tissue. Moreover, the solubilized ECM fractions were shown to possess low viscosities alone but to impart strong shear thinning properties when combined with the previously developed IPN. When integrated into MSC laden bioinks, the solubilized ECM fractions failed to improve the fibrochondrogenic potential of the IPNs.

Chapter 6 explored scaling up the bioprinting process in order to 3D bioprint an anatomically correct, complex large scale meniscus constructs. Viscosity and spreading ratio analyses of the previously developed bioinks identified the optimal printing conditions. Next, *z-printing*, a novel 3D bioprinting technique was implemented in order to facilitate easier printing of complex, large scale constructs due to the movement of printheads along the z-axis instead of the x and y-axis, which decreases the duration of the printing process, enables additional quality control and enables additional intermittent material modification stages. Finally, an MSC-laden construct mimicking the shape and size of the human meniscus was 3D bioprinted, which considered the non-linear and heterogeneous biomechanics and spatial composition of the native meniscus tissue, including pores for gas and nutrient exchange important for engineering geometrically large constructs.

In summary, this thesis describes the development of a 3D bioprinted meniscus construct which mimics the external size and shape of the human meniscus as well as its internal heterogeneous structure. The fibre reinforced IPN constructs employed in this study were shown to mimic key bi-phasic biomechanical attributes of the normal meniscus. Moreover, the developed bioink showed its potential for 3D bioprinting in the field of cartilaginous tissue engineering, being both shear thinning and supportive of a

chondrogenic phenotype. Furthermore, the creation of this large, multi-material biological constructs was facilitated through the development of a novel 3D bioprinting technique which successfully addresses several key challenges of 3D printing as a manufacturing process.

ACKNOWLEDGEMENTS

Ich will mich zuerst bei meiner Famile bedanken, die mich immer unterstützt und mir all das ermöglicht hat und immer an mich geglaubt hat.

I am entirely grateful to Danny and Cathal for being my mentors and supervisors, who allowed me to go my own way while guiding and supporting me in the lab and in my future career and served as shining examples to me. Thank you for your guidance, trust and patience.

None of this would have been possible without all the other members of TCBE who showed me how to science but were also there for me to celebrate successes and pick me back up after my losses. Special thanks have to go out to Rossana, Simon, Dinorath, Gra, Kev, Sophia, Criti, Xavi, Bin, Pier, Dan, Mathieu, Michele, Matteo, Pedro, Paola, Jessie and Ollie but most of all Dave, who I abused so often as my own personal post-doc and seemingly never got tired of looking at histology slides and experiment plans. I have been all around the world but nobody makes a place feel like home quite the way you guys do. Thanks for exploring the lab, Gingerman and even Mexico and Rhodes together with me.

After a long day of work I really enjoyed coming back home to the château de PhD with Jenny and Kian, so thanks for keeping me going with some science-based baking and fence-fuelled BBQ.

I also want to thank my friends in Austria, Dublin and all over the world, like Suni, Tami and Jens, my quidditch friends and the Molbio masters, who showed me that life outside the lab exists and always believed in me.

I would be nowhere without Julia, though, and I could not imagine anyone who I would rather share a lab and a life with.

TABLE OF CONTENTS

LIST OF FIGURES

LIST OF EQUATIONS

LIST OF TABLES

NOMENCLATURE

AC	Articular cartilage
ACL	Anterior cruciate ligament
Alg	Alginate
BMSCs	Bone marrow stem cells
BSA	Bovine serum albumine
$CaCl_2$	Calcium chloride
CDM	Chondrogenically defined media
Col I	Collagen type I
Col II	Collagen type II
CTGF	Connective tissue growth factor
DMEM	Dulbecco's modified Eagle's media
ECM	Extracellular media
FDM	Fused deposition modelling
GelMA	Gelatin methacryloyl
HAc	Acetic acid
inECM	ECM of inner meniscus zone
IPN	Interpenetrating network
MEW	Melt electrowriting
MRI	Magnetic resonance imaging
MSCs	Mesenchymal stem cells
OA	Osteoarthritis
outECM	ECM of outer meniscus zone
PCL	Polycaprolactone
PFA	Paraformaldehyde
pfDMEM	phenol free DMEM
PG	Proteoglycan
PGA	Polyglycerol acid
PLA	Polylactic acid
PU	Polyurethane
SD	Standard deviation
SEM	Standard error of the mean
sGAGs	sulphated glycosaminoglycans
TE	Tissue engineering
TGF-β	Transforming growth factor beta
XPAN	Expansion media

PUBLICATIONS

Co-author publications

- SCHIPANI, R., **SCHEURER, S.,** FLORENTIN R, CRITCHLEY, S.E., KELLY, D. J. 2020, *Reinforcing interpenetrating network hydrogels with 3D printed polymer networks to engineer cartilage mimetic composites.* Biofabrication, 12

Conference abstracts

- **SCHEURER, S**., KELLY, D. J., MORAN C. J. *3D printed polycaprolactone scaffolds for meniscus regeneration*. Bioengineering in Ireland Conference (BINI), Templepatrick, Northern Ireland, January 20th/21st 2017
- **SCHEURER, S**., KELLY, D. J., MORAN C. J. *Bioinks of solubilized porcine ECM and GelMA for meniscus tissue engineering*. 4th annual Meeting of the Matrix Biology Society Ireland (MBI), Dublin, Ireland, November 30th-December 1st 2017
- **SCHEURER, S**., KELLY, D. J., MORAN C. J. *3D bioprinting of ECM functionalized bioinks reinforced with polycaprolactone fibres for meniscus tissue engineering*. Bioengineering in Ireland Conference (BINI), Dublin, Ireland, January 26th/27st 2018
- **SCHEURER, S**., SCHIPANI R., KELLY, D. J., MORAN C. J. *3D bioprinting of ECM functionalised bioinks reinforced with polycaprolactone fibres for meniscus tissue engineering*. 8th World Congress of Biomechanics (WCB), Dublin, Ireland, July 8th-12th 2018
- **SCHEURER, S**., SCHIPANI R., KELLY D. J., MORAN C. J. *3D printing of scaffolds for meniscus tissue engineering mimicking function through structure.* Annual Conference of the International Society for Biofabrication (ISBF), Würzburg, Germany, October 28th/31st 2018
- **SCHEURER, S**., SCHIPANI R., KELLY D. J., MORAN C. J. *3D printing of scaffolds for meniscus tissue engineering – mimicking structure through function*. Bioengineering in Ireland conference (BINI), Limerick, Ireland, January 18th/19th 2019

- **SCHEURER, S**., SCHIPANI R., KELLY D. J., MORAN C. J. *Meniscus tissue engineering through 3D printing*. Tissue engineering and Regenerative Medicine International Society (TERMIS) European Chapter, Conference, Rhodes, Greece, May 27th/31st 2019

Other publications during candidacy

- LANARO M., FORRESTAL D. P., **SCHEURER, S**., SLINGER D. J., LIAO S., POWELL S. K., WOODRUFF M.A. 2017, *3D printing complex chocolate objects: Platform design, optimization and evaluation*. Journal of Food Engineering, 215

Chapter 1
INTRODUCTION

1.1. Structure and function of the meniscus

Menisci are a pair of semilunar, fibrocartilaginous structures in the knee located between the femoral and the tibial joint plateaus, and are responsible for load distribution and maintenance of stability within the joint. Since menisci are deformable as well as mobile in the joint they protect the articular cartilage (AC) in the knee by serving as pillows between the relatively flat tibial plateau and the rounded femoral heads. They translate vertical forces into hoop stress within the meniscus and more than double the contact area between the tibia and femur.

The fibrocartilage-like meniscus tissue is compositionally and structurally different to the AC that lines the ends of bones within synovial joints, since it contains more type I collagen (Col I) fibres and lower amounts of type II collagen (Col II) and sulfated glucosaminoglycans (sGAGs). The highly organized network of collagenous fibres provides the meniscus with tensile strength and stiffness and prevents the radial extrusion of the tissue. In particular, the circumferential orientated collagen fibres within the meniscus contribute to it biomechanical function and also anchor the tissue to the tibial plateau by extending through the entire outer rim through the insertional ligaments to the horns of the meniscus.

There are other notable differences between AC and meniscal cartilage. The meniscus has a region that is vascularized, the outer “red” zone of the tissue. Further inwards the tissue becomes less and less vascularized and is often referred to as the “white” zone. Apart from their degrees of vascularization, these zones also differ from each other in their structure and composition, with the outer zone characterized by a higher Col I content and the presence of elongated fibroblast-like cells, whereas the

inner zone is composed of more Col II and sGAGs and is populated with more rounded chondrocyte-like cells (Collier & Ghosh, 1995; Nakata et al., 2001; Tanaka, Fujii, & Kumagae, 1999).

1.2. Meniscus tears and current treatment options

Meniscus tears are a common injury in most age groups and an increasingly common surgical treatment option with good patient-reported outcome is to repair the torn region through sutures. However, meniscus repair surgeries have a high re-operation rate and in many cases repairing tears is not possible (Caiqi Xu & Zhao, 2015). Age and lifestyle of the patient are important factors as well as the location, size, pattern and chronicity of the tear in order to choose the right treatment option. For example, tears located in the inner third of the tissue, the only slowly regenerating white zone of the meniscus, are often treated with partial or complete meniscectomies (Hutchinson, Moran, Potter, Warren, & Rodeo, 2014). Here the surgeon removes the torn section of meniscus in order to relieve patients from accute symptoms such as pain or locking of the joint in the short term. Removing parts of the tissue does not restore the function of the meniscus which was lost through the tear in the long term and typically leads to further joint degeneration. If only 20% of the meniscus is removed the contact forces in the knee are increased by 350% (Seedhom & Hargreaves, 1979). Partial meniscectomies are the most common treatment method for smaller tears, even though they are still known to be associated with OA in the long term. However, some cases of larger tears require total meniscectomies. Allograft transplants are considered by many to be the gold standard for severe meniscus injuries, but like all organ transplants suffer from logistical problems and shortage of donors (Moran, Busilacchi, Lee, Athanasiou, & Verdonk, 2015a).

Alternatives to meniscectomy and allograft transplants are the commercially available cell-free scaffold products Actifit^{TM}(Spencer et al., 2012) and

CMI®(Bulgheroni et al., 2010; Monllau et al., 2011). Here the damaged meniscus tissue is surgically removed and replaced by a polyurethane scaffold (Actifit^{TM}) or a bovine collagen sponge (CMI®). While such commercially available implants have shown some reasonably promising results, they still do not mimic the complex internal architecture and biomechanical function of the native meniscus tissue. Long term studies of these products have demonstrated an improvement compared to meniscectomies in terms of pain relief as well as regaining mobility after 2 to 10 years. However failure rate of between 7% and 30% have been reported and patients were still not able to perform sports at the same level as prior to their injury. Furthermore, the mentioned artificial products are only available for repairing partial meniscectomies (Leroy et al., 2016; Monllau et al., 2011).

1.3. Tissue engineering approaches to create improved meniscus implants

There is a big interest in regenerative medicine and biological approaches to meniscus tissue engineering (Hutchinson et al., 2014; Matteo, Tarabella, & Tomba, 2016; Moran, Orth, et al., 2015; Moran, Atmaca, Declercq, Cornelissen, & Verdonk, 2014; Moran, Barry, Maher, Shannon, & Rodeo, 2012; Moran, Busilacchi, et al., 2015a; Moran, Busilacchi, Lee, Athanasiou, & Verdonk, 2015b; Romanazzo, S., S.Vedicherla, C. Moran, 2011; Romanazzo, Vedicherla, Moran, & Kelly, 2017; Vedicherla, Romanazzo, Kelly, Buckley, & Moran, 2018). In particular the emerging field of 3D bioprinting offers a solution to the limitations associated with existing meniscal scaffolds due to the ability to pattern cells and bioactive factors in mechanically functional three-dimensional (3D) scaffolds. Recent approaches to bioprinting meniscal constructs have focused on 3D printing polymeric constructs to mechanically reinforce cell-laden hydrogels, with the goal of creating biological implants which mimic the biomechanics of the native tissue more closely than existing commercially available

implants (G Bahcecioglu, Bilgen, Hasirci, & Hasirci, 2019; C H Lee et al., 2014; Nakagawa et al., 2019a; Szojka et al., 2017; Zheng-zheng Zhang et al., 2019).

The internal structures of CMI® and Actifit™ are homogenous porous meshes, which do not accurately mimic the complexity of the native meniscus tissue. As noted previously, circumferentially arranged collagen fibres are essential to the biomechanical function of the meniscus. Meniscal scaffolds produced by 3D printing of thermopolymers like PCL can mimic aspects of this structural complexity and the associated biomechanical properties of the tissue (Z.-Z. Zhang et al., 2017)(Balint, Gatt, & Dunn, 2012). 3D printing not only enables the deposition of biodegradable fibres with controlled directionality, but also with varying diameters and spacings, and therefore can facilitate the production of scaffolds with tunable compressive and tensile mechanical properties. 3D printing strategies such as FDM and Melt Electrowriting (MEW) are particularly useful for producing highly porous PCL scaffolds, and previously have been used to produce scaffolds that mimic the mechanical properties of musculoskeletal tissues such as bone and cartilage (Balint et al., 2012; Chang H Lee et al., 2014; Visser, Melchels, et al., 2015).

Despite recent advancements in tissue engineering (TE) and 3D bioprinting, cell-laden implants that mimic the complex biomechanical properties of normal meniscal tissue have yet to be developed. While 3D printing has enabled the engineering of constructs with compressive properties similar to the native human meniscus (Gokhan Bahcecioglu, Hasirci, Bilgen, & Hasirci, 2019; Szojka et al., 2017), they are typically homogenous in both their internal architecture and associated mechanical properties, whereas the native tissue is highly heterogeneous with distinct compositions and architectures within the inner and outer zones, the horns and the center as well as superficial and deep layers. This thesis aims to develop a 3D bioprinting strategy that is able to generate meniscal implants that considers such spatial complexity in its mechanical properties. In particular, this thesis will explore the

use of anisotropic printing architectures to produce implants with an improved resistance to the anisotropic forces in the joint (Bas et al., 2017; Driscoll, Nerurkar, Jacobs, Elliott, & Mauck, 2011; X. Li, Lu, Yang, & Yang, 2018; Maroti et al., 2019).

CMI® and Actifit™ are acellular porous scaffolds of bovine Achilles tendon and polyurethane, respectively (de Groot, 2010; W. G. Rodkey et al., 2008; W. G. D. Rodkey, Steadman, & Li, 1999), and require the ingrowth of cells from the remaining outer rim of the meniscus in order to regenerate lost meniscus tissue and ultimately replace the implanted scaffold. Using scaffolds that are already populated with cells or ECM molecules before being implanted is therefore a promising TE in order to improve the functionality of the implant and accelerate neo-tissue formation and meniscus regeneration (Chang H Lee et al., 2014; Romanazzo, S., S.Vedicherla, C. Moran, 2011). Several different cell sources for meniscus tissue engineering have been used in the past, each with their own advantages and disadvantages. Allogenic meniscus cells suffer from low donor availability, while isolating autologous meniscus cells requires further damage to the meniscus of the patient (Kwon et al., 2019; Makris, Hadidi, & Athanasiou, 2011a; Zellner et al., 2017). This has motived increased interest in the use of bone marrow derived stem/stromal cells (BMSCs) for meniscus TE. BMSCs have the advantage of multilineage plasticity, are immunomodulatory and anti-inflammatory. Moreover, they show macroscopic and microscopic healing effects, ECM production of fibrocartilage-like tissue with improved mechanical properties and chondroprotective effects (Mandal, Park, Gil, & Kaplan, 2011; Nerurkar, Han, Mauck, & Elliott, 2011; Pabbruwe et al., 2010). Furthermore, in order to provide specific cues for the controlled differentiation of cells, constructs with spatio-temporal release profiles have been developed. Localizing signals to the inner and outer zones of the printed construct enables spatial differentiation towards fibrochondrogenic or chondrogenic phenotypes that are found in the outer and inner zones of the native tissue, respectively (C H Lee et al., 2014; Romanazzo, S., S.Vedicherla, C. Moran, 2011;

Zheng-zheng Zhang et al., 2019). When cultivated in scaffolds or hydrogels functionalized with decellularized and/or solubilized meniscus ECM, BMSCs have also been shown to differentiate into the different cell types found in the native meniscus tissue (Rothrauff, Shimomura, Gottardi, Alexander, & Tuan, 2017)(Visser, Levett, et al., 2015)(Rothrauff et al., 2017). Such decellularization and solublization processes have also enabled the creation of scaffolds from meniscus ECM that retain native signals while removing inflammatory signals like xenogeneic DNA. This strategy has already been developed in the Kelly lab using other tissues like AC (Almeida et al., 2014; Browe, Kelly, Mahon, & Díaz-payno, 2019).

1.4. Objectives of this thesis

The existing CMI® and Actifit™ products possess a relatively simple porous internal architecture that does not replicate the internal structure and anisotropic biomechanics of native meniscus tissue. 3D printing has been used in the past to create fibre based scaffolds in order to mimic the internal architecture of soft biological tissues such as the meniscus (G Bahcecioglu et al., 2019; C H Lee et al., 2014; Nakagawa et al., 2019a; Szojka et al., 2017). This thesis aims to develop a 3D bioprinting strategy that enables the creation of anatomically accurate, tissue engineered meniscus constructs with heterogeneous and anisotropic biomechanics and ECM compositions which mimics key aspects of the native meniscus. To this end, ***the first objective of this thesis (Chapter 3) is to use FDM to create PCL scaffolds with compressive and tensile properties mimicking that of the human meniscus by varying the PCL fibre diameter, spacing and architecture (*****Fig. 1.1*****)***. As part of this project, the pores between the PCL fibres will be filled with hydrogels in order to produce mechanically reinforced constructs that are both bi-phasic (a fluid phase and a solid phase) and cell compatible. This was successfully shown in the past with UV-crosslinkable gelatin methacryloyl (GelMA) and hyaluronic acid (Bas et al., 2015; Visser, Melchels, et al., 2015).

Currently commercially available implants have failed to promote tissue regeneration with a quality high enough to allow full joint regeneration. While cell-laden, fibre-reinforced hydrogels have been used to produce bi-phasic constructs with robust mechanical properties that are simultaneously supportive of abundant ECM secretion (Bas et al., 2015; Schipani, 2019; Visser, Melchels, et al., 2015), these studies have so far have concentrated on regenerating AC, rather than meniscus. Therefore ***the second objective of this thesis (Chapter 4) is to 3D bioprint a composite construct consisting of a BMSC laden hydrogel reinforced with a PCL fibre network, and to assess the capacity of this construct to support fibrochondrogenesis of BMSCs (*****Fig. 1.1*****).***

The cell populations and ECM composition found in native meniscus are heterogeneous and vary between the inner and outer zone. Tissue engineering enables the creation of constructs which reflect these characteristics by employing different materials for the inner and outer zones (G Bahcecioglu et al., 2019). However, only limited differences in the levels of ECM deposition have been observed in the created zones. Therefore *the third objective of this thesis (Chapter 5) is to functionalize hydrogel bioinks with decellularized and solubilized porcine meniscus tissue, and to assess (i) the rheology and printability of such bioinks and (ii) their capacity to support the differentiation of BMSCs into zonally defined meniscal fibro-chondrocytes (***Fig. 1.1***).*

Lastly, CMI® and Actifit™ are designed only to repair partial meniscectomies (de Groot, 2010; W. G. Rodkey et al., 2008; W. G. D. Rodkey et al., 1999) whereas allografts transplants are still the gold standard to repair total meniscectomies, but suffer from limitations due to donor shortage. In recent years, large scale 3D bioprinted constructs have been created with inner and outer zones and biomechanical properties similar to the native tissue (G Bahcecioglu et al., 2019)(C H Lee et al., 2014; Nakagawa et al., 2019a), with some studies employing circumferential and radial fibre orientation in their scaffold designs (Szojka et al., 2017; Zheng-zheng Zhang et al.,

2019). However, these approaches have generally not considered the complex mechanical properties of the native meniscus (e.g. tension-compression non-linearity), and scaling-up the production of such large TE constructs remains a significant challenge. Therefore ***the fourth and final objective of this thesis (chapter 6) is to develop a scalable 3D bioprinting strategy capable of creating meniscal constructs of anatomical size and shape which mimic the anisotropic, heterogeneous and non-linear biomechanical properties of the native meniscus (*****Fig. 1.1*****).***

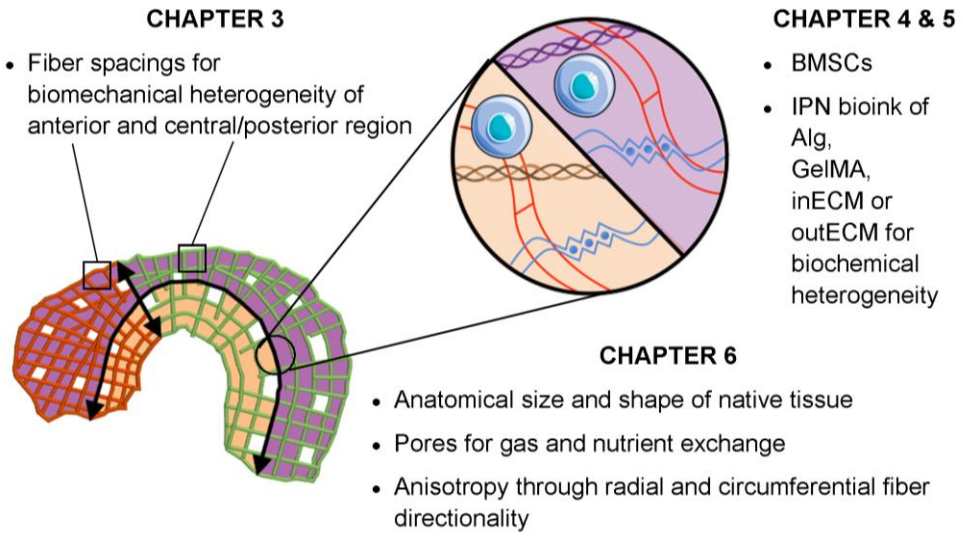

Fig. 1.1 Objectives of this thesis: Chapter 3 is focused on mimicking the biomechanical properties of the native tissue, chapter 4 concentrates on creating a BMSC loaded IPN of Alg and GelMA, chapter 5 adds solubilized porcine inner and outer meniscus ECM and chapter 6 creates a meniscus construct of anatomical size and shape of the native human tissue.

Chapter 2
LITERATURE REVIEW

2.1. General introduction

Menisci are a pair of semilunar cartilaginous tissues in the knee responsible for load distribution, joint stability, shock absorption and distribution of lubricating synovial fluid (Proctor, Schmidt, Whipple, Kelly, & Mow, 1989)(Hugh & MacNab, 1972; Newman, Anderson, Daniels, & Dales, 1989) (Tissakht, Ahmed, & Chan, 1996). The menisci have a wedge shaped profile and are located between the femur and tibia. Their shapes are essential for increasing the contact surface between the relatively planar tibial plateau and the more rounded femoral head (Fig. 2.1 a-c). Furthermore, the menisci transmit more than 50% of the vertical axial forces within the knee joint and convert them to hoop stresses (Fig. 2.1 f). Moreover, the tissues move slightly during bending and flexing of the knee joint and are therefore attached within the joint at several different points in a way that allows a degree of freedom of movement. The outer zone of the menisci is attached to the joint capsule which supplies the tissue with blood and nutrients. Furthermore, the horns of the menisci are attached to the tibial plateau through the meniscotibial ligaments and to the femoral head through the meniscofemural ligaments. In addition to that, the lateral and medial menisci are also attached to each other via the transverse inter-meniscal ligament (Mark A Sweigart & Athanasiou, 2001). The meniscus possesses two distinctly different zones: the outer, more vascularized and innervated zone, and the inner, more cartilaginous and therefore slower regenerating zone (Fig. 2.1 c). These two zones differ in cell populations and ECM composition and therefore in their biomechanical properties and function (Fig. 2.1 e).

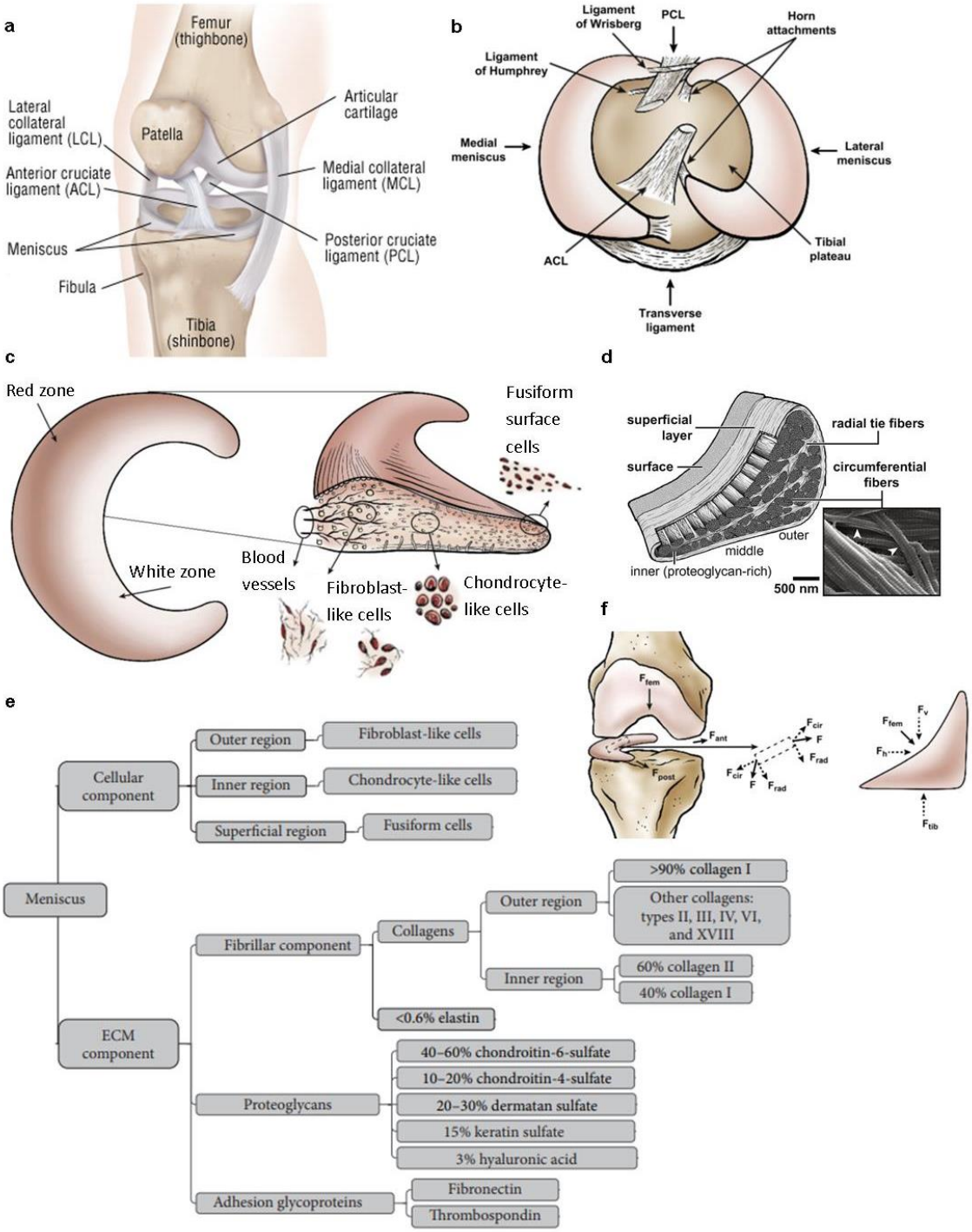

Fig. 2.1. Meniscus structure and function: The menisci are located within the knee joint(a) between the tibial plateau and femoral head (b) and consist of distinct zones of varying cell populations(c) and ECM compositions(e). The circumferentially and radially directed fibres provide anisotropy(d) which is essential for the load distribution functions(f).

(a, (www.drugs.com) b, c, f (Makris et al., 2011b), d (Q. Li et al., 2017), e (Guo et al., 2015))

2.2. Extracellular matrix composition

2.2.1 Introduction

Meniscus tissue is a fibrocartilaginous tissue and is often described as a composite material with collagen fibres inside a hydrophilic matrix (Tissakht & Ahmed, 1995). The fibres form a solid phase and their electrostatic charges bind water inside the tissue which forms a liquid phase (60-70% of the tissue wet weight). Meniscus therefore has bi-phasic properties (Mow & Huiskes, 2005).

The matrix of the vascularized, outer zone is primarily composed of collagen type I as well as traces of Col II-VI and is therefore more fibrous (Fithian, Kelly, & Mow, 1990; Makris, Hadidi, & Athanasiou, 2011b). Col I fibres are strong in tension and are oriented in a circumferential direction inside the tissue. This orientation is crucial in preventing radial extrusion of the tissue during stress and in preventing structural integrity (Ghosh & Taylor, 1987; Setton, Guilak, Hsu, & Vail, 1999)(Fig. 2.1 d).

The matrix of the inner, more cartilaginous zone is composed of approximately 60% Col II as well as 40% Col I. Furthermore, the inner zone also contains proteoglycans (PG) like aggrecan and glycoproteins (McDevitt & Webber, 1990) which are important to provide the tissue with viscoelasticity, compressive stiffness and hydration and to reduce friction between the tibial and femoral surfaces(Ghosh & Taylor, 1987; Setton et al., 1999)(Fig. 2.1 e).

To summarize, the meniscus is a bi-phasic tissue with a solid and a liquid phase. Furthermore, the solid phase is a composite, which consists of collagen fibres in a hydrophilic matrix. The various forms of collagen fibres and matrix molecules are not spread out homogenously throughout the tissue, but are located to different degrees throughout the inner and outer zones, the horns and the centre, as well as the surface and the deep layers of the tissue. In addition to that, the fibres and matrix

molecules show a distinct orientation inside the tissue resulting in a specific anisotropy. (Fig. 2.1 d)

In the following sections the heterogeneity as well as anisotropy of the meniscus tissue as a result of the different localization and orientation of the mentioned fibres and matrix molecules as well as the resulting biomechanical properties will be discussed.

2.2.2 Meniscus heterogeneity

Meniscus tissue possesses a heterogeneous composition of collagen fibres and matrix molecules that creates biomechanical differences between its inner and outer zone, through its depth and spatially from the horns to its centre (Fig. 2.1 c).

The biomechanical differences of the various matrix compositions can be partially attributed to the molecules' varying electrochemical charges and therefore ability to bind water. This results in regional differences in degrees of swelling, as well as physiochemical, electrical and mechanical properties like resistance to tensile, compressive and shear stress. The following zones are differentiated in the literature:

2.2.2.1. Outer and inner zone

The meniscus can be differentiated between an outer and an inner zone. The outer zone is the thicker part of the wedge shaped tissue and due to its vascularization it is also referred to as the "red zone". Due to this vascularization and connection to the joint capsule the outer zone possesses a higher healing capacity then the inner, so called "white" zone. Furthermore, the dry weight of the red zone is composed of 80% collagen I and traces of less than 1% of Col II, III, IV, VI and XVIII and therefore possesses a more fibrous phenotype(Arnoczky & Warren, 1982; Longo et al., 2012). In addition, the red zone is mainly populated by fibroblast-like cells.

Often an intermediate zone is defined as a ‘third’ zone between the outer and inner zone. This fibrocartilaginous zone is populated by fibroblast-like cells as well as chondrocyte-like cells.

Lastly, the inner or white zone can be described as a hyaline cartilage-like tissue that is not vascularized and has therefore a low healing capacity. The matrix of the white zone is composed of 70% collagen per dry weight, of which 60% is type II and 40% col I. Furthermore, the white zone consists of 17% sGAGs per dry weight and 1% PGs and is populated with fibrochondrocyte cells (Arnoczky & Warren, 1982; Herwig, Egner, & Buddecke, 1984; Longo et al., 2012; Proctor et al., 1989) (Fig. 2.1 e).

As a cartilaginous tissue, menisci have similar structural and functional features to AC tissue except a few differences with the presence of a vascularized zone being the biggest one. Furthermore, as mentioned above, the ECM possesses a fibrocartilaginous composition and therefore contains a higher Col I content overall and a lower PG content, particularly in the outer red zone.

After birth, the entire meniscus is vascularized, whereas the white, non-vascularized zone only develops during adolescence. The loss of vascularization in the inner zone during adolescence is believed to be due to an increase of weight bearing and knee movement (Petersen & Tillmann, 1995).

2.2.2.2. Superficial and deep layers

Furthermore, the ECM of the meniscus can be differentiated between its superficial and its deep zone through differences in ultrastructure and water content. The superficial zone consists of randomly orientated fibrils with split lines similar to the ones found in the surface of AC. The ultrastructure of the tissue changes at a depth of approximately 100 μm, and in contrast to the thinner, more randomly orientated fibrils on the surface consists of thick, collagen fibre bundles, which are oriented in a horizontal, circumferential direction going from horn to horn. Additionally, smaller,

radially oriented fibres tie the circumferential ones together and reinforce the tissue going from the outer to the inner zone (Mow & Huiskes, 2005).

2.2.2.3. Horns vs central region and medial vs lateral

Furthermore, within the deep layer, which makes up the majority of the meniscus volume, uniform collagen and PG contents are reported, aside from differences between inner and outer zones as described above. However, slightly higher tensile moduli have been reported in the horns of the medial meniscus compared to the central part, which can be attributed to the anisotropy through fibre directionality rather than ECM contents. In contrast, the posterior horn of the lateral meniscus shows a reduced amount of circumferentially oriented fibres, which can be correlated with a higher amount of lesions reported in the clinic in that region (Fithian et al., 1990).

In contrast, the size and density of radial fibres in bovine menisci have been reported to increase from the anterior to posterior horn, which leads to higher tensile moduli and ultimate tensile strength in the radial direction in the posterior horn (Skaggs, Warden, & Mow, 1994).

2.2.3 Anisotropy

As described above, meniscus tissue has a similar structure and composition to AC, but with a number of key differences. The ECM fibre directionality sets meniscus tissue further apart from AC, which has been described with horizontal, parallel fibres in the superficial zone, randomly orientated fibres in the middle zone and vertically oriented fibres in the deep zone. In contrast, as described above, meniscus tissue possesses randomly oriented fibres in the superficial layer and circumferentially and radially directed fibre bundles in the deep layers. Furthermore, this distinct fibre orientation causes anisotropy in the tissue, which means the mechanical properties depend on the direction in which the tissue is loaded. Stronger tensile properties have therefore been reported in the circumferential direction of the semilunar shaped tissues

compared to the radial direction, which corresponds to the higher number of thick, circumferentially oriented fibre bundles in the meniscus (Proctor et al., 1989). This circumferential arrangement of ECM components is essential for one of the most important functions of the meniscus: the conversion of compressive stresses to hoop stresses (Fig. 2.1 d, f).

To summarize, due to the anisotropic fibre orientation the compressive forces, shear stresses and tensile stresses in circumferential and radial direction can therefore be endured and redirected (Mow & Huiskes, 2005).

2.3. Biomechanical properties of the meniscus

Since menisci consist of a matrix with electrostatic charges, the tissue is able to bind and store large amounts of liquids, with 60-70 % (by wet weight) of the tissue consisting of water. Menisci are therefore characterized as bi-phasic materials with a solid and a liquid phase (Fithian et al., 1990; Mow & Huiskes, 2005) displaying rate dependent mechanical properties (Bullough, Munuera, Murphy, & Weinstein, 1970; Proctor et al., 1989; Skaggs et al., 1994). The following section will consider the compressive and tensile properties of the meniscus.

2.3.1 Compressive properties

As described above, the compressive properties of native menisci are determined by its permeability and water content which is facilitated by the electrostatic charges of its matrix components. Since liquids cannot be compressed the liquid phase of the tissue is displaced from the solid phase instead during compressive loading. The resistance to compressive forces of meniscus tissue is therefore depending on the permeability of the tissue and changes with varying rates of compression (Mow & Huiskes, 2005).

With an average aggregate modulus under axial compression of 100-150 kPa meniscus tissue possesses slightly lower compressive properties than the ones of AC

(M A Sweigart & Athanasiou, 2005). As described above, meniscus tissue consists of a heterogeneous ECM composition which means the compressive properties vary between the inner and outer zones and the horns and the centre. Moreover, there are also slight variations between menisci of different species of human, bovine, porcine and lapine sources, which are the most common ones reported in the literature. Moreover, due to the described heterogeneity it is important where sections of samples have been taken from. As reported below in table 2.1, the aggregate modulus is slightly higher in the anterior region (~0.15 MPa) than of the central and posterior regions (~0.1 MPa). However, the biggest source of variation in comparing mechanical properties of human tissues is donor variability. In many cases the available human menisci are often from patients of a wide age range, or solely from older patients who suffer from degenerated an injured knee joints. However, the most concise testing of human meniscus tissue has been excellently reviewed by Makris et al (M A Sweigart & Athanasiou, 2005) and are reported in Table 2.1.

Table 2.1 Compressive properties of native meniscus tissue

Study	Location	Aggregate modulus (±SD), MPa	Permeability (±SD, 1015 m4 N—1s-1)
(M A Sweigart et al., 2004)	Medial superior		
	Anterior	0.15 ± 0.03	1.84 ± 0.64
	Central	0.10 ± 0.03	1.54 ± 0.71
	Posterior	0.11 ± 0.02	2.74 ± 2.49
	Medial Inferior		
	Anterior	0.16 ± 0.05	1.71 ± 0.48
	Central	0.11 ± 0.04	1.54 ± 0.49
	Posterior	0.09 ± 0.03	1.32 ± 0.61

2.3.2 Tensile properties

The meniscus tissue possesses anisotropic tensile properties due to radial and circumferential collagen fibre directionality, as well as spatial differences in fibre density (e.g. between the anterior/posterior and surface/deep layers as well as between the medial and lateral menisci).

Under elongation testing the initial region of a stress/strain curve can be described as a non-linear toe region and correlates to an elastic behavior of coiled up collagen fibre bundles being uncoiled. When the tissue is elongated under tension, the fibres stretch and the amplitude of the coiled fibres decreases. The stiffness of the tissue then gradually increases until all fibres are straightened (Mow & Huiskes, 2005). Following that, the linear region of the stress-strain curve the correlates to stretching of the now straightened collagen fibres concluded by their eventual fracture (Mow & Huiskes, 2005; Tissakht & Ahmed, 1995).

Similarly, to compressive testing, published results on tensile properties of native tissue vary significantly and depend on donor, sample location and size, preparation and testing method. Examples of variation in preparation process are preparing frozen or fresh samples, testing them in a humidified chamber or in solutions with protease inhibitors to prevent degradation (M A Sweigart & Athanasiou, 2005; Tissakht & Ahmed, 1995). Another step towards elimination of testing variations have recently been described through the uniform use of “extended tab” and rectangular shaped samples to test circumferential and radial specimen, respectively. The most concise collection of data, as reviewed by Makris, is presented in Table 2.2.

The tensile moduli of human meniscus tissue reaches 100 – 300 MPa in circumferential direction and shows its lowest values in the medial posterior horn with approximately 100 MPa and has its highest moduli in the anterior and posterior horns of the lateral meniscus with 135-300 MPa. The tensile moduli in the radial direction are with approximately 30-50 MPa lower and show reduced tensile properties in both posterior horns (Fithian et al., 1990; Lechner et al., 2000; Tissakht & Ahmed, 1995).

Table 2.2: Tensile properties of native meniscus tissue

Study	Direction	Location	Modulus (±SD, MPa)
(Fithian et al., 1990)	Circumferential	**Lateral meniscus**	
		Anterior	159.1 ± 47.4
		Central	228.8 ± 51.4
		Posterior	294.1 ± 90.4
		Medial meniscus	
		Anterior	159.6 ± 26.2
		Central	93.2
		Posterior	110.2
(Tissakht & Ahmed, 1995)	Circumferential	**Lateral meniscus**	
		Anterior	124.5 ± 39.51
		Central	91.4 ± 23.04
		Posterior	143.7 ± 38.91
		Medial meniscus	
		Anterior	106.2 ± 77.95
		Central	78.0 ± 25.09
		Posterior	82.4 ± 22.23
	Radial	**Lateral meniscus**	
		Anterior	48.5 ± 25.67
		Central	45.9 ± 24.20
		Posterior	29.9 ± 12.77
		Medial meniscus	
		Anterior	48.5 ± 25.67
		Central	46.2 ± 27.56
		Posterior	32.6 ± 11.27
(Lechner, Hull, & Howell, 2000)	Circumferential	**Medial meniscus**	
		Anterior	141.2 ± 56.7
		Central	116.4 ± 47.5
		Posterior	108.4 ± 42.9

2.4. Cell population

The meniscus also possesses a spatially heterogeneous cell population. During early development the tissue only consists of a red zone so similarly, all cells have same morphology before adolescence. Later in development, when the white zone forms, two morphologically and phenotypically distinct cell populations can be observed. Cells can therefore be classified according to their shape and absence or presence of a pericellular matrix (Ghadially, Thomas, Yong, & Lalonde, 1978). Currently different terms are found throughout the literature for the distinct cell populations (Fig. 2.1 c)

2.4.1 Chondrofibroblast-like cells of the inner zone

Cells primarily found in the inner white zone possess a rounded shape, form lacunae and are surrounded by a pericellular matrix which consists of col II and GAGs as well as smaller volumes of collagen I similarly to hyaline cartilage. These cells are therefore called fibrochondrocytes or chondrocyte-like cells (Hellio Le Graverand et al., 2001; Melrose, Smith, Cake, Read, & Whitelock, 2005).

2.4.2 Fibroblast-like cells of the outer zone

Furthermore, the outer red zone is populated by cells of an oval, fusiform shape with similar behavior and characteristics to fibroblasts. Furthermore, their long cell extensions enable them to interact with other cells and their surrounding matrix. This pericellular matrix consists mostly of col I with traces of GAGs and Col III and V (Mcdevitt, Mukherjee, Kambic, & Parker, 2002; Nakata et al., 2001).

2.4.3 Cells in superficial layer

A third, recently recognized population can be found in superficial layer of tissue. The cells possess a flattened fusiform shape without cell extensions and are thought to be progenitor cells with therapeutic and regenerative capabilities (Bracht, Verdonk, Verbruggen, Elewaut, & Verdonk, 2007).

2.4.4 Mechanical stimulation of cells

The homeostasis of this heterogeneous cell population is maintained by a complex cocktail of genetic and biochemical factors like growth factors and cytokines (Collier & Ghosh, 1995; McNulty, Rothfusz, Leddy, & Guilak, 2013; Pangborn & Athanasiou, 2005; Riera et al., 2011) as well as physical factors during joint loading. Mechanical factors play an especially critical role in the development, maintenance, degeneration, and repair of the meniscus and could therefore provide insights into prevention and treatment of traumatic lesions and degeneration of the tissue.

Meniscus cells therefore respond to mechanobiological signals like tension, compression and hydrostatic pressure and together with genetic and biochemical ones metabolic and pro- or anti-inflammatory responses are created (Mcnulty & Guilak, 2016). Specifically, *in vivo* studies have shown that joint immobilization leads to a loss of proteoglycans (Klein, Player, Heiple, Bahniuk, & Goldberg, 1982; Videman, Eronen, Friman, & Langenskiold, 1979) in gene level (Djurasovic et al., 1998) as observed in histological staining as well as a decrease in the mechanical function of the tissue (Anderson, Gershuni, Nakhostine, & Danzig, 1993; Ochi, Kanda, Sumen, & Ikuta, 1997). This described disuse atrophy can be prevented and lesions repaired through passive or active motion without bearing of weight in order to increase the blood flow throughout the joint system (Bray et al., 2001; Burr, Frederickson, Pavlinch, Sickles, & Burkart, 1984; Klein, Heiple, Torzilli, Goldberg, & Burstein, 1989). This mechanism which also improved regeneration after surgery (Dowdy, Miniaci, Arnoczky, Fowler, & Boughner, 1995) and induced anti-inflammatory response in osteoarthritis model can also be observed through an increase in IL-10 in fibrochondrocytes (Ferretti et al., 2005).

Abnormally high loading however, can be damaging to the meniscus tissue as well, as shown through lower cell viability levels in a rabbit joint model and an increase in pro-inflammatory cell signals like nitric oxide (Killian, Haut, & Haut Donahue, 2014). Furthermore, explant cultures show that 10% strain under dynamic loading causes anabolic responses in cells through decreased release of pro-inflammatory mediator NO (Gupta, Zielinska, McHenry, Kadmiel, & Haut Donahue, 2008) and increased aggrecan expression (Aufderheide & Athanasiou, 2006). However, strains of 20% surpass the healthy physiological levels and cause a catabolic cell response demonstrated through the release of matrix metalloproteases, nitride oxide synthase 2 and interleukin 1a (Gupta et al., 2008; McHenry, Zielinska, & Donahue, 2006; Zielinska, Killian, Kadmiel, Nelsen, & Haut Donahue, 2009), whereas the secretion of

Col I, tissue inhibitor of metalloproteases 1 and TGF-β (Gupta et al., 2008; Zielinska et al., 2009).

To summarize, meniscus tissue possesses a heterogeneous cell population with a homeostasis maintained by a complex mixture of biochemical, genetic and mechanical signals. Abnormal mechanical loading, however, can lead to decreased function of the meniscus tissue through degeneration or lesions.

2.5. Biomechanical and clinical impact of meniscus deficiency

2.5.1 Meniscus tears

As described above the circumferentially aligned collagen fibres are essential for the function of the meniscus tissue. However, the load bearing and distributing function of the meniscus can be disrupted when those fibres are torn through trauma or degeneration. Meniscus injuries are very common in all age groups and symptoms are swelling, mechanical blocking of the knee and joint line pain as well as a decrease in muscle strength and altered gait pattern (Hall et al., 2014). Furthermore, athletes have even higher chances of injury (B. E. Baker, Peckham, Puparo, & Sanborn, 1985), usually from trauma during axial loading and rotation (Browner, 2009) which is often also coupled with anterior cruciate ligament (ACL) injuries in more than 80% of patients (Rubman, Noyes, & Barber-Westin, 1998). 81% injuries occur in the medial meniscus, and 19% in the lateral one, with skiing and soccer being the recreational activities with the highest knee injury risks (Majewski & Susanne, 2006). Tears in middle aged and elderly patients, however occur due to degeneration than from sports and in 68-90% of patients meniscus tears are also correlating with OA. Due to degeneration and declining vascularization of the joint with age meniscus repair has been less successful in older patients (Barrett, 1998)(M Englund et al., 2007). Moreover, degenerative tears are commonly of a more complex nature and occur mostly in the posterior horn (Mcdermott & Amis, 2006).

The nature of lesions can be classified according to the depth of the tear (partial or full thickness), as well as the tear pattern (radial, bucket handle, oblique, or complex for example) (Fig. 2.2 a). Untreated meniscus tears are a potent risk factor for the development of OA (Martin Englund et al., 2009). Identifying and classifying the injury is therefore essential to choosing the correct treatment option (Noyes & Barber-Westin, 2010). A common surgical treatment method is meniscectomy, which entails the removal of the torn section to facilitate acute pain relieve and reduction in joint swelling. Following a partial meniscectomy, patients can return to their normal life after short time, especially since the introduction of minimally invasive arthroscopic surgery methods. Meniscectomies are conducted in 61 per 100 000 people per year, in young patients to treat acute lesions or as part of degenerative process in older patients (B. E. Baker et al., 1985).

However, the removal of the damaged meniscus tissue causes knee instability and accelerates osteoarthritis, leading to more chronic pain and the eventual need to undergo total meniscectomy or knee arthroplasty in the future (Salata, Gibbs, & Sekiya, 2010). Meniscus deficiencies due to lesions or meniscectomies therefore have a number of biomechanical and clinical impacts.

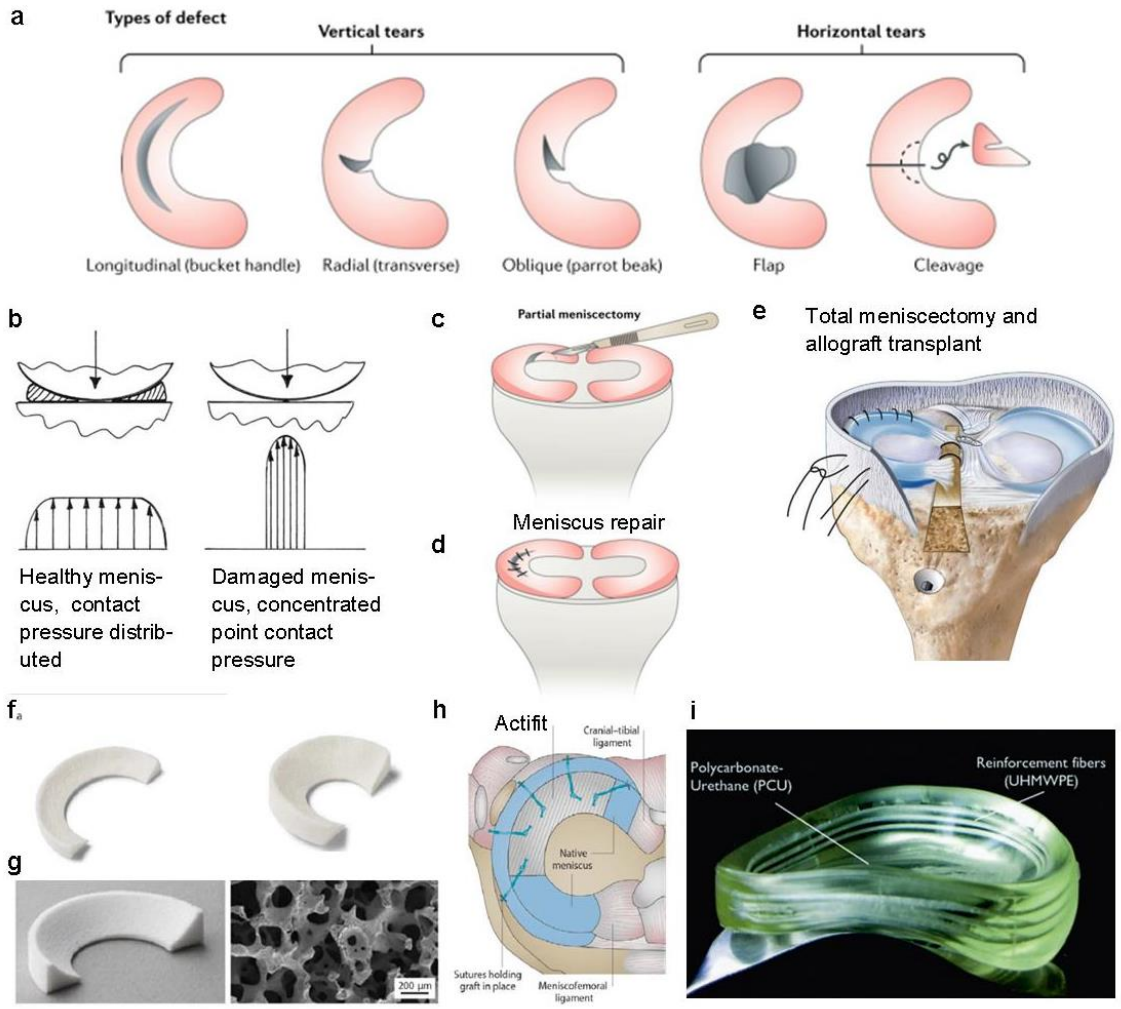

Fig. 2.2 Meniscus tears, repair and replacement: Various types of meniscus tears (a) reduce the total contact area between femur and tibia and increase the concentrated point contact pressure (b). Popular repair methods are partial meniscectomies (c) or repair through sutures (d). Total meniscectomies require allograft transplants, often via fixation through bone tunnels (e). Partial meniscus defects can be replaced with commercially available products Actifit™ (f) or CMI® (g) via arthroscopic surgery (h). Further novel implants like NUsurface® are currently in development too (i).

(a, c, d: (Kwon et al., 2019), b (Mcdermott & Amis, 2006), e (Noyes & Barber-Westin, 2010) f Ivy Sports Medicine, Germany, g –h Orteq Ltd, UK), i (Active Implants, 2018)

2.5.2 Biomechanical impact

2.5.2.1. Partial meniscectomy

As a load bearing tissue, the structure of menisci is essential to their function. Partial deficiencies after a tear and subsequent removal of the damaged tissue, however, decrease the tissue volume and contact area and therefore lead to an impairment of their function (Fig. 2.2 c).

Specifically, menisci transmit more than 50% of the axial stresses within the knee joint and convert them to hoop stresses. The tissue is wedge shaped and semilunar and therefore can cover approximately 60% of the joint surface between the spherical shaped femoral condyles and more flat tibial plateau. It thereby increases the contact surface within the joint (Noyes & Barber-Westin, 2010) which is essential to the load distributing function of the tissue. Partial lesions and subsequent meniscectomy of the torn and sometimes even dislocated tissue, however also causes a decrease in meniscus area and therefore an increase in pressure which the tissue cannot withstand over time. In particular, a reduction of 16-34% of the contact area between menisci and femur and tibia through a partial meniscectomy leads to more than 350% force increase on the AC on average(Fig. 2.2 b)(Seedhom & Hargreaves, 1979). Meniscus tears and associated deficiencies are not all equally severe to the joint function due to the heterogeneity of the tissue: Tears in the peripheral region for example often lead to no significantly decreased contact area and peak contact stress only increase by 4 - 27%. Conducting a partial meniscectomy to treat such a lesion, however has been shown to increase peak contact areas by 110% (Baratz, Fu, & Mengato, 1986).

This increase in peak contact area stresses furthermore also leads to changes on the biomolecular level of the tissue. An increase in stress has been shown to lead to a loss and disaggregation of proteoglycans in the ECM and hydration of the tissue. Furthermore, meniscus cells also showed a change in PG synthesis through a lack of

incorporation and attachment of the molecules to their surrounding matrix as well as a changed ratio of produced chondroitin-sulphate-rich compared to keratan-sulphate-rich PGs. These biomolecular changes have also been shown to be symptoms of OA (Lanzer & Komenda, 1990). Moreover, a disruption in meniscus function has been shown to lead to damages in the underlying layer of AC of the joint as evident through fibrillation, loss and necrosis (Lanzer & Komenda, 1990). Degenerative tears like this can be commonly detected through their high intensity signals in magnetic resonance imaging (MRI) scans due to their increased water mobility corresponding to the tissue's change in permeability which is facilitated through the proteoglycan levels (Hutchinson et al., 2014). The loss of function and morphological changes of AC on the tibial plateau can therefore be directly correlated to the amount of removed meniscus tissue in a defect (M Englund, Roos, Roos, & Lohmander, 2001; Hede, Larsen, & Sandberg, 1992).

2.5.2.2. Total meniscectomy

The most significant reduction in meniscus function, however, can be observed in tissues with horizontal radial tears which disrupt a large number of circumferential fibres and entail large biomechanical impacts on the function of the knee joint. In these cases total meniscectomies have to be conducted through the removal of large sections of the injured meniscus until mostly only the peripheral rim remains. Bucket handle tears located in the inner third of the meniscus decrease the contact area of the meniscus by 10% only but increase peak contact stresses by 65%. After treatment via total removal of the lateral meniscus a 235-335% increase in localized contact load peaks was shown in cadavers (Paletta, Manning, Snell, Parker, & Bergfeld, 1997). Similarly, the total loss of the medial meniscus was shown to lead to a decreased contact area by 75% and an increase of peak contact pressure of 235% (Baratz et al., 1986). Due to slight biomechanical differences between lateral and medial compartment of the knee joint total meniscectomies of the lateral meniscus have been

shown to have lower post-surgical evaluation scores than procedures on the medial meniscus. Since the lateral condyle and lateral meniscus are both mirrored in convexity, more point loading within the lateral side of the joint was recorded. The lateral meniscus therefore carries 70% of the load of the lateral compartment compared to the medial meniscus which due to its reduced convexity carries only 50% of the load of the medial compartment (Mcnicholas et al., 2000)(Makris et al., 2011b).

2.5.3 Clinical impact

Patient related symptoms of meniscus deficiencies are joint instability, locking, effusion, grinding and pain as well as physical findings on knee examination like limitation in motion, joint line tenderness, effusion, and provocative signs like pain when squatting. Furthermore, the clinical impact also varies depending on the site of the lesion. Specifically, a worse decrease in joint function was detected after posterior tears compared to anterior or bucket handle tears and consequitive partial meniscectomies (Hede et al., 1992). Preserving as much healthy meniscus tissue as possible is imperative in order to prevent further degeneration of the joint (Matteo et al., 2016; Moran, Orth, et al., 2015). Consequentially, it has been shown that the retention of the posterior third as well as the peripheral rim of the meniscus correlate with successful long-term recovery results (Chatain et al., 2001; Hede et al., 1992). However, vertical, radial tears have been shown to disrupt a high number of essential circumferential collagen fibres and indicate the necessary removal of large contact areas of the tissue through a total meniscectomy (R. S. Jones et al., 1996). Further clinical consequences when a total meniscectomy was necessary are radiographic changes in the whole knee joint like ridge formation, narrowing of joint space and flattening of femoral condyle within the first 5 months of the operation. These symptoms become more severe over time due to the loss of the weight-bearing function of meniscus (Fairbank, 1947). In fact, a 4% loss of AC per year could be

detected after conducting total meniscectomies (Y. J. Wang et al., 2010)(Mcdermott & Amis, 2006).

2.5.4 Current clinical approaches to meniscus deficiencies

2.5.4.1. Repair

Menisci are cartilaginous tissues similar to AC but possess a limited self-healing capability due to their small degree of vascularization. It has furthermore been shown that lesions in the peripheral red zone of the meniscus can regenerate without surgical intervention through physical therapy, especially in younger patients. The self-repair capabilities of tears can therefore be classified according to the location of the lesion relative to the blood supply of the meniscus. Stable, vertical and longitudinal tears in the vascularized, peripheral red zone of the anterior region have the highest chances of healing, whereas lesions in the white zone have only low chances of regeneration without surgical intervention (Dehaven & Arnoczky, 1994)(Weiss, Lundberg, Gillquist, & Hospital, 1989).

In recent years preserving meniscus structure and function has become a priority in the treatment of lesions. Hence, instead of removing sections of torn meniscus tissue lesions, which cannot regenerate minimally invasive surgery is used more commonly to repair tears using anchors and sutures (Fig. 2.2 d). Highest success rates have been achieved here once more in younger patients in paediatric or adolescent ages regardless of tear or location due to their higher healing potential stemming from higher vascularization and rate of metabolism (Makris et al., 2011b). Meniscus repair surgery is often conducted in conjunction with reconstruction of a torn ACL, which can be correlated to a number of meniscus lesions due to the nature of many meniscus injuries stemming from trauma in recreational activities. In fact, combined repair surgeries like these even have a higher success rate than of

meniscus surgeries alone (Wasserstein et al., 2008). This has been correlated to the possible release of cells, growth factors and bone marrow to the meniscus when drilling bone tunnels necessary for ACL reconstruction (Hutchinson et al., 2014). Tears in the peripheral, vascularized zone have higher recovery rates again, especially in younger patients. In older patients, repair procedures are only conducted in order to treat peripheral tears. Contraindications to repair are poor vascularization in the region and degenerative nature of the tear, knee instability or osteoarthritis as well as patient age and compliance with rehabilitation (Hutchinson et al., 2014).

A number of different repair techniques apart from suturing are using a fibrin clot, rasping, trephination as well as using stem cell therapy or growth factors (Henning CE, Lynch MA, Yearout KM, Vequist SW, Stallbaumer RJ, 1990; Taylor & Rodeo, 2013)(van Trommel, Simonian, Potter, & Wickiewicz, 1998). Success rates range from 63% - 91% with a higher rate of re-operation than meniscectomies, long term follow-up studies are still lacking and there is only little knowledge about possible deterioration of the meniscus and AC (Morgan, Wojtys, Casscells, & Casscells, 1991; Caiqi Xu & Zhao, 2015). Furthermore, repairing meniscus lesions is still challenging, which is why the most commonly used method to treat meniscus lesions is still meniscectomy, despite the known risk of joint degeneration (E. M. Roos, Östenberg, Roos, Ekdahl, & Lohmander, 2001).

2.5.4.2. Replacement

Some meniscus lesions have very low chances of success in repair like longitudinal, bucket handle tears in the white zone which often leads to locking of the knee (Mcdermott & Amis, 2006) as well as radial horizontal tears from trauma, horizontal, flap or complex lesions associated with degenerating tissue which are more often found in elder patients (Greis, Bardana, Holmstrom, & Burks, 2002). Those lesions are often indicated for treatments with partial or total meniscectomies in order to remove the torn region and reduce the acute pain and locking of the joint in case of

bucket handle tears. Contrary to today's knowledge in 1897 menisci were described in 1897 as remnants of intra-articular leg muscles and torn menisci were primarily treated with total meniscectomies. Later, in 1949 the opinion in the field changed and total meniscectomies were recognized as damaging the joint and their connection to osteoarthritis (Greis et al., 2002). Hence, in order to preserve meniscus tissue and function partial meniscectomies were introduced as the primary treatment method for lesions. Moreover, in long term studies it was shown that even the regenerative potential in paediatric patients with still opened epiphyses in the age of 15 years old was insufficient to recover from a total meniscectomy but instead lead to degeneration of the joint (Medlar, Mandiberg, & Lyne, 1980). However, as described above over the last few decades it was found out now that meniscus tears and subsequently indicated partial meniscectomies cause still too much tissue loss to regain full meniscus function and novel repair methods have been developed (Matteo et al., 2016; Moran, Orth, et al., 2015; Moran et al., 2012).

In scenarios where repair is not possible and partial or total meniscectomies are deemed necessary, however, several implants are available in order to replace the damaged and removed meniscus tissue. Actifit™ and CMI® are currently commercially available implants following partial meniscectomies and show promising results in the clinic, whereas the gold standard to replace removed tissue during total meniscectomies are still allograft implants (Makris et al., 2011b; Moran, Orth, et al., 2015) (Fig. 2.2 e-h).

Actifit™ and CMI® are off-the-shelf products made of polyurethane and collagen scaffolds which reduce pain and improve the knee function as well as radiological diagnosis. CMI® is slightly stiffer than Actifit™, degrades slightly slower, consists of porous Col I – chondroitin sulphate and hyaluronic acid from bovine Achilles tendon and has been shown to support tissue ingrowth (Pieter Buma, Tienen, & Veth, 2007). Specifically, histology shows immature collagen fibrils and lacunae,

blood vessels and fibroblast-like cells in the constructs 6 months after implantation without degradation of joint surfaces visible in MRI scans. Furthermore, after midterm studies of 6 years patient activity scores had improved but second look arthroscopy and MRI scans still showed inferior tissue compared to native meniscus tissue and shrinkage of the implant. In long-term studies after 10 years, however 64% - 85% of patients returned to pre-injury activity levels. However, most significant increases in patient scores and beneficial developments have only been recorded in younger patients with chronic meniscus deficiencies so far (Bulgheroni et al., 2010; W. G. Rodkey et al., 2008; Zaffagnini et al., 2011; Zaffagnini & Giordano, 2007)(Spencer et al., 2012)(Harston, Nyland, Brand, Mcginnis, & Caborn, 2012)(Myers, Sgaglione, & Kurzweil, 2013). Other studies on the other hand still show a scaffold shrinkage and MRI signal differences compared to healthy knees (Monllau et al., 2011). Furthermore, necessary improvements to the currently available studies on CMI® are the lack of randomization and control groups which is an unfortunate difficulty when conducting clinical studies.

Actifit™ on the other hand is an artificial implant made of polyurethane, a combination of PCL and urethane. PCL degrades in the body over a course of 5 years whereas urethane requires longer to degrade. Actifit™ has promising tissue ingrowth results too, shows the development of a trilayered organisation pattern and improvements in pain and activity scores in patients but clinical studies so far have only been short and midterm over a course of 2 years (Schüttler et al., 2016; Rene Verdonk, Verdonk, Huysse, Forsyth, & Heinrichs, 2011).

NUsurface® and Trammpolin® are two more implants which are currently in development and are aimed at treating deficiencies which indicated total meniscectomies. Both devices are based on polycarbonate urethane and are non-resorbable. NUsurface® is currently in clinical trials in the USA and seems to mimic the essential circumferential fibre structure more closely than CMI® or Actifit™. The

polycorbonate urethane meniscal device reinforced with free floating, ultra-high molecular weight polyethylene fibres (UHMWPE)(Active Implants, 2018)(NUsurface®, AIC, Memphis, Tennessee, (Elsner & Linder-ganz, 2010)) (Fig. 2.2 i). However, short-term clinical results point at a high failure rate in 78% of patients after 2 years due to dislocation, tears or development of OA and motivate further development of novel implants (Van Der Straeten et al., 2016). Similarly to NUsurface®, Trammpolin® is currently investigated in clinical trials but animal studies failed to provide chondroprotection compared to meniscectomy due to suboptimal fixation method and size matching (A C T Vrancken, Madej, Hannink, Verdonschot, & Tienen, 2015; Anne C T Vrancken et al., 2017).

To summarize, both CMI® and Actifit™ show very promising results in tissue ingrowth, and pain and activity scores in patients but also MRI signal abnormalities and scaffold shrinkage after 10 years. Furthermore, only a small number of long-term clinical studies have been conducted so far without necessary blinding or control groups. Moreover, both products can be used to treat patients with segmental meniscus defects but require an intact peripheral rim of the tissue and intact AC (Tienen, Hannink, & Buma, 2009).

Allograft transplants are therefore still the gold standard to replace meniscus defects and are the only available implants to treat lesions, which indicated total meniscectomies. Half of all arthroscopic knee surgeries in the US every year are therefore still the removal of unstable and damaged sections of meniscus tears (Kim et al., 2006) to treat acute joint pain and loss of joint function despite the known retained connection of the tear to development of osteoarthritis in long-term (Papalia et al., 2013). Meniscus allograft transplants are available in cryo-preserved or fresh conditions and suffer from donor shortage due to difficulties in shape and size matching which is important for healing and preservation of joint mechanics (Dienst, Greis, Ellis, Bachus, & Burks, 2007; S. R. Lee, Kim, & Nam, 2012). Allografts are either

fixated to the tibial plateau via bone channels or bone plugs, a bone bridge, a hemi-plateau for better load transmission or via suture fixation through tunnels (Fig. 2.2 e)(Rodeo, 2001). Long term studies of more than 10 years show improved joint function and patient satisfaction but have not been proven to prevent joint narrowing (S. Lee et al., 2019; Vundelinckx, Vanlauwe, & Bellemans, 2014). Patient age is also negatively correlated with good treatment outcome for allograft transplants (R Verdonk et al., 2013), indicating that patients with stable, well aligned knees but acute, traumatic lesions might need different treatment options than older patients with degenerative lesions. It is therefore important to choose a fitting treatment option to restore the joint anatomy and function as well as to prevent the risk of developing osteoarthritis.

To summarize, the developed implants of Actifit™ and CMI® showed promising healing results but do not show full meniscus regeneration or halt the progression of osteoarthritis and are difficult for surgeons to handle, while allograft implants suffer from donor shortage (Kwon et al., 2019). Therefore, despite good progress in meniscus repair and replacement procedures over the last decades there is still a demand for improved cell-based meniscus implants for partial and total meniscectomies via tissue engineering.

2.6. Tissue engineering approaches

The currently available surgical meniscus replacement approaches show promising results, but it is unclear if they provide long-term solutions for meniscus regeneration. This has motivated increased interest in meniscus tissue engineering strategies to create more advanced cell-based implants for joint regeneration (Hutchinson et al., 2014; Matteo et al., 2016; Moran, Orth, et al., 2015; Moran et al., 2014, 2012; Moran, Busilacchi, et al., 2015a; Romanazzo et al., 2017; Vedicherla et al., 2018). Central to these efforts include the development of advanced biomaterials

like polylactides, polyglycosides, silk and others in order to create scaffolds, which can mimic the complex biomechanical functions of the meniscus tissue. A common strategy in tissue engineering for orthopaedics is therefore to create implants which provide the necessary mechanical integrity and function to the joint after their implantation, until the repopulated cells regenerate tissue which can fulfil these requirements (Makris et al., 2011b).

2.6.1 Cell sources

The non-vascularized white zone of the meniscus has a low regenerative potential. Trephination or rasping for example allows access of autologous progenitor cells from blood vessels and the bone marrow to travel to damaged sites and repair lesions. Growth factors have been used in the past to further entice this migration, or exogenous cells can also be delivered to damaged sites directly through the implant. The specific cell choices for such strategies have will be discussed here briefly but have recently been reviewed in detail elsewhere (Hutchinson et al., 2014)(Niu et al., 2016).

2.6.1.1. Autologous meniscus cells and chondrocytes

Using autologous meniscus cells and chondrocytes has a number of advantages, including donor acceptance and the fact that the cells will produce meniscus or cartilage specific ECM molecules without any further priming or modification. However, the biggest disadvantage is that this strategy requires two surgical procedures: first a biopsy to extract the cells followed by a second procedure to re-implant the autologous cells after their expansion *in vitro* (Kon et al., 2008)(Martinek et al., 2006).

Furthermore, the number of viable cells which can be isolated from patients is often highly limited since patients who need a meniscus treatment often already suffer from degenerating tissue, which means a biopsy may not contain cells ideal for expansion and matrix production *in vitro*. In addition, the currently available protocols

for meniscus cells and chondrocytes mostly produce cells which do not secrete a sufficient amount of sGAGs and dedifferentiate when growing on tissue culture plastic(Tanaka et al., 1999)(Collier & Ghosh, 1995)(Gunja & Athanasiou, 2007)(Darling & Athanasiou, 2005). This is a particular challenge for tissue engineering large scale constructs like menisci, which require a high number of cells and abundant matrix deposition. This has motivated the use of alternative cell sources for meniscus tissue engineering.

2.6.1.2. Allogenic meniscus cells and chondrocytes

Allogenic meniscus cells or chondrocytes have been explored as cell sources for meniscus tissue engineering due to their higher availability and better quality compared to autologous cells of patients with potentially degenerative cartilage or menisci. Specifically, articular, auricular and costal chondrocytes have been used in different studies and show good potential (Weinand, Peretti, Adams, et al., 2006; Weinand, Peretti, Jr, et al., 2006). Xenogenic chondrocytes and meniscus cells have also been explored as well and show promising results. Moreover, they have shown little to no immune response in rabbits over a course of 24 weeks (Ramallal et al., 2004).

2.6.1.3. Bone marrow Mesenchymal Stem Cells

Perhaps the most prominent cell type in musculoskeletal tissue engineering are multipotent, marrow stromal / mesenchymal stem cells which can be isolated from the adult bone marrow (*BMSCs*). They were first described as mesenchymal stem cells and shown to differentiate into cells capable of producing tissues resembling cartilage, bone, fat and other connective tissue *in vitro* (Caplan & Dennis, 2006). However, their roles *in vivo* might be different, since they can secrete immune-regulatory molecules which contribute to healing processes (Caplan, 2017). Specifically, they are able to present paracrine mediators and recruit other cells to repair tissue and regulate the immune response. This function has prompted some to propose re-classifying these

cells as Medicinal Signalling Cells (Caplan & Dennis, 2006). Furthermore, their use in tissue engineering strategies has now also shifted to enticing their healing potential in damaged tissue rather than simply use the cells to replace the tissue. To summarize, MSCs possess multilineage plasticity, immunomodulatory, anti-inflammatory and proliferative abilities which make them highly attractive cell sources for musculoskeletal tissue engineering.

Their ability to migrate to meniscus lesions and secrete trophic factors, their potential to differentiate into cartilaginous cells and drive matrix fibrocartilagenesis as well as their chondroprotective properties have therefore been used in several studies for meniscus tissue engineering.

However, as described above, repair methods using autologous MSCs are still limited by the age of the patient as well as the size of the lesion, which is why isolation, expansion and implantation of MSCs is sought to improve those shortcomings. In contrast to using chondrocytes or meniscus cells, however, MSCs require specific culture conditions in order to drive them towards a chondrogenic phenotype. Various different strategies have been explored to achieve this like different chondrogenic media conditions with signalling molecules like growth factors, mechanical stimulation, matrices for 3D culture, hypoxic oxygen culture conditions or centrifugation into micro pellets. These different treatment methods all have their advantages and disadvantages and have to be adapted to fit each implant. For example, after isolation and expansion MSCs have been seeded into hyaluronan-collagen scaffolds and implanted directly into a rabbit and canine defect models without where they presented good healing and tissue integration (Abdel-hamid, Hussein, Ahmad, & Elgezawi, 2005; Izuta et al., 2005). However, increased matrix production but less integration into the host tissue and cell migration has been detected when the cells were pre-cultured in chondrogenic media with TGF-β1 prior to implantation (Pabbruwe et al., 2010). Furthermore, increased ECM deposition was detected under dynamic culture

conditions and mechanical stimulation as well as when cultured on scaffolds of decellularized meniscus tissue and electrospun PCL (B. M. Baker, Shah, Huang, & Mauck, 2011)(Nerurkar, Sen, Baker, Elliott, & Mauck, 2011).

In contrast, instead of seeding MSCs into constructs prior to implantation growth factors and ECM molecules have also been used to recruit local endogenous stem/progenitor cells to migrate to the site of interest through *in situ* activation in an attempt to promote a repair process. In this approach the cells are targeted to migrate into the lesion or construct after implantation, proliferate and differentiate into the desired cell type using acellular scaffolds or delivery of growth factors such as vascular endothelial growth factor (Forriol, 2009; Nerurkar, Sen, et al., 2011). Furthermore, a number of studies have also sought to create vascular access channels via trephination or rasping the red zone of the remaining peripheral meniscus to allow blood flow and stem/progenitor cell migration into the meniscus lesion as described above (Uchio, Ochi, Adachi, Kawasaki, & Iwasa, 2003; Zhongnan Zhang, Arnold, Williams, & McCann, 1995).

2.6.1.4. Synovium derived MSCs

Furthermore, a cell source similar to bone marrow derived MSCs used in meniscus tissue engineering are synovium derived MSCs. They have similar characteristics as bone marrow MSCs like multilineage plasticity, regenerative potential and their ability to generate fibrocartilage (Hatsushika et al., 2014). Similarly to bone marrow MSCs growth factors like TGF-β3 and connective tissue growth factor (CTGF) have been used to attract them to migrate from the synovium to damaged areas to promote healing (Chang H Lee et al., 2014) but have shown the additional advantages of simplified harvesting for isolation (Shirasawa, Sekiya, Sakaguchi, Yagishita, & Ichinose, 2006). After isolation and expansion synovium derived MSCs have been used in clinical trials to treat meniscus defects and osteoarthritis via direct injection (Jr et al., 2014). However, current issues of injection-based stem cell treatments are still

the limited number of cells which can be delivered via embedding in construct and the lack of localization of the cells at the target site. A possible solution for the latter issue, however is the co-localization of growth factors to implanted biomaterials which will be discussed in the following sections.

2.6.2 Biomaterials

Both natural and synthetic biomaterials have been used in meniscus tissue engineering in the past in order to create implants which are biocompatible, biodegradable and ideally capable of supporting meniscal tissue regeneration. A wide range of polymeric scaffolds have been developed, the functions of which are to provide some initial biomechanical stability to the joint environment as well as providing an environment which is conducive to maturation of an engineered tissue (Athanasiou & Eswaramoorthy, 2013). A number of scaffold-free tissue engineering strategies have also been developed in order to avoid potential toxic degradation processes or unfavourable immune responses associated with some polymers (Hoben et al., 2007).

Requirements to biomaterials for meniscus tissue engineering applications are to provide a support structure for cells which shields them from compressive and shear forces in the joint environment of the knee and to maintain its shape until cells produce their own matrix. In addition, they need to be degradable in order to facilitate remodelling and host tissue integration. Furthermore, a number of biomaterials also provide differentiating cues and guides to attract host cells to migrate to an injury site.

2.6.2.1. Synthetic polymers

A number of synthetic polymers have been used in the past for meniscus tissue engineering like PU, PCL, polylactic acid (PLA), polyglycolic acid (PGA) and polylactic co-glycolic acid for example. Their advantages are their high bulk availability as well as their robust mechanics which allows many of them to them to withstand the

environment of the joint. Moreover, 3D printing enables the creation of anatomically shaped constructs which can be fitted to the exact target site of each individual patient as well as a variation of internal pore sizes, fibre sizes and above described mechanical behaviour. In contrast, some of their biggest disadvantages are, however their lack of bioactivity, tissue integration and bi-phasic mechanical properties. Specifically, synthetic polymers consist of a solid phase only, whereas menisci and other cartilaginous tissues are viscoelastic and bi-phasic, which means they also possess a liquid phase (Makris et al., 2011a).

2.6.2.2. Hydrogels

Hydrogels, on the other hand, can be characterized by their viscoelastic behaviour due to their high water content which means they are able to absorb and store liquids similar to meniscus ECM. Hydrogels consist of polymer chains which form a network that is either crosslinked ionically or covalently, temporarily or permanently. Hydrogels used commonly in meniscus tissue engineering are natural as well as artificial gels and examples include: fibrin, heparin, alginate, gelatin methacrylamide or hyaluronic acid methacrylamide. Furthermore, another advantage of hydrogels in tissue engineering applications is that they provide a 3D environment for cells to interact with and grow in which mimics their native surroundings more closely than 2D tissue culture plastic would. Moreover, if the hydrogels contain cell binding sites then encapsulated cells are able to interact with their surrounding matrix and migrate or assume an elongated fibroblast-like morphology. Contrary to that, alginate for example does allow cell binding so cells are forced to assume a rounded morphology than their ECM synthesis and proliferation could be reduced (Aufderheide & Athanasiou, 2006; Johannah Sanchez-A & Athanasiou, 2009; Thie, Schlumberger, Rauterberg, & Robenek, 1989; P. Verdonk et al., 2005). Since the gel matrix can influence the cell phenotype, a number of hydrogels used in AC tissue engineering strategies are also used in meniscus tissue engineering since they are believed to be generally supportive

of a cartilaginous phenotype. However, only the inner zone of the meniscus is populated by chondrocytes similar to that in AC, while the outer peripheral zone is populated by fibroblast-like cells. Many tissue engineering constructs therefore employ different types of hydrogels in order to stimulate encapsulated cells to assume morphologies similar to that observed in the inner and outer zones of the meniscus (G Bahcecioglu et al., 2019; Gokhan Bahcecioglu, Hasirci, Bilgen, & Hasirci, 2018).

Furthermore, other smart biomaterials have been developed for meniscus tissue engineering applications, such as injectable gels based on chitosan-hyluronan-poly N-isopropyl acrylamide for minimally invasive surgery, since arthroscopic surgery is a commonly used technique in orthopaedic procedures. The hydrogel reversibly solidifies with temperature changes, encapsulated meniscus cells maintain their viability and during culture ECM production increases. Disadvantages of this as well as many other hydrogels are their relatively poor mechanical properties, even after solidifying (J. Chen & Cheng, 2006). Modest improvements in mechanical properties can be achieved through increased hydrogel crosslinking and/or polymer concentration, however this can be associated with decreased cell viability and ECM production (Bryant, Chowdhury, Lee, Bader, & Anseth, 2004).

To summarize, hydrogels have the advantage of simulating a 3D matrix similar to the one encountered by cells in their native environment. Moreover, many hydrogels also promote ECM synthesis and so-called smart hydrogels gels are even tuneable to adapt to the needs of the heterogeneous cell population in the meniscus tissue. The main limitations associated with hydrogels for meniscus tissue engineering applications are their relatively poor mechanical properties, potentially making then unsuitable for implantation into the challenging mechanical environment of the knee joint.

2.6.2.3. ECM based biomaterials

In order to increase the bioactivity of biomaterials for tissue engineering applications, several studies describe the use of ECM derived biomaterials, either alone or in combination with a hydrogels, for meniscus tissue engineering.

Development of such ECM derived biomaterials requires certain physical and/or chemical treatment steps in order to minimise the risk of an immune reaction and to facilitate the creation of a gel-like material, which can be shaped to the user's requirements. Specifically, in order to remove any immunogenic potential from the ECM material, DNA needs to be removed from the tissue below the widely accepted threshold of 50ng/mg (Crapo, Gilbert, & Badylak, 2011a). However, a challenge to this procedure is to retain key compositional and structural cues associated with the native tissue in order to ensure the biomaterial retains its capacity to direct cell differentiation. For example decellularization treatments of porcine menisci have been described using pepsin digestion, urea, acids, or freeze-thaw cycles leaves which leaves sGAGs and collagen molecules intact but removes PGs (Y.-C. Chen et al., 2015)(Stapleton, Ingram, Fisher, & Ingham, 2011)(Wu et al., 2015). Moreover, the solubilization treatment furthermore enabled injectability of the biomaterial which is a necessity for the development of bioinks for tissue engineering through 3D bioprinting (Pati et al., 2014). Furthermore, human bone marrow MSCs cultured within the matrix material showed enhanced proliferation and Col II and sGAG secretion (Y.-C. Chen et al., 2015), (Stapleton et al., 2011)(Wu et al., 2015).

Moreover, since the ECM compositions of the inner and outer meniscus zones differ in collagen, sGAG and PG molecules as described above, several studies have created ECM based materials which have been isolated from the specific zones separately (Romanazzo et al., 2017; Rothrauff et al., 2017; Shimomura, Rothrauff, & Tuan, 2017). In these studies the observed collagen expression of encapsulated cells was higher in presence of the decellularized ECM components than without them.

Furthermore, an additional stimulation through growth factors TGF-β and CTGF in the media further increased matrix production significantly.

However, phenotypic differences between cells cultured in inner and outer ECM based materials are often still small and require additional culture in presence of TGF-β. For example, human MSCs cultured in constructs of decellularized inner and outer ECM material via on urea based treatment mixed with GelMA showed differences in gene expression in earlier time points between groups of inner and outer ECM only. However, equalization of differences between gene transcription levels and ECM secretion was detected after 21 to 42 days in culture (Shimomura et al., 2017)(Rothrauff et al., 2017). These findings go in parallel with a recently published review which concludes that many cells only take cues from their surrounding ECM based biomaterials only in early culture phases, whereas if not exposed to stronger signalling molecules like growth factors they will follow their previous phenotype and remodel their surrounding matrix accordingly in later stages (Blache, Stevens, & Gentleman, 2020).

2.6.2.4. Growth factors

As described above, many biomaterials and ECM based components have been used in tissue engineering strategies in the past in order to drive cell differentiation of MSCs towards chondrogenic or fibroblast-like phenotypes. However, only a small number of them achieved this over prolonged culture periods without the additional use of growth factors to stimulate encapsulated cells (Rothrauff et al., 2017; Shimomura et al., 2017). CTGF and hepatocyte growth factor have shown to stimulate matrix production and vascularization associated with the outer zone of the meniscus, whereas platelet derived growth factor-BB and insulin-like growth factor drive secretion of matrix molecules similar to the inner zone. (Chang H Lee, Moioli, & Mao, 2006; K. H. Park & Na, 2008) Furthermore, CTGF and platelet-derived growth factor have recently

been used to create a spatio-temporal release profile in a 3D printed construct (Chang H Lee et al., 2014; Nakagawa et al., 2019a)

The most commonly used growth factor to induce chondrogenesis, TGF-β, is also heavily featured in AC tissue engineering and has been shown to be essential for matrix production (Tuli et al., 2003). However, it has been shown that it also prevents tissue integration. This indicates, that a combination of different growth factors as well as other elements like oxygen concentration, mechanical stimulation and 3D environment are necessary in order to drive the differentiation of cells towards the phenotypes found in native meniscus tissue.

To that end, various biofabrication techniques have been explored in order to create more complex tissue engineered implants, which could enable a more complex stimulation of encapsulated cells.

2.6.3 Biofabrication

2.6.3.1. Casting

Biofabrication enables the creation of complex outer shapes similar to anatomical size and form of native meniscus tissue which is especially important for a tissue like the meniscus with its function of load distribution between the tibial and femoral heads.

Injection moulded alginate constructs with the anatomical shape of menisci have been described in the past (G.-Q. Chen & Wu, 2005; Heijkants et al., 2004; Klompmaker et al., 1991; Maher et al., 2010; Ramrattan et al., 2005). However, some of them suffered from heterogeneous tissue generation due to the limited nutrient and gas exchange through diffusion to encapsulated cells within the centre of a large scale construct like a human sized meniscus (Ballyns et al., 2008). This could be improved

through the creation of pores to reduce the diffusion distance towards cells or by cultivation in an agitation bioreactor (Grayson et al., 2008; Rouwkema et al., 2013).

Furthermore, many constructs which are based on hydrogels alone often suffer from low mechanical properties. However, a small number of biofabrication strategies have achieved tensile and compressive moduli similar to the ones of native meniscus tissue. Their ability to create a scaled up construct as well as to survive in a joint environment in long term studies still remains to be proven (Gunja, Huey, James, & Athanasiou, 2009; Makris, Macbarb, Paschos, Hu, & Athanasiou, 2014).

In contrast, constructs based on PCL and hyaluronan polymers provide more mechanical support and have been casted with structural support through polyethylene therephtalate or PLA fibres in order to withstand the hostile mechanical forces in the native joint. After 4 months, promising tissue ingrowth and tissue integrity were reported using *in vivo* sheep models when seeding autologous chondrocytes on top of the implant. However, after 12 months due to the rigid mechanical properties of the casted polymers the developed implants caused increased damage to the AC while still suffering from implant dislocation and deformation (Chiari et al., 2006; Kon et al., 2008, 2012).

Moreover, recently zonal variation and anisotropy has been induced in casted constructs through a variation of collagen density and alignment of pores (Higashioka, Chen, Hu, & Athanasiou, 2014). In addition, 3D printing enables the creation of meniscus constructs of further complexity.

2.6.3.2. 3D printing of meniscal implants

3D printing has become an important technology in tissue engineering over the previous decades due to its ability to create more complex constructs. It enables the control over the inner structures and allows the development of constructs that mimic the architecture of collagen fibres found in the native meniscus tissue. For example, by

modifying the orientation of electrospun PCL fibres dramatic increases in the tensile properties of scaffolds can be achieved (Teberg et al., 1982). Furthermore, it was also shown that aligned PCL fibres influenced cell and ECM alignment in culture which additionally strengthened the tensile properties of the resulting constructs (B. M. Baker & Mauck, 2007). Another biofabrication technique which showed promising results in cartilage tissue engineering based on aligned PCL and PGA fibres is based on weaving and could provide a means of further mimicking the anisotropic fibre orientation of native ECM fibres (F. Moutos & Guilak, 2010; F. T. Moutos, Freed, & Guilak, 2007). Circumferentially aligned PCL fibres have also been explored in 3D printing via FDM, which enabled the manipulation of both the compressive and tensile moduli of the constructs to better mimic the native tissue values (Szojka et al., 2017; Zheng-zheng Zhang et al., 2019).

In addition to mimicking the ECM fibre orientation by controlling the inner architecture of the scaffolds, 3D printing also enables the control over tissue heterogeneity. As described above, pores for supporting nutrient diffusion can be introduced, but 3D printing strategies can also be used to re-create the inner and outer zones of the native meniscus tissue, for example by spatially localizing cells, hydrogel matrices or growth factors. Zone-specific tissue engineered meniscus constructs have previously been fabricated using a 3D printed PCL scaffold loaded with CTGF and TGF-β3 encapsulated in microspheres within the outer and inner zones of the construct, with the goal of creating a spatio-temporal growth factor release profile. The developed construct showed very promising tissue development *in vitro* and *in vivo* in sheep but still require improved fixation of the tibial plateau to avoid meniscus extrusion and damage of the underlying cartilage (Chang H Lee et al., 2014; Nakagawa et al., 2019b). A more recent study filled varying compositions of GelMA and agarose into the pores of a meniscus shaped PCL scaffold in order to create an inner and outer zone where the authors reported varying cell morphologies and ECM

composition to some degree. (G Bahcecioglu et al., 2019) Similar zonally engineered constructs were also achieved through a combination of dynamic mechanical and biochemical stimulation through CTGF and TGF-β3 in vitro and led to promising tissue regeneration in rabbit studies *in vivo* (Z.-Z. Zhang et al., 2017; Zheng-zheng Zhang et al., 2019).

To summarize, many recent studies take on number of different complex architectural challenges using 3D bioprinting in order to better mimic the native meniscus tissue. Although promising in vitro and in vivo results have been promising, so far such approaches have failed to translate their success from *in vitro* and small animal *in vivo* studies to large animal *in vivo* models. More advanced biofabrication techniques and increasingly biomimetic constructs could overcome these challenges and create tissue engineered implants, which are capable of promoting meniscus regeneration in challenging environments.

Chapter 3

3D PRINTING OF POLYMER NETWORKS WITH MENISCUS-LIKE MECHANICAL PROPERTIES

3.1. Introduction

Menisci play an essential role in the knee joint and every year 1.5 million people in the US and Europe require surgery due to trauma or degeneration of the tissue (OECD & Chapter7EU, 2016; Parker, Hurwitz, Spang, Creighton, & Kamath, 2016). Meniscus tears are common in all age groups and dramatically increase the risk of developing OA in later life (Hall et al., 2014). Partial meniscectomies are a very common treatment option and in recent years a number of scaffolds have been used clinically to replace the damaged section of the meniscus (Bulgheroni et al., 2010; Monllau et al., 2011; Spencer et al., 2012). Such implants do not restore normal tissue and joint function after surgery, which is due to, at least in part, to a number of limitations associated with existing meniscus scaffolds. In particular, these biomaterials do not mimic the internal architecture and associated mechanical properties of the native meniscus tissue. Therefore tissue engineering strategies are required to develop meniscus scaffolds that are not only supportive of a meniscal cell phenotype, but which also mimic the complex biomechanical properties of the native meniscus tissue. Such biomimetic scaffolds could transform treatment options for patients with damaged menisci, resulting in improved recovery after surgery.

The menisci function to increase the contact area in the knee joint, thereby reducing the stresses developed within joint tissues during normal daily activities. Vertical loads acting on the meniscus are translated into hoop stresses within the meniscus, which are accommodated by the complex structure and composition of its ECM (Makris et al., 2011b). Meniscal tissue displays spatially inhomogeneous and

anisotropic mechanical properties, which can be related to the composition and organization of its ECM (Mow & Huiskes, 2005). The tissue has a higher amount of collagen fibres orientated in a circumferential orientation throughout its semilunar shape than in a radial direction, hence its tensile stiffness is approximately an order of magnitude higher in the circumferential direction (Makris et al., 2011a). Furthermore, meniscus tissue also displays significant tension-compression non-linearity, being significantly stiffer in tension than in compression (Mow & Huiskes, 2005).

Existing scaffolds used clinically for meniscal repair possess relatively simple and homogenous pore structures, and do not mimic the complex internal architecture and biomechanics of the native meniscus. Emerging biofabrication techniques such as 3D printing allow for development of anatomically accurate scaffolds with complex internal architectures mimicking key features of biological tissue (G Bahcecioglu et al., 2019; Chang H Lee et al., 2014; Nakagawa et al., 2019b). A further benefit of 3D printing is that it enables diverse material sets to be combined to produce composites with desirable mechanical and biological properties; for example cell compatible hydrogels that are typically mechanically weak can be reinforced with stiffer fibrous networks to produce composites suitable for implantation into load bearing environments (Malda et al., 2013). Tough and elastic IPN hydrogels have also been combined with such fibre networks in order to create composites that are more biomimetic of soft biological tissues (D. S. Jones, Mclaughlin, Mccoy, & Gorman, 2005; Liao, Moutos, Estes, Zhao, & Guilak, 2013; Schipani, 2019; Schipani, Scheurer, E, & Kelly, 2020). For example, IPNs have been created by combining GelMA and alginate to create biomaterials uniquely suited to tissue engineering applications (Jeon et al., 2017; Krishnamoorthy & Zhang, 2019a). In isolation, GelMA and alginate are either too brittle or weak to be used as tissue engineering scaffolds for load bearing applications. However, when combined as an IPN the resulting biomaterial displays increased fracture toughness, elasticity, stiffness and strength, enabling its use for cartilage and

bone tissue engineering applications (Chimene, Lennox, Kaunas, & Gaharwar, 2016; Cancan Xu, Dai, & Hong, 2019).

The aim of this chapter was to develop biomimetic scaffolds for meniscus tissue engineering consisting of an IPN hydrogel mechanically reinforced with PCL networks displaying tension-compression nonlinearity. To this end various PCL print patterns were first investigated in order to produce scaffolds with mechanical properties (specifically tension-compression non-linearity) mimetic of the native human meniscus. These PCL scaffolds were then combined with IPN hydrogel bioinks consisting of GelMA and alginate in order to bioprint composites that were (i) supportive of high levels of cell viability and (ii) biomimetic of the dynamic mechanical properties of the meniscus.

3.2. Materials and Methods

3.2.1 Fused deposition modelling

Polycaprolactone (CAPA 6500D, Perstorp, Sweden) was printed using a RegenHU Discovery 3D printer (Switzerland). Fibres with diameters of 120 µm were printed using a 30G needle, fibres of 240 µm were printed with a 25G needle. Scaffolds were designed with 0.25, 1 and 2 mm fibre spacing, respectively, in a 90° orthogonal orientation in double layers in either aligned or offset patterns.

3.2.2 Calculation of scaffold porosity

The porosity of printed samples was calculated using the gravimetric method. Briefly, the mass $m_{scaffold}$ and volume $V_{scaffold}$ of samples was recorded and put into Eq. 3.1 and **Error! Reference source not found.**, where $\rho_{scaffold}$ denotes the apparent density of the scaffold and ρ_{PCL} describes the density of PCL of 1.145 g/ml.

$$\rho_{PCL}\ (g/ml) = \frac{m_{scaffold}}{V_{scaffold}}$$

Eq. 3.1

$$PCL\ content\ (\%) = \frac{\rho_{scaffold}}{\rho_{PCL}}$$

Eq. 3.2

3.2.3 Meniscus sample preparation

Medial menisci from 3 months old female pigs were harvested and biopsies of 6 mm diameter of the outer zones were taken. Biopsies were then cut to cylinders with parallel bases for more even contact with the compression platens and more robust testing.

3.2.4 Compressive testing

Samples for compressive testing were printed as cubes of 6 mm edge length and height. Before testing, all samples (n = 4) were soaked in phosphate buffered saline solution (PBS) (Sigma) over night. Uniaxial, unconfined compressive testing was then performed in wet conditions at room temperature using a bath of PBS and a 2.5 kN load cell in a Zwick/Roell Twin Column (Germany) with a preload of 0.005 N, preload speed of 2 mm/min, waiting time of 2 min and then compressed with a speed of 0.0167 mm/s. The samples were subject to a strain cycle load of 3 cycles with nominal amplitude of 10, 20 and 30% strain in sequence. The compressive modulus was calculated using the linear section, the ultimate compressive strength was recorded as the highest recorded stress during the testing regime. The permanent deformation of the scaffold was defined as uniaxial plastic strain of the sample and calculated using Eq. 3.3 where Δt (s) describes the interval of time between two cycles when force stops being recorded and is recorded again and h_0 (mm) is the sample height prior to the test (Fig. 3.1 h)

$$PD\ (\%) = \frac{Test\ speed * \Delta t}{h_0} * 100$$

Eq. 3.3

3.2.5 Tensile testing

Dog-bone structures were printed for tensile testing with a gauge length of 15 mm and a thickness and width of 1.5 mm and 4.2 respectively. Both ends of the samples were glued to frames of sand paper using 2 components epoxy glue. A 2.5 kN load cell in a Zwick/Roell Twin Column used to measure the tensile moduli with a preload of 0.05 N a speed of 1 mm/min, paused for 10 seconds and then applying 50% strain with a speed of 1 mm/min. To account for sample slippage, the dog-bones were marked before testing and analysed via video recording during the test. The ramp modulus was calculated using the linear section between 2 and 5% strain.

3.2.6 Fabrication of single component and interpenetrating network (IPN) hydrogels

As described elsewhere (Loessner et al., 2016) gelatin methacrylamide (GelMA) was created by adding methacrylamide groups to gelatin. Briefly, porcine type A gelatin (Sigma- Aldrich, average molecular weight 40-50 kDa) was dissolved in distilled water in 20% ratio (w/V) at 40°C. 10% methacrylic anhydride (Sigma) was then added dropwise and stirred under protection from light at 50°C for 2 hours. The solution was then diluted with DI water by 1:5 and its pH adjusted to 7.4 before dialysis against distilled water for 7 days at 37°C in bags of 12-14 kDa pore size. The dialysate was then sterile filtered and freeze-dried.

To create the IPN hydrogels, Alginate (LVG, Pronova, Norway) and GelMA were dissolved in Dulbeco's Modified Eagle's Media (DMEM) (Gibco) and mixed with irgacure 2959 (Sigma) to create a gel of 3.5% alginate, 5% GelMA and 0.05% irgacure.

3.2.7 Casting and crosslinking gels in PCL scaffolds

Before filling the IPN hydrogel into printed PCL constructs, the printed scaffolds were soaked in 45 mM $CaCl_2$ (Sigma) under rotation over night. The PCL cubes were then put into casted moulds of 3% agarose (Sigma) and 45 mM $CaCl_2$. Their pores

were then filled with the IPN hydrogel by extruding it through a 23G needle. The constructs inside the moulds were then exposed to UV light (6W) for 7.5 minutes from the top and the bottom each. Furthermore, the constructs were then left for 5 additional minutes of crosslinking inside the $CaCl_2$ containing moulds.

3.2.8 Statistical analysis

Data was expressed as mean and standard error of the mean. Significance was calculated using the student-t test with Welch's correction or ANOVA and Tukey's post-hoc test was calculated with * > 0.05, ** > 0.001, *** > 0.0005, **** > 0.0001, n = 4.

3.3. Results

3.3.1 The influence of fibre diemater on the tensile and compressive properties of 3D printed PCL networks

First, the influence of fibre diameter (120 µm or 240 µm) on the compressive and tensile mechanical properties of 3D printed PCL scaffold networks was explored (Fig. 3.1 a,b). With a constant 1 mm fibre spacing, decreasing the fibre diameter from 240 µm to 120 µm slightly decreased the measured PCL content of the scaffolds from 18.7% to 17.4% and the compressive modulus from 7.1 MPa to 4.3 MPa (Fig. 3.1 c-d). Somewhat unexpectedly, the ultimate compressive strength increased from 0.33 MPa 0.86 as the fibre diameter reduced (Fig. 3.1 e). The tensile modulus decreased more significantly with reductions in fibre diameter, from 50.6 MPa 17.7 MPa, as did the ultimate tensile strength, reducing from 4.34 to 1.38 MPa (Fig. 3.1 f-g). The permanent scaffold deformation recorded after the application of 10% compressive strain was lower than the value recorded for native porcine meniscus tissue (~4%), and decreased significantly with decreasing fibre diameters, from 2.49% for the 240 µm fibre diameters, to 1.49% for the 120 µm diameter fibre diameters. After the application

of 20% strain, all permanent deformation levels were higher than that recorded after the application of 10% strain. Furthermore, native tissue and scaffold with a 240 µm fibre diameter displayed similar values of 5.9%, decreasing to 3.55% for scaffolds with a 120 µm fibre diameter (Fig. 3.1 i).

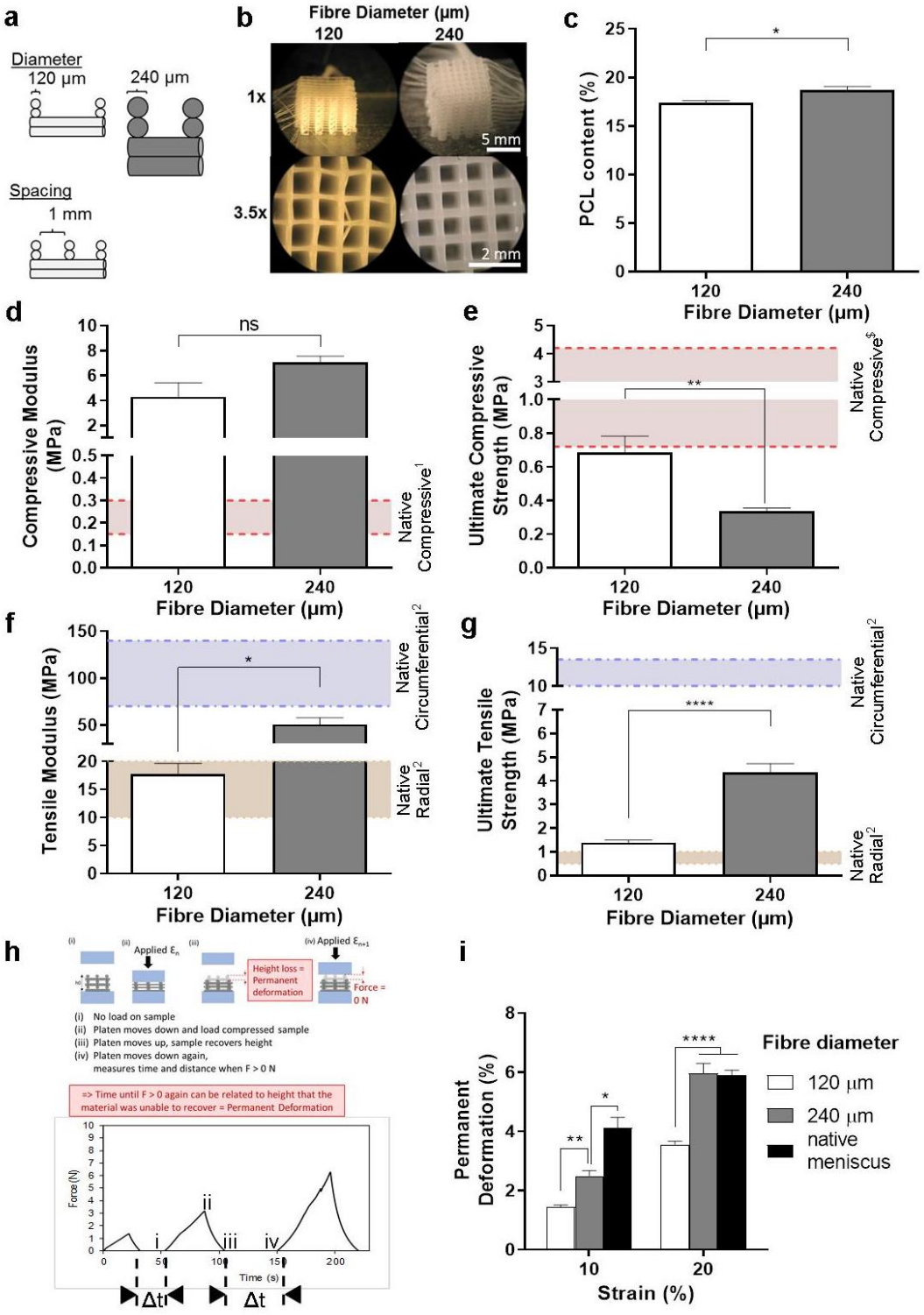

Fig. 3.1 Effect of PCL fibre diameter on mechanical properties: Printed PCL fibres with 1 mm spacing, aligned pattern and 120 µm or 240 µm diameter and (a-b), their PCL contents (c), compressive moduli (d), ultimate compressive strength (e), tensile moduli (f), ultimate tensile strength (g), and permanent deformation (h-i). $p \leq 0.05$ (*), $p \leq 0.001$ (**), $p \leq 0.0001$ (****), n = 4

(1) Sweigart et al, (2) Tissakht et al, ($) stress at 30% strain

3.3.2 The influence of fibre spacing on the compressive and tensile properties of 3D printed PCL networks

As expected, decreasing the fibre spacing increased the mechanical properties of the resulting scaffold network, while also increasing the overall PCL content. The measured PCL content increased from 12.35% for scaffolds with a 1 mm spacing, to 48.35% in scaffolds with 0.25 mm spacing (Fig. 3.2 a-c). The compressive modulus also increased with reductions in PCL fibre spacing, from 1.3 MPa to 16.2 MPa (Fig. 3.2 d), while the ultimate compressive strength increased from 0.18 MPa to 4.06 MPa (Fig. 3.2 e). Similarly, the tensile modulus increased from 14.8 MPa to 53.8 MPa (Fig. 3.2 f), as did the ultimate tensile strength, increasing from 1.07 MPa to 4.58 MPa (Fig. 3.2 g). Finally, the permanent deformation after the application of 10% compressive strain was lower than that observed for native porcine meniscus tissue in all scaffolds, decreasing with decreasing fibre spacing from 3.37% for a spacing of 2 mm to 0.22% at a 0.25 mm spacing. As expected, the levels of scaffold permanent deformation were higher after the application of 20% strain, with 0.25 mm spacing scaffolds still undergoing the lowest levels of permeant deformation (0.52%) (Fig. 3.2 h).

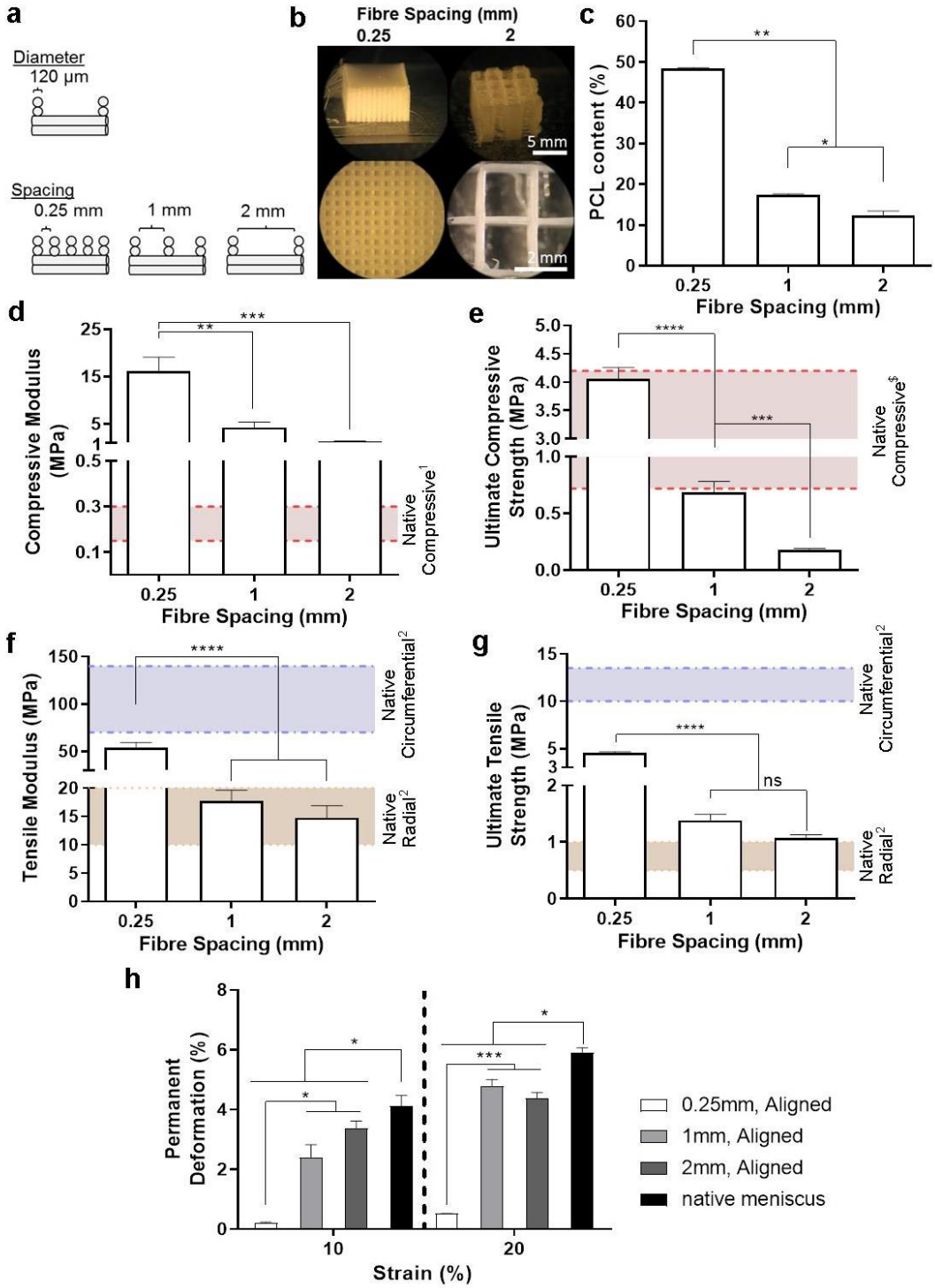

Fig. 3.2 Effect of PCL fibre spacing on mechanical properties: Printed PCL fibres with 120 µm fibre diameter, aligned pattern and 0.25, 1 or 2 mm spacing (a-b), their PCL contents (c), compressive moduli (d), ultimate compressive strength (e), tensile moduli (f), ultimate tensile strength (g), and permanent deformation (h). $p \leq 0.05$ (*), $p \leq 0.001$ (**), $p \leq 0.0005$ (***) and $p \leq 0.0001$ (****), n = 4

(1) Sweigart et al, (2) Tissakht et al, ($) stress at 30% strain

3.3.3 The influence of fibre pattern on the tensile and compressive properties of 3D printed PCL scaffolds

Next the influence of fibre print pattern was explored by 3D printing scaffolds where consecutive parallel layers of fibres were either directly 'aligned' with the underlying layer, or were 'offset' to the underlying layers (Fig. 3.3 a). To test the effect of such print patterns on the tensile and compressive moduli of the resulting networks, the fibre diameter was maintained constant (120 µm), whilst the fibre spacing was set to either 0.25 mm, 1 mm or 2 mm. When applying an offset pattern, the compressive modulus of the scaffolds reduced compared to the corresponding aligned scaffolds for all fibre spacings (Fig. 3.3 b), whilst the ultimate compressive strengths did not significantly change (Fig. 3.3 c). It should be noted that the stress-strain curve for 3D printed scaffolds with an offset configuration was typically J-shaped, demonstrating behaviour more representative of soft biological tissues such as the meniscus (Fig. 3.3 b-c). Furthermore, an offset print pattern was found to reduce the tensile modulus, from 14.8 MPa to 8.23 MPa for scaffolds with a large (2mm) fibre spacing, and also resulted in a reduction in the ultimate tensile strength (Fig. 3.3 d-e). The PCL content was not affected by the fibre pattern (Fig. 3.3 f). It was noted that the reduction in compressive moduli with changes in the printed fibre pattern (from 'aligned' to 'offset') was relatively higher than that observed for the tensile moduli. The result of this was that the ratio of the tensile to compressive modulus was highest for offset designs with a 2mm fibre spacing. In fact, this design was the only scaffold with a ratio > 35:1, which was comparable to that observed in native meniscal tissue in the radial direction (Fig. 3.3 g). No changes in permanent deformation were recorded in scaffolds with offset patterns compared to the corresponding scaffold with aligned patterns after the application of either 10% or 20% compressive strain (Fig. 3.3 h). In conclusion, it is possible to reduce the compressive modulus of 3D printed scaffolds more than its

tensile modulus without changes in other scaffold properties (e.g. PCL content, permeant deformation), by changing the print pattern from ‘aligned’ to ‘offset’

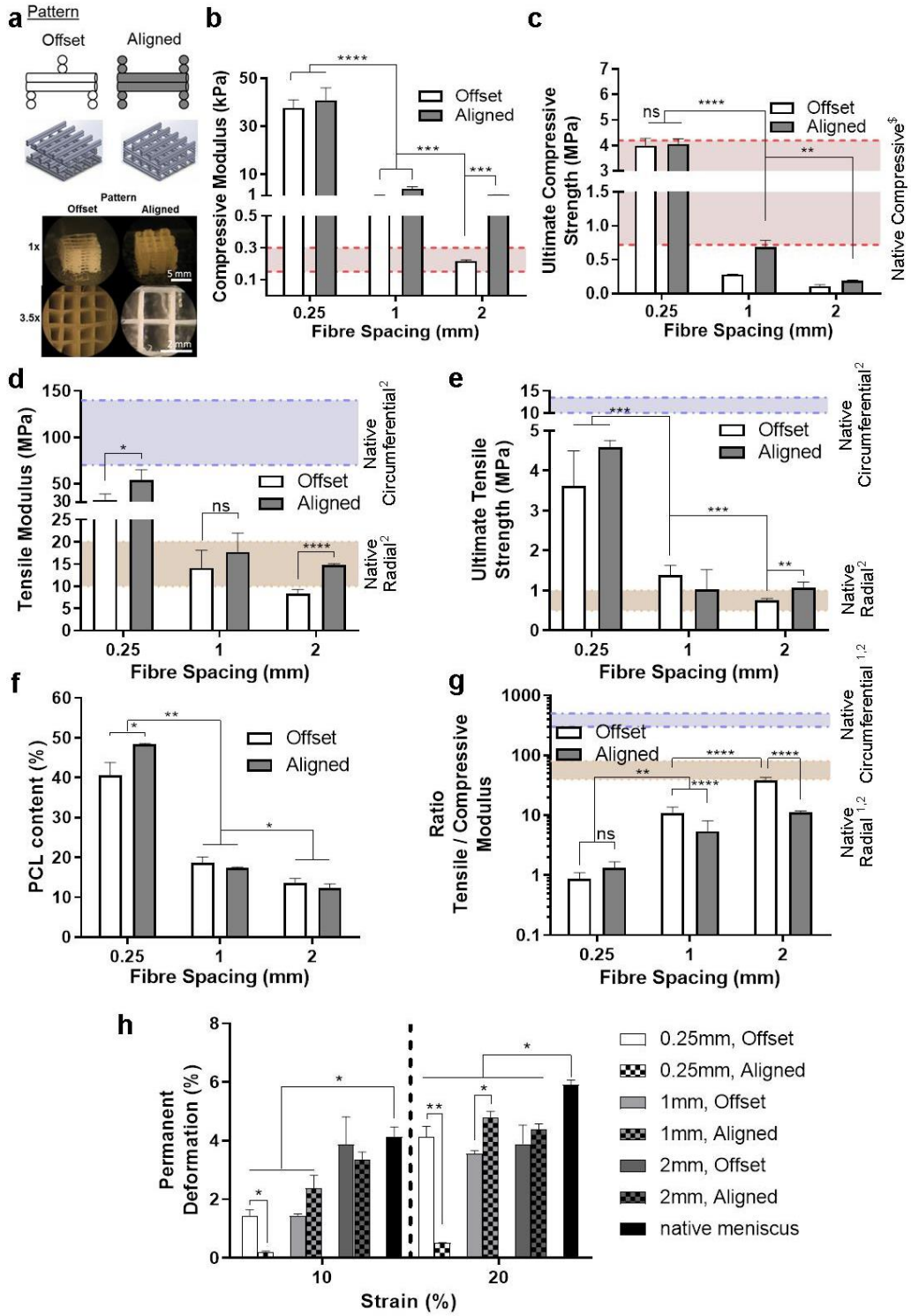

Fig. 3.3 Effect of PCL pattern on mechanical properties: Printed PCL fibres with 120 µm fibre diameter, aligned or offset pattern and 0.25, 1 or 2 mm spacing (a), their compressive moduli (b), ultimate compressive strength (c), tensile moduli (d), ultimate tensile strength (e), PCL contents (f), tensile/compression ratio (g) and permanent deformation (h). $p \leq 0.05$ (*), $p \leq 0.001$ (**), $p \leq 0.0005$ (***) and $p \leq 0.0001$ (****), n = 4

(1) Sweigart et al, (2) Tissakht et al, ($) stress at 30% strain

3.3.4 Reinforcing IPN hydrogels with 3D printed PCL fibre networks to produce highly hydrated composites mimetic of soft biological tissues

With a view to 3D bioprinting a cell laden, PCL fibre-reinforced IPN hydrogel suitable for meniscal tissue engineering, this thesis next sought to explore how integrating the previously developed PCL network into an IPN hydrogel would influence the tensile and compressive properties of the resulting composite. To this end, 3.5% GelMA, 5% alginate and 0.05% irgacure 2959 were mixed to create an IPN which was then filled into the pores of a PCL network (120 µm fibre diameter, double layer, 2 mm fibre spacing, offset pattern), which was subsequently cross-linked using $CaCl_2$ and UV light (Fig. 3.4 a). In agreement with previous findings from our lab (Schipani, 2019), the compressive modulus of the composite construct (0.55 MPa) was significantly higher than both the IPN alone (0.08 MPa) and the PCL scaffold alone (0.22 MPa). In fact, combining the IPN and PCL network led to a synergistic increase in compressive properties, with the compressive modulus of the composite greater than the sum of the moduli of the IPN alone and the PCL alone (Fig. 3.4 b). However, the ultimate compressive strength of the PCL fibre reinforced composite construct did not increase compared to the strength of the PCL scaffold alone, with both groups still displaying a J-shaped stress-strain profile (Fig. 3.4 c). Furthermore, the tensile modulus and ultimate tensile strength of the composite was comparable to the PCL only (Fig. 3.4 d-e). However, for the 'offset' design, adding the IPN into the PCL network reduced the permanent deformation of the composite after the application and removal of 10% compressive strain (Fig. 3.4f). After the application and removal of 20% compressive strain, the permanent deformation of all tested constructs was similar, independent of the chosen print pattern, but was still lower than that measured for native meniscal tissue (Fig. 3.4 f).

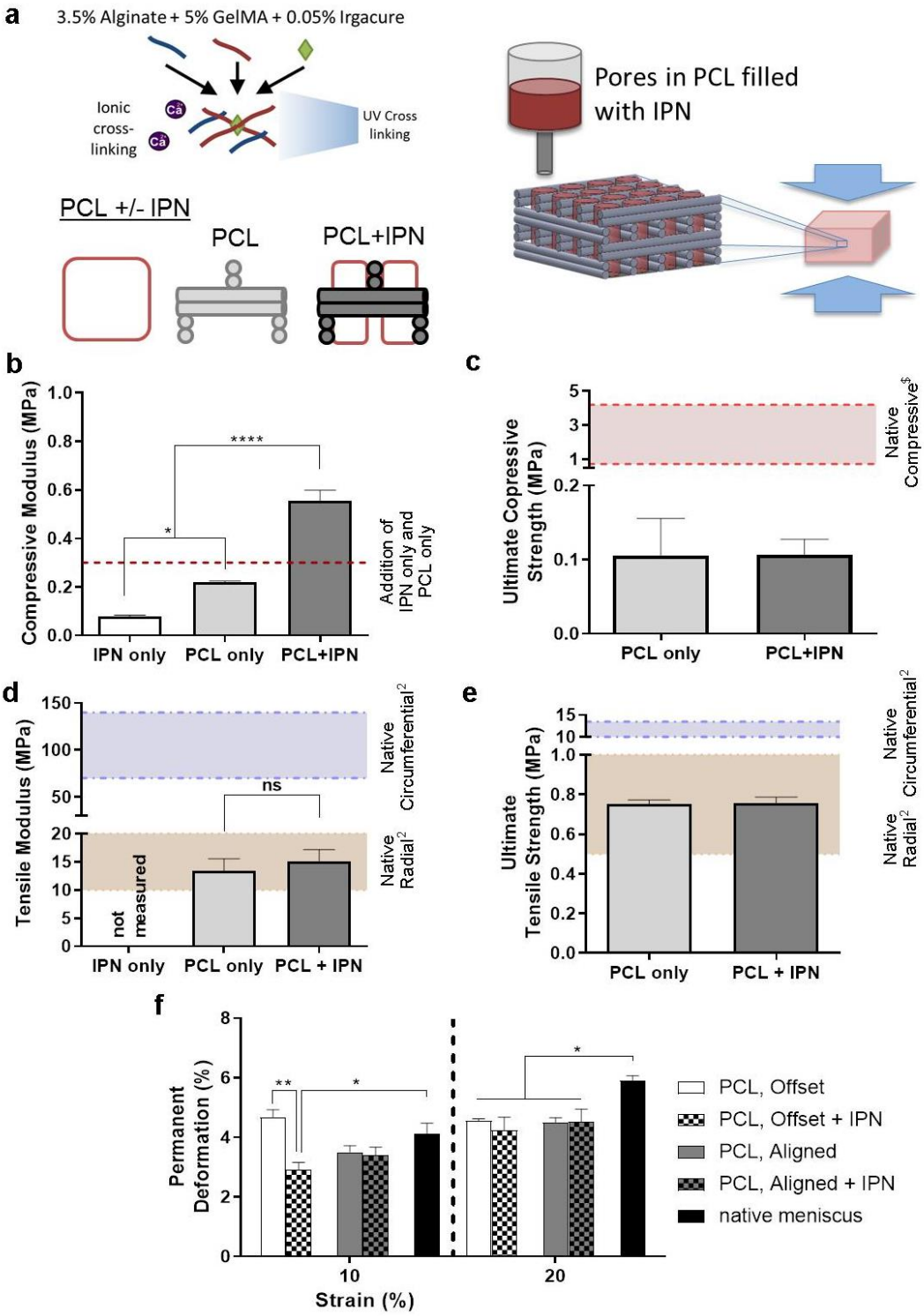

Fig. 3.4 Effect of IPN reinforcement on mechanical properties: IPNs of alginate and GelMA with printed PCL fibres with 120 µm fibre diameter, 2 mm spacing and aligned or offset pattern (a), their compressive moduli (b), ultimate compressive strength (c), tensile moduli (d), ultimate tensile strength (e), and permanent deformation (f). $p \leq 0.05$ (*), $p \leq 0.001$ (**) and $p \leq 0.0001$ (****), n = 4

(1) Sweigart et al, (2) Tissakht et al, ($) stress at 30% strain

3.4. Discussion

Currently commercially available meniscus implants do not mimic the complex internal structure and biomechanical function of the native meniscus tissue. The aim of this chapter was to engineer composites that mimicked the compressive and tensile properties of native human meniscus tissue by combining 3D printed PCL scaffolds with IPN hydrogels. The compressive and tensile properties of 3D printed PCL scaffolds were found to decrease with decreasing fibre diameters and increasing fibre spacings, which was associated with a decrease in the overall PCL content of the biomaterials. The ratio between the tensile and compressive modulus of the PCL constructs was found to depend on the print pattern, with more meniscus biomimetic scaffolds generated using an 'offset' design. Finally, it was possible to engineer fibre-reinforced composites by reinforcing IPN hydrogels with networks of 3D printed PCL. These composites possessed superior elasticity and compressive properties compared to PCL networks only.

This chapter first sought to identify PCL network designs that mimicked both the compressive and tensile moduli of the native human meniscus tissue. Using PCL as a biomaterial, and within the design parameters explored in this study, it was not possible to print scaffolds that fully mimicked the complex compressive and tensile properties of human meniscus tissue. Scaffolds with fibre diameters of 120 μm, a fibre spacing of 2 mm and offset print pattern matched the compressive modulus of the tissue (M A Sweigart et al., 2004), as well as its tensile modulus and ultimate tensile strength in the radial direction (Tissakht & Ahmed, 1995). While the tensile modulus of the native tissue in circumferential direction could be approached using a fibre spacing of 0.25 mm, these scaffolds were not mimetic of other meniscus properties and suffered from other drawbacks. Firstly, the PCL content of scaffolds with 0.25 mm spacing was as high at 48%, which is deemed impractical for applications in surgery, since the degradation time of such a high amount of polymer *in vivo* increases

significantly (Abedalwafa, Wang, Wang, & Li, 2013; Woodruff & Hutmacher, 2010). Secondly, scaffolds with a PCL content this high showed a significantly increased compressive modulus, exceeding that of native tissue in compression by nearly two full orders of magnitude. High PCL content has been shown before to be associated with higher scaffold compressive moduli, so this result was to be expected (Malda et al., 2013; Woodruff & Hutmacher, 2010). While it is unclear what impact implanting such constructs would have in the joint, damage to the AC in the knee would be a concern (Kwon et al., 2019). It was concluded, therefore, that it is not possible to engineer fully biomimetic meniscus scaffolds using PCL alone, but this was deemed an acceptable shortcoming of proposed design. Alternative material choices to solve those problems might be more silk fibre (Warnecke et al., 2018) or Ultra High Weight Polyethylene (NUsurface®, AIC, Memphis, Tennessee)(Active Implants, 2018; Balint et al., 2012; Elsner & Linder-ganz, 2010) to provide greater tensile strength in the backbone of the construct, either as an alternative to PCL or within the backbone of the present meniscus construct to provide additional tensile strength in the circumferential direction.

Instead of pursuing higher circumferential tensile strength, it was decided to focus on developing a scaffold that mimicked the axial compressive and radial tensile properties of the native meniscus. The tensile and compressive moduli of native meniscus tissue have a specific ratio, with the tensile modulus being dramatically higher than the compressive modulus (>35:1), a feature referred to as tension-compression non-linearity (X. Chen et al., 2017). This ratio could not be achieved using an ‘aligned’ print pattern, as the compressive modulus was too high, while their tensile moduli was too low compared to native human tissue. An increase in PCL content would bring the tensile modulus of the printed scaffold closer to the values of native tissue, but it also resulted in a dramatic increase in the compressive modulus, again resulting in the development of a scaffold with a non-physiological ratio of tensile to

compressive modulus. This design challenge was addressed using an offset printing pattern, which was found to decrease the compressive properties of the scaffold more than the tensile properties. Using a printing architecture of 2 mm spacing, 120 μm fibre diameter and an offset printing pattern, it was possible to produce scaffold with a physiological ratio of tensile to compressive modulus. Previous studies have demonstrated how such changes in scaffold design can alter the compressive properties of printed PCL networks (Szojka et al., 2017). However, to our knowledge it is the first time that the ability to modulate the tensile behaviour more than the compressive one has been described using this approach. Furthermore, the J-shaped stress-strain profile observed during compression testing of the offset printing pattern suggests a more biomimetic mechanical behaviour under compression compared to scaffolds with an aligned print pattern.

The final stage of this chapter investigated the mechanical properties of composites generated by mechanically reinforcing IPN hydrogels with networks of 3D printed PCL. The compressive modulus of the fibre-reinforced composites were superior to that of the IPN and PCL alone, and to the sum of their individual moduli combined. This effect has been attributed to the fact that the IPN limits the radial expansion and buckling of the PCL fibre walls, and increases the generation of hydrostatic pressure with the IPN under compressive loading. Previously, MEW has been used to engineer such composites, using PCL fibres of a thickness of about one order of magnitude smaller than the ones created by FDM (Bas et al., 2015; Castilho, Hochleitner, Wouter, Rietbergen, & Paul, 2018; Schipani et al., 2020; Visser, Melchels, et al., 2015). These earlier studies have demonstrated little or no synergistic reinforcement when hydrogels are combined with PCL scaffold produced by FDM. Using an ‘offset’ print pattern results in the development of PCL scaffolds with a softer compressive modulus, but which can be used to synergistically reinforce hydrogels (Schipani et al., 2020). Furthermore, the stress-strain curve of the combined sample

under compressive testing revealed an elastic J-shaped profile, somewhat mimetic of that observed in soft biological tissue (Kendall & Fuller, 1987). It should be noted that the tensile modulus and ultimate tensile strength of the fibre-reinforced IPN composite was comparable to the PCL scaffold alone. This is most likely due to the drastically lower resistance of the IPN to tensile forces, therefore combining them resulted in no benefit to the overall tensile properties.

The composites also displayed low levels of permanent deformation (the portion of the original height of a material that cannot be recovered after a particular strain is applied and removed) following the application and removal of compressive strain. The levels of permeant deformation in such biomaterials are dependent on the applied strain levels, the rate of loading as well as the time given for the sample to recover its original height following the removal of load. While 10% strain represented a physiological loading regime, 20% strain represented a more degenerative loading regime (Gupta et al., 2008; Mcnulty & Guilak, 2016; Zielinska et al., 2009). While menisci in the joint endure a high number of compressive strain cycles and recover from them, he tested meniscus tissue showed higher permanent deformation levels than all printed samples. This could be attributed to the fact that the interval between cycles during testing was chosen as too short and native tissue would usually swell and recover given more time (Mow & Huiskes, 2005). In subsequent chapters a longer recovery period was employed, which allowed further time for recovery of the sample. Similar to the compressive and tensile moduli, the level of permanent deformation under compressive loading decreased with increasing PCL content, fibre diameter and decreasing fibre spacing. The chosen fibre pattern had little influence on permanent deformation levels under 10% strain. However, not only did an offset pattern facilitate the development of scaffolds with compressive moduli similar to native values, the levels of permanent deformation within such constructs could be reduced when combined with the IPN. Therefore, future chapters of this thesis will employ an offset

printing pattern, with a 120 μm fibre diameter and 2 mm fibre spacing to produce PCL networks to reinforced IPN hydrogels designed for meniscus tissue engineering and 3D bioprinting.

3.5. Conclusions

To conclude, 3D printed PCL scaffolds with a fibre diameter of 120 μm, a spacing of 2 mm and an ‘offset’ print pattern, when combined with an IPN of alginate and GelMA, result in development of highly hydrated composites with axial compressive and radial tensile properties similar to native human meniscus tissue. Chapter 4 of this thesis will explore the potential of the IPN to support chondrogenesis of MSCs, and further characterise the biphasic mechanical properties of such tissue engineered constructs with time in culture.

Chapter 4

3D BIOPRINTING OF FIBRE-REINFORCED INTEPENETRATING NETWORK HYDROGELS FOR ENGINEERING OF FIBRICARTILAGINOUS TISSUES

4.1. Introduction

In order to create a tissue engineered implant for meniscus regeneration which can fulfil the complex tasks of the meniscus within the knee joint, it is essential that the construct mimics the biomechanical properties of the native tissue. In chapter 3 of this thesis a 3D printing strategy was developed which enables the fabrication of PCL scaffolds mimicking the elastic modulus of native meniscus tissue in compression and in tension (in the radial direction). However, cartilagenous tissue like the meniscus have complex bi-phasic (time-dependent) mechanical properties as the tissue consists of both a fluid and solid phase (Mcnulty & Guilak, 2016). PCL scaffolds do not display such bi-phasic mechanical properties. In contrast, hydrogels such as alginate or GelMA are characterized by both a solid and liquid phase and generally display time-dependent mechanical properties. They consist of a matrix of polymer chains with electrostatic charges which bind water molecules in a similar manner to that within cartilagenous tissues. A significant limitation of such hydrogels (and hydrogel bioinks) for the engineering of musculosketelal tissues is their relatively poor mechanical properties, generally making them unsuitable for meniscus tissue engineering applications.

A number of strategies have been employed to improve the mechanical properties of hydrogels and bioinks for the tissue engineering of cartilagenous tissues.

One common approach is to reinforce softer, more chondrogenic hydrogels with stiffer polymer networks (Bas et al., 2015; Visser et al., 2015). Another involves the use of IPNs with mechanical properties comparable to soft biological tissues (Chimene, Kaunas, & Gaharwar, 2020; Malda et al., 2013). IPNs are mixtures of two hydrogels which are crosslinked ionically and covalently, respectively but will remain uncrosslinked to one another. This provides an IPN with its superior mechanical properties like increased elasticity and lower fracture progression which be tailored to the tissue of interest (Chimene et al., 2020; Schipani, 2019).

Such IPNs have also been used in the engineering of musculoskeletal tissues. For example, highly elastic and tough IPN hydrogels have been developed using alginate and gelatin, which were also shown to support the proliferation and osteogenic differentiation of MSCs (Jeon et al., 2017; Krishnamoorthy & Zhang, 2019a). Such IPNs can also be used as bioinks for 3D bioprinting applications (Y. X. Chen, Cain, & Soman, 2017; Do, Hong, Cha, Shin, & Bae, 2018)(Krishnamoorthy & Zhang, 2019b)(Z.-Z. Zhang et al., 2016)(Colosi et al., 2016)(Ansari et al., 2017)(Zhu et al., 2018)(Costantini, Onofrillo, Duchi, Daly, & Critchley, n.d.)(Tamayol et al., 2015). It remains unclear whether such IPN hydrogels are capable of supporting the fibrochondrogenic differentiation of MSCs, and furthermore if they could be mechanically reinforced to produce composites that mimic the complex viscoelastic mechanical properties of the native meniscus.

Specifically, IPNs of alginate and GelMA has been used in bioprinting in the past, albeit not for cartilagenous tissue engineering.(Y. X. Chen et al., 2017)(Krishnamoorthy & Zhang, 2019b)(Z.-Z. Zhang et al., 2016)(Colosi et al., 2016)(Ansari et al., 2017)(Zhu et al., 2018)(Costantini et al., n.d.)(Tamayol et al., 2015).

Many hydrogels commonly used in tissue engineering due to their promotion of cell proliferation and tissue regeneration only have mechanical properties too low to

withstand the forces in a native joint environment (Malda et al., 2013). An additional difficulty in tailoring bioinks for cartilage tissue engineering is that common methods of increasing the mechanical properties of hydrogels is to increase the polymer density or the degree of crosslinking. However, both strategies have shown to decrease the cells' ability to produce matrix. This lack of chondrogenesis in many gels with high mechanical stiffness has been linked to a lack of nutrient transport and cell migration through the hydrogels which can then lead to hypertrophy of MSCs (Chimene et al., 2020)(Freeman & Kelly, 2017).

In recent years cartilage biofabrication research has therefore employed scaffolds which reinforce softer, more chondrogenic hydrogels with stiffer PCL fibres (Bas et al., 2015; Schipani, 2019; Visser, Melchels, et al., 2015). The phenomenon of a soft hydrogel and a stiff PCL construct reinforcing each other has been reported to stem from the ability of the gel to prevent the PCL fibres from buckling under compression (Visser, Melchels, et al., 2015) and has been demonstrated in chapter 3 already in case of the elastic modulus. Consequently, in the following chapter the mechanical properties of the created composite scaffolds were explored more in depth by employing a rheological analysis as well as a more complex compressive testing methodology which analyse the equilibrium and the dynamic moduli as well. Those characteristics provide insight into the ability of the scaffold to retain its liquid phase under compression.

The aim of this chapter was to 3D bioprint a composite construct consisting of an MSC laden IPN hydrogel reinforced with a PCL fibre network, and to assess the capacity of this construct to support fibrochondrogenesis of MSCs. To this end this chapter will first characterise the rheological properties of alginate, GelMA and a mixture of both hydrogels, with a view to determining their shear thinning properties and suitability of 3D bioprinting applications. Next, the capacity of an alginate-GelMA IPN to support chondrogenesis of bone marrow mesenchymal stem cells (BMSCs) was

assessed *in vitro*. In particular, this chapter sought to determine if both the equilibrium and dynamic mechanical properties of these *in vitro* maturated tissues would fall within the range of native meniscus tissue.

4.2. Methods

4.2.1 Printing PCL scaffolds

Cylindrical PCL scaffolds of 6 mm diameter and 6 mm height were printed in a pattern of double layered 2 mm offset as described in chapter 3 (Fig. 4.2 a).

4.2.2 Preparation of constructs

Printed PCL scaffolds were sterilized via ethylene oxide treatment for 12 hours and allowed to degas for 48 hours. All following steps were conducted under sterile conditions. To ensure homogenous crosslinking of IPN + PCL samples, the printed scaffolds were first incubated in sterile 45 mM $CaCl_2$ overnight under rotation in order to ensure diffusion into all pores. To prepare crosslinking of IPN only gels a mould of 3% agarose and 45 mM $CaCl_2$ was prepared.

First, 16% (w/v) LVG sodium alginate (Pronova, Norway) and 17.5% (w/v) GelMA were dissolved separately in DMEM and then mixed with 0.5% irgacure 2595 (Sigma) in a ratio of 2:2:1 using two syringes connected via a luer lock adapter. Expanded BMSCs were then trypsinized and resuspended in expansion media (XPAN) at a concentration of $40x10^6$ cells/ml and mixed with the remaining IPN components in a ratio of 1:1 to obtain a final cell seeding density of $20x10^6$ cells/ml. IPN + PCL samples were then prepared by pipetting the IPN with cells into the pores of the prepared PCL scaffolds using a conical 23G needle while IPN only gels were pipetted into the prepared agarose and $CaCl_2$ moulds to obtain cylindrical gels (4.7 mm diameter and 4 mm height).

Samples were then crosslinked in 45 mM $CaCl_2$ under a 6 W UV lamp with 20 mm distance to samples for 15 minutes and another 5 minutes of $CaCl_2$ only.

4.2.3 Rheology

Rheological characterization was conducted using an MCR 102 Anton Paar Rheometer (Austria) with a 25 mm diameter parallel plate and a measurement gap of 0.5 mm. 10% Uncrosslinked gels were allowed to equilibrate at 13°C for 20 minutes before measuring viscosity as a function of shear stress by conducting shear rate sweeps from 0.1 to 100 s^{-1}. Each sample was measured in both technical and biological triplicates. The data was then fitted to the Herschel-Bulkley power law equation where τ describes the yield stress, k is the consistency index, γ describes the shear stress and n describes the flow index Eq. 4.1.

$$\tau = k\gamma^n$$

Eq. 4.1

4.2.4 Cell culture

Porcine bone marrow mesenchymal stem cells were harvested and isolated from femurs of 3 month old female pigs. Cells were expanded on 2D cell culture plastic XPAN, composed of DMEM (Gibco), 1% penicillin (100 U/ml), streptomycin (100 µg/ml), 0.1 µl/ml amphotericin B, 0.05 µl/ml FGF-2 and bovine serum albumin (all Sigma) in 20% pO_2. Chondrogenic potential was confirmed via tripotentiality assay and cells were expanded until passage 2 before seeding into scaffolds.

After crosslinking, the constructs containing cells were transferred to XPAN medium at 20% pO_2 overnight and then cultured in chondrogenically defined media consisting of DMEM supplemented with 1% penicillin (100 U/ml), streptomycin (100 µg/ml), sodium pyruvate (100 µg/ml), L-proline (40 µg/ml), L-ascorbic acid 2-phospate (50 µg/ml), linoleic acid (4.7 µg/ml), bovine serum albumine (1.5 mg/ml), 1x insulin-transferrin-selenium, dexamethasone (100 nM) (all Sigma Aldrich), human TGF-β3 (10

ng/ml) (ProSpec-Tany TechnoGene) and 0.1 µl/ml amphotericin B and 5% pO_2 for 42 days. Media changes were performed twice per week.

4.2.5 Live/Dead confocal microscopy

Cell viability was analysed at 1, 21, and 42 days after crosslinking using a Live/Dead assay kit (Bioscience). Samples were first washed in phenol free DMEM (pfDMEM) (Sigma) before incubating them in 4 µM ethidium homodimer-1 and 2 µM calcein in pfDMEM for 1 hour. After washing again in pfDMEM they were imaged using a Leica SP8 Confocal microscope and the viability quantified using the software ImageJ.

4.2.6 Biochemical analysis

The biochemical content of samples was quantified after 1, 21 and 42 days of culture. Samples were tab dried and weighed before digesting them in papain (125 µg/ml) in 0.1 M sodium acetate, 5 mM L-cysteine-HCl, 0.05 M ethylene-diamine-tetracetic acid (EDTA) (all Sigma) and pH 6 under rotation at 60°C for 18 hours. Finally, since PCL remains undigested the melted remains of each sample were blot tried and weighed separately in order to calculate the weight of the gel of alone of each sample by deducting their PCL weights from the total weight of each sample.

The DNA content was analyzed using a Quant-iT PicoGreen dsDNA assay kit (Invitrogen) immediately after completing the papain digest. The amount of secreted sulphated glycosaminoglycans (sGAGs) was determined using a DMMB assay kit (Blyscan, Biocolor). The collagen levels were quantified through the hydroxyproline levels using a (dimethylamino)benzaldehyde and chloramine T assay and calculated through a hydroxyproline : collagen ratio of 1:7.69. All biochemical analysis results were normalized to gel weights.

4.2.7 Histological and immunohistological analysis

Samples were analysed via histological and immunohistological stainings after 1, 21 and 42 days in culture. After L/D microscopy samples were incubated in 100 mM $CaCl_2$ for 3 minutes before fixing them in 4% paraformaldehyde with 21.4 g/l sodium cacodylate and 2.6 g/l $BaCl_2$, pH adjusted to 7.4 under rotation at 4°C overnight. Samples were then washed in UPW and dehydrated in a graded series of ethanol, xylene, embedded in paraffin wax, sectioned at 7 µm thickness and affixed to microscopy slides. Sections were then stained with Aldehyde Fuchsin/Alcian Blue stains to analyze sGAG, Alizarin Red for calcium and Picrosirius Red for collagen deposition, respectively.

Immunohistological analysis was conducted to assess secretion of Col I, II and X. Firstly, slides were rehydrated and treated with chondroitinase ABC (Sigma) in a humidified chamber at 37°C to ease access to antigens before goat serum was used to block unspecifc antigen binding sites. The primary antibodies collagen I (abcam 90395, 1:400), collagen II (St.Cruz sc52658, 1:400) and collagen X (abcam 49945, 1:200) were applied in goat serum overnight at 4°C. After washing in PBS a 3% hydrogen peroxide solution was applied for 20 minutes at RT under protection light and another washing step in PBS before applying secondary antibodies for collagen I & II (mouse monoclonal, Sigma B7151, 1.5:200) and col X (mouse monoclonal, abcam ab97228, 1:500) at room temperature for 1 hour. Then, sections were incubated in ABC reagent (Vectastain, Vecta Labs) for 45 minutes at room temperature and DAB peroxidase substrate until positive controls showed staining. Finally, sections were dehydrated again with a series of ethanol and xylene and mounted with Vectamount (Vector Labs).

4.2.8 Meniscus sample preparation

Compressive testing of sections of porcine menisci was conducted as described below in case of samples in cell culture. Medial menisci from 3 months old female pigs were harvested and biopsies of 6 mm diameter of the inner and outer

zones were taken. Biopsies were then cut to cylinders with parallel bases for more even contact with the compression platens and more robust testing (Fig. 4.4 c).

4.2.9 Mechanical characterization

Uniaxial unconfined compressive testing of meniscus biopsies, and PCL and IPN constructs after 1, 21 and 42 days of culture was conducted using a 100 N load cell in a twin column Zwick universal testing machine (Zwick/Roell). Samples were tested under compression in a bath of PBS in room temperature as published previously (Gannon, Nagel, & Kelly, 2012; Olvera, Daly, & Kelly, 2015). After a preload of 0.005 N to ensure contact between the sample surface and the testing platen, a stress relaxation test was performed by applying a strain of 20% with a strain rate of 0.04%/s. Then equilibrium stress was recorded after a relaxation period of 45 minutes. Finally, directly after measuring the equilibrium stress, a cyclic testing protocol was conducted by applying a 1% amplitude sinusoidal strain for 5 cycles with a speed of 1 Hz at 0.01%/s strain rate. The elastic modulus ($E_{elastic}$) was calculated by first determining the stress at the linear region of the generated stress/strain curve ($\sigma_{elastic}$) by the dividing the applied force ($F_{elastic}$) by the sample's cross sectional area (A)Eq. 4.2 and then dividing $\sigma_{elastic}$ by the applied strain ($\epsilon_{elastic}$) Eq. 4.3.

$$\sigma_{elastic} = \frac{F_{elastic}}{A}$$

Eq. 4.2

$$E_{elastic} = \frac{\sigma_{elastic}}{\epsilon_{elastic}}$$

Eq. 4.3

The equilibrium Young's modulus ($E_{equilibrium}$) was determined as the force at equilibrium ($F_{equilibrium}$) divided by the cross sectional area (A) of the sample (Eq. 4.4) divided by the applied strain ($\epsilon_{equilibrium}$)Eq. 4.5.

$$\sigma_{equilibrium} = \frac{F_{equilibrium}}{A}$$

Eq. 4.4

$$E_{equlibrium} = \frac{\sigma_{equilibrium}}{\epsilon_{equilibrium}}$$

Eq. 4.5

The dynamic stress ($\sigma_{dynamic}$) was then calculated by dividing the average change of force (ΔF) during each cycle by the sample's cross sectional area (A) Eq. 4.6.

$$\sigma_{dynamic} = \frac{\Delta F}{A}$$

Eq. 4.6

The dynamic modulus ($E_{dynamic}$) was then determined by dividing the dynamic stress ($\sigma_{dynamic}$) by the applied strain ($\epsilon_{dynamic}$) Eq. 4.7.

$$E_{dynamic} = \frac{\sigma_{dynamic}}{\epsilon_{dynamic}}$$

Eq. 4.7

4.2.10 Statistical analysis

Data was expressed as mean and standard error of the mean. Significance was calculated using the student t-test with Welch's correction or ANOVA and Tukey's post-hoc test. Differences were considered to be statistically different at $p \leq 0.05$ (*), $p \leq 0.001$ (**), $p \leq 0.0005$ (***) and $p \leq 0.0001$ (****), n = 3.

4.3. Results

4.3.1 Rheological analysis

A rheological characterization of the alginate (1%, 3.5%) and GelMA (5%, 10%), as well as the corresponding mixtures (1% Alg / 10% GelMA, 3.5% Alg, 5%

GelMA), was first conducted and fitted to the Herschel-Bulkley model in order to assess their shear thinning properties (Fig. 4.1). At 13°C GelMA was found to have the highest viscosity, uncrosslinked alginate was found to have the lowest viscosity and the mixture with GelMA an intermediate value. Furthermore, the viscosity increased with increasing polymer concentration in all materials. Viscosity decreased dramatically as a function of shear rate for the GelMA and the mixture with alginate, whereas alginate alone maintained a reasonably constant viscosity with increasing shear rate (Fig. 4.1 a). The measured levels of shear stress increased in all hydrogels with increasing shear rates, but the steepest increase was seen in the alginate inks (Fig. 4.1 b). All materials could be fitted to the power law or the Herschel-Bulkley model Eq. 4.1 in order to describe their non-Newtonian behaviour (Table 4.1). The measured yield stress τ_0 increased with polymer concentrations and was found to be highest in the 10% GelMA alone and 1% Alg/10% GelMA mixture. Furthermore the flow index *n* of both alginate inks was ~ 0.75, which indicates a weak shear thinning behaviour (values less than one indicate shear thinning behaviour). A significantly lower flow index, closer to 0, was observed for both GelMA concentrations, indicating strong shear thinning behaviour. Both mixtures displayed some degree of shear thinning behaviour, approximately midway between their respective alginate and GelMA components (Fig. 4.1 c). The calculated consistency index k showed a similar trend, with higher consistency in GelMA than in alginate, with values for the mixtures between their respective GelMA and alginate concentrations (Fig. 4.1 d). To summarize, using the Herschel-Bulkley model it could be shown that the mixtures of alginate and GelMA have shear thinning properties, but less so than the GelMA inks alone.

Table 4.1 Herschel-Bulkley model of rheological analysis

	n	k [Pa*s^n]	τ_0 [Pa]	R^2
1% Alg	0.756	0.086	0.003	0.936
3.5% Alg	0.807	3.620	0.609	0.999
5% GelMA	0.105	29.929	21.873	0.960
10% GelMA	0.179	252.910	131.925	0.852
3.5% Alg / 5% GelMA	0.594	20.600	8.851	0.997
1% Alg / 10% GelMA	0.170	142.690	81.019	0.836

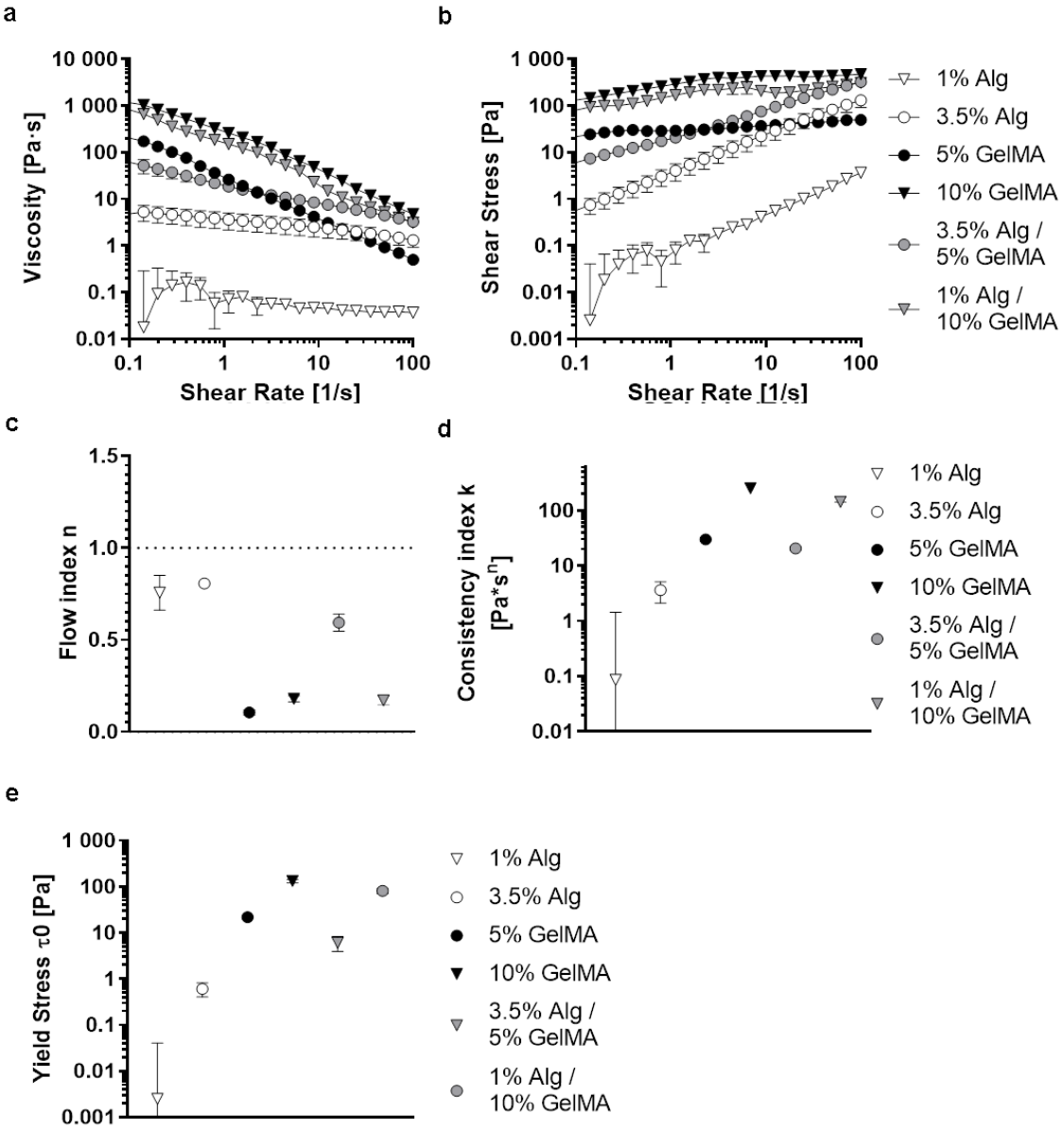

Fig. 4.1 Rheological analysis: A rheological analysis to assess the viscosity (a) and shear stress (b) as a function of shear rate was fitted to the Herschel-Bulkley model to calculate the flow index (c), consistency index (d) and yield stress (e). n = 3 in triplicates

4.3.2 Fibrochondrogenetic differentiation of BMSCs in fibre-reinforced IPNs

Next, 3.5% Alg/5% GelMA IPNs laden with BMSCs were either cultured alone or within 3D printed PCL networks in chondrogenic media and physioxic conditions for 42 days (Fig. 4.2 a). Live/Dead staining at day 1 revealed lower levels of cells viability in IPN + PCL constructs, but overall levels of viability remained high (typically >60%) and were comparable in both PCL reinforced and unreinforced constructs after 21 and 42 days in culture (Fig. 4.2 b-c). This was confirmed by the biochemical analysis, which demonstrated that DNA levels were comparable in both groups after 21 and 42 days of culture (Fig. 4.3 a). Collagen synthesis was estimated via a hydroxyproline assay and revealed a significant increase in collagen production in both constructs over the course of 42 days in culture (Fig. 4.3 b). Comparable levels of sGAG synthesis was also observed in the IPN alone and IPN + PCL constructs after 6 weeks in culture (Fig. 4.3 c).

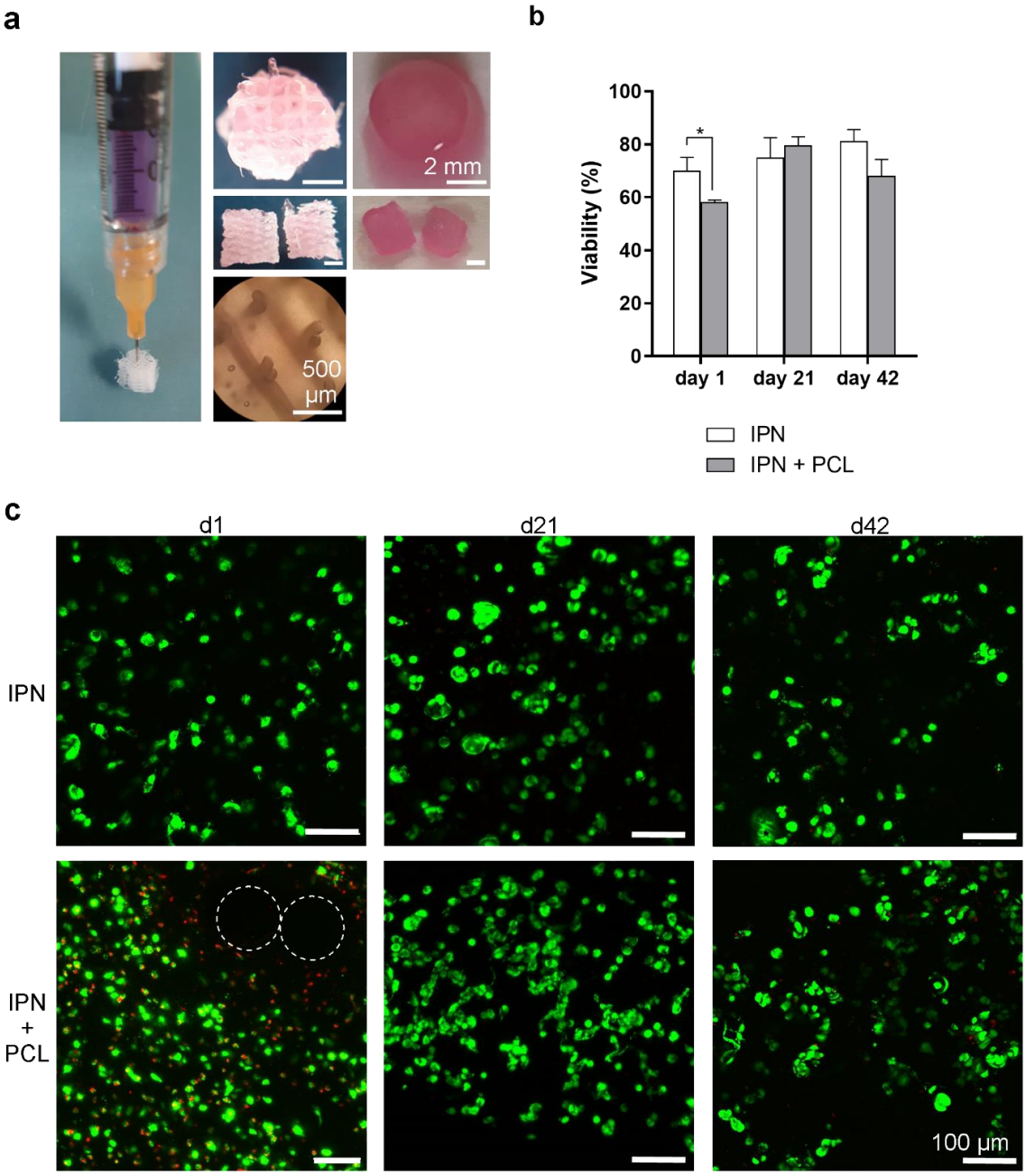

Fig. 4.2 BMSC viability in fibre-reinforced IPNs. BMSCs were seeded into IPNs of alginate and GelMA and either injected into the pores of printed PCL scaffolds or casted into an agarose mold. Scale bars: 2 mm and 500 µm (a). The cell viability was analyzed via Live/Dead imaging under confocal microscopy. The dotted circles show the location of PCL fibres. Scale bar: 100 µm (b-c). * indicates $p \leq 0.05$, $n = 3$

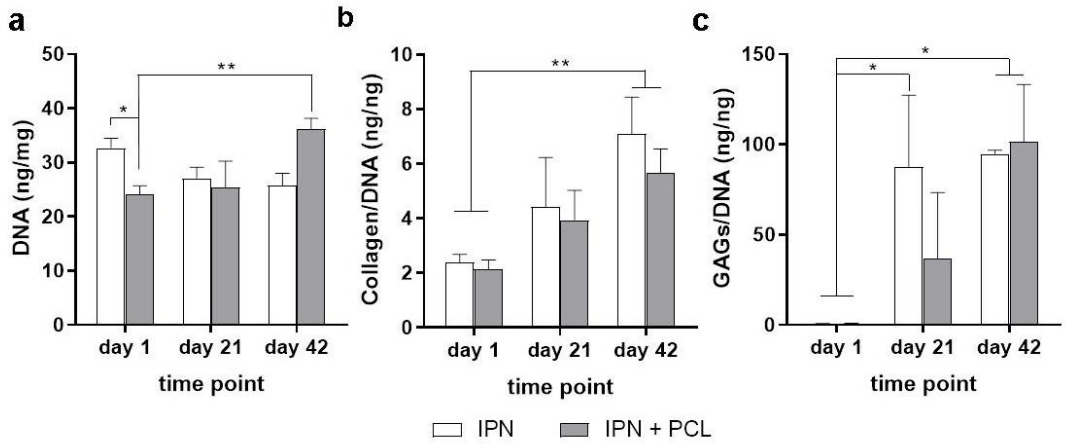

Fig. 4.3 Biochemical analysis of fibre-reinforced IPNs. (a) DNA, (b) collagen and (c) sGAG levels in IPN hydrogels and IPN hydrogels reinforced with a networks of PCL (IPN + PCL). $p \leq 0.05$ (*), $p \leq 0.001$ (**). n = 3

4.3.3 Mechanical testing

The mechanical properties (equilibrium and the dynamic moduli in compression) of MSC laden constructs after 42 days of *in vitro* culture was next assessed, and compared to samples of the inner and outer zone of porcine meniscus tissue (Fig. 4.4 a-c). As expected, the mechanical properties of PCL reinforced IPNs were notably higher than that of the IPNs alone. The elastic modulus of the PCL + IPN constructs significantly increased with time in culture, falling into the same range as that of outer meniscus tissue, but significantly higher than that of the inner meniscus. The elastic modulus of IPN alone was comparable to that of inner meniscus tissue (Fig. 4.4 d).

The equilibrium modulus of the PCL + IPN and the IPN alone constructs did not significantly increase with time in culture (Fig. 4.4 e). The equilibrium modulus of the IPN alone constructs was comparable to that of inner and outer zone of the meniscus, while the PCL + IPN constructs were found to have a significantly higher equilibrium modulus than the native tissue.

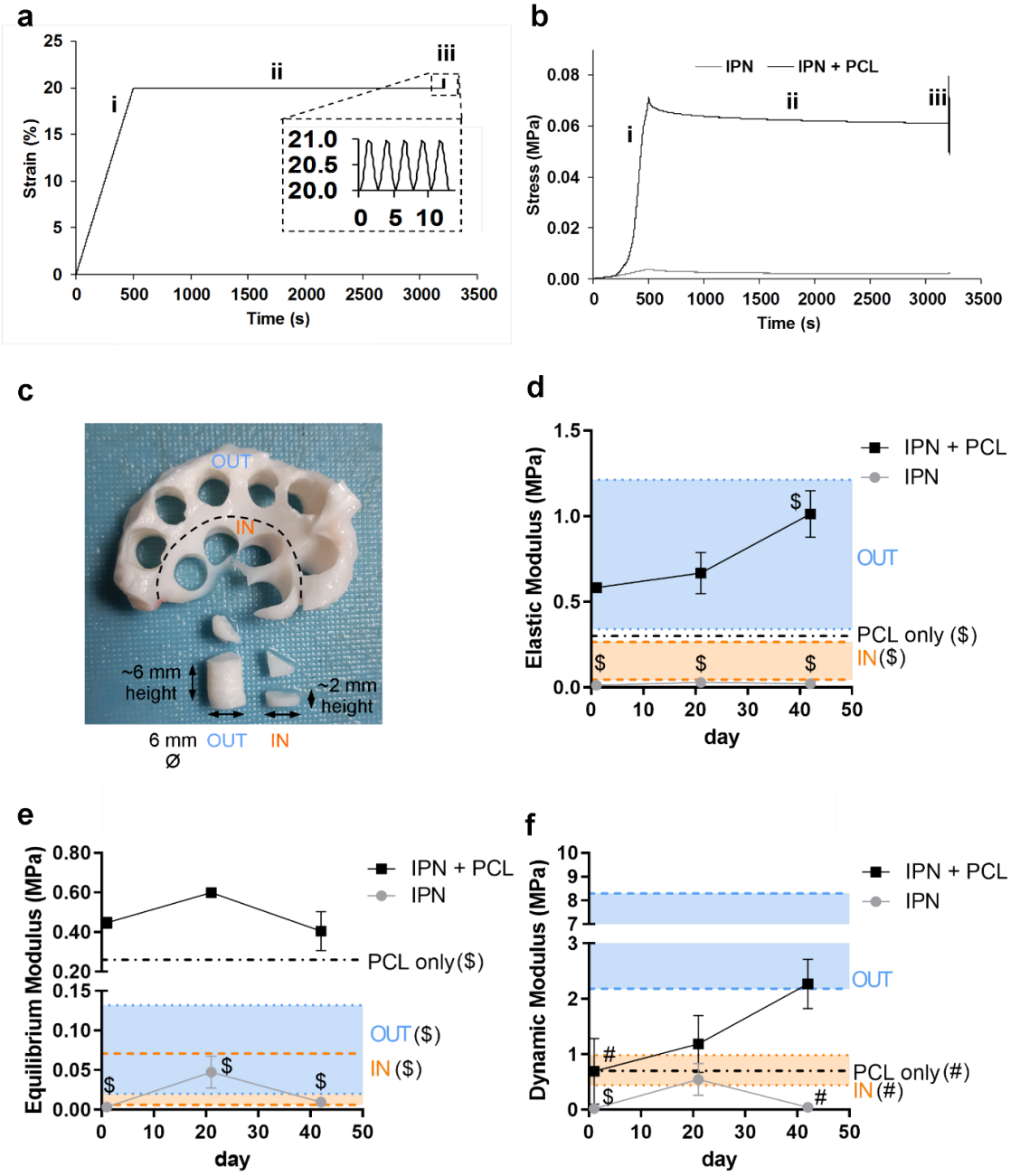

Fig. 4.4 Mechanical testing: A compressive testing regime was employed to test the elastic (i), equilibrium (ii) and dynamic modulus (iii)(a-b) of engineered constructs and compare them to tested native porcine meniscus (c). Analysis of the elastic modulus (d), the equilibrium modulus (e) and the dynamic modulus (f) furthermore uncovered the compressive properties of the created constructs after 42 days of culture as well as the moduli of PCL scaffolds alone and native porcine meniscus samples of the inner and outer zone. $ represents $p < 0.05$ compared to IPN + PCL d1, # represents $p < 0.05$ compared to IPN + PCL d42, n = 3

The dynamic modulus of the PCL + IPN constructs were significantly higher than the modulus of PCL alone and increased with time, albeit not significantly ($p=0.08$), falling into the same range as that of the inner meniscus tissue after 3 weeks and into the range of the outer one after 6 weeks. The dynamic modulus of PCL alone was comparable to inner meniscus tissue while the modulus of IPN alone increased briefly after 3 weeks but decreased again after 6 weeks (Fig. 4.4 f).

4.3.4 Histological and immunohistological analysis

A histological and immunohistological analysis was next conducted in order to assess the fibrochondrogenic potential of the IPN based constructs. Alcian Blue/Aldehyde Fuchsin and Picrosirius Red staining demonstrated an increased secretion of sGAGs and collagen, respectively, in both groups over 42 days of culture. This aligns with the results shown in the biochemical analysis. Alizarin Red staining also revealed the presence of calcific deposits within the IPN only constructs. Immunohistological analysis of the sectioned engineered tissues revealed an increase in Col II staining over the culture period in both groups, whereas only low levels of Col I and Col X were detected. Porcine meniscus tissue used as control showed intense Col I staining (Fig. 4.5).

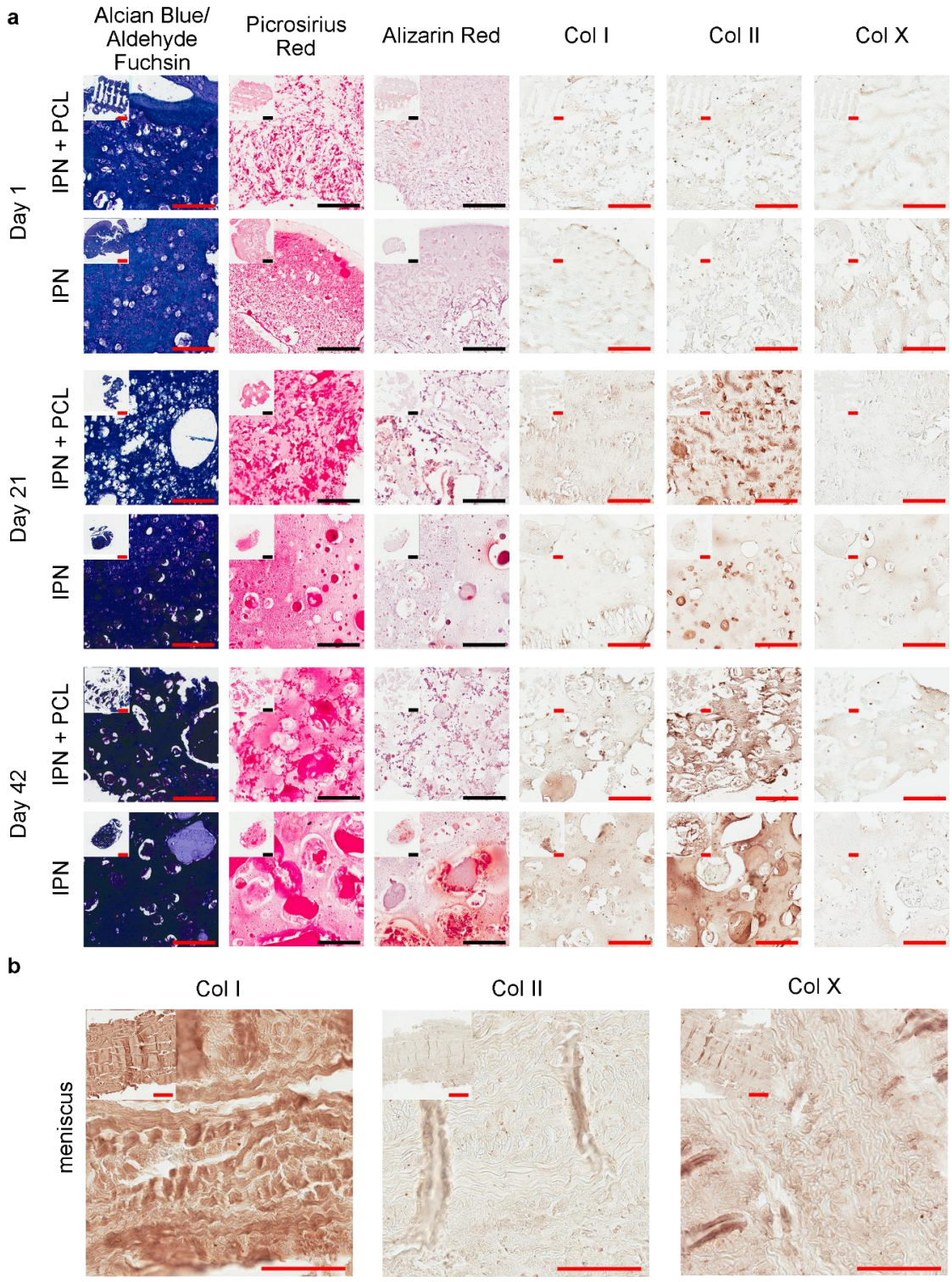

Fig. 4.5 Histological and Immunohistochemical analysis: (a) Histological analysis of cultured scaffolds over the course of 42 days via Alcian Blue/Aldehyde Fuchsin, Picrosirius Red and Alizarin Red staining. (b) Immunohistochemical analysis of Col I, II and X. Scale bars: 1 mm and 100 µm. n = 3

4.4. Discussion

Providing stem or progenitor cells with surroundings which stimulate the production of cartilaginous or fibrocartilaginous matrix remains a major challenge in the field of tissue engineering. Many materials are either too soft to withstand the harsh mechanical stresses of the native joint environment, or are too dense/stiff to support robust cartilage matrix production. The research goal of this chapter was therefore to develop a printable IPN based hydrogel with fibrochondrogenic potential. It was demonstrated that an IPN of alginate and GelMA has shear thinning properties, that BMSCs secrete a cartilaginous matrix within this hydrogel and that this secreted matrix improves the mechanical properties of the PCL reinforced IPN, resulting in tissues with dynamic mechanical properties closer to native meniscal tissue.

Rheological analysis methods have only been employed recently to develop bioinks and describe their viscoelastic properties through comparable parameters. The viscosity as a function of shear rate is hereby calculated through fitting the data to the Herschel-Bulkley model (Chimene et al., 2016; Melchels et al., 2016; Pati et al., 2014). Consequently, it was demonstrated that the GelMA and IPN hydrogels possess shear thinning properties. This characteristic of decreasing shear forces with an increase in shear rate is beneficial for the development of injectable and printable bioinks for several reasons. Firstly, the shear forces acting on the material and the encapsulated cells decrease with increasing shear rates during extrusion from a syringe and therefore support higher levels of cell viability post-printing. The observed shear thinning effect is caused by the alignment of polymer fibres within the gel as reviewed thoroughly elsewhere (Malda et al., 2013). Furthermore, after extrusion when the shear rate decreases, the viscosity of the bioink increases which ensures higher mechanical integrity and fidelity of the printed construct. The calculated flow index n of 0.59 of the IPN of 3.5% alginate / 5% GelMA lies below 1 and therefore confirms the non-Newtonian and shear thinning behaviour of the developed IPN. The yield stress τ_0

describes the minimum stress needed for extrusion and the ability of the bioink to retain its shape after extrusion. Bioinks with a higher consistency index k have been shown to form a 'plug' during extrusion which protects the cells in the centre of the syringe and needle from high shear forces near the walls, which further increases the viability of the cells (Chimene et al., 2018; Mouser et al., 2016). The shear thinning behaviour of the IPN can be associated with the GelMA, which in agreement with this study has been shown to have shear thinning properties at 13°C (Chimene et al., 2018). In contrast, uncrosslinked alginate does not shear thin to the same extent and has previously been shown to be unprintable unless modified to increase its viscosity (Freeman & Kelly, 2017). To conclude, an IPN of 3.5% alginate and 5% GelMA, with a value of n below 1, k to be 20.6 Pa*s^n and τ_0 of 8.851 Pa were found to be in the range of other reported bioinks and were therefore considered suitable for biofabrication (Chimene et al., 2018; Melchels et al., 2016).

In addition to having rheological properties compatible with 3D bioprinting applications, the developed IPN bioink has also been found to promote the secretion of (fibro)cartilaginous matrix components, specifically Col II and sGAGs. Immunohistochemical analysis showed that the secreted matrix proteins were low in Col X, but rich in Col II, which suggests the development of a stable cartilage matrix without hypertrophic chondrocytes. However, some calcification of the IPN was observed after 6 weeks of chondrogenic culture conditions, suggesting progression along an endochondral pathway. Similar observations have been made in the past (Krishnamoorthy & Zhang, 2019b)(Z.-Z. Zhang et al., 2016)(Colosi et al., 2016) (Ansari et al., 2017)(Zhu et al., 2018)(Rathan et al., 2019) when alginate and GelMA had been used in tissue engineering, suggesting further improvements in bioink design is required to engineer phenotypically stable cartilage. Interestingly, IPNs reinforced with PCL did not spontaneously calcify during chondrogenic culture. While the exact mechanism for this remains unclear, it may be related to the different bulk mechanical

properties of the fibre-reinforced IPN, which in turn will alter contraction of the construct as well as nutrient transport during *in vitro* culture. Alginate alone has been used in cartilage tissue engineering in the past since it forces cells to assume a rounded phenotype (Daly, Critchley, Rensock, & Kelly, 2016a; Rowley, Madlambayan, & Mooney, 1999) due to its lack of cell-matrix interaction sites. In contrast GelMA possesses cell-binding RGD motifs for example which enable encapsulated cells to spread and assume a more fibrochondrocyte-like phenotype as they have been found in meniscus cell populations (Daly, Critchley, et al., 2016a; Levett et al., 2014)(Makris et al., 2011b).

Stimulation of MSC encapsulated within the IPNs supported the development of a cartilaginous tissue rich in sGAGs and Col II, which stained less intensely for Col I deposition. Compositionally, this is similar to the inner region of the meniscus, but different to the outer region of the meniscus, which consists predominately of Col I. Engineering tissues more mimetic of the outer region of the meniscus will likely require altering the biochemical and biophysical cues used to direct the differentiation of BMSCs. For example, different combinations of growth factors can be used to promote fibro-chondrogenic differentiation of stem/progenitor cells. The spatio-temporal use of CTGF and TGF-β has been shown to stimulate secretion of Col I, or Col II and sGAGs in sections of constructs designed to mimic the outer and inner zone of the meniscus, respectively (Chang H Lee et al., 2014; Nakagawa et al., 2019a). Alternatively, the composition of the bioink can be altered to module BMSC phenotype. The addition of meniscus ECM of the inner or outer zones has previously been shown to induce increased gene expression of Col I or Col II and AGG, respectively.(Rothrauff et al., 2017; Shimomura et al., 2017)

The dynamic mechanical properties of the fibre-reinforced IPNs were found to increase with time in culture as the encapsulated BMSCs secreted a cartilaginous matrix. This resulted in the development of engineered tissues that better mimicked the

biomechanical characteristics of meniscal tissue. An unexpected drop in stiffness of the IPN alone between day 21 and day 42, however, can be related to errors in testing due to changes in sample shapes over time in culture. This was only corrected in later studies through removal of swollen volumes in order to ensure flat surfaces for even contact with the compression platens. A complex compressive testing protocol was employed to analyse both the flow dependent (ramp & dynamic modulus) and flow independent (equilibrium modulus) mechanical properties of the hydrogels and engineered tissues. The equilibrium modulus provides insight in the behaviour of the solid phase of the construct once fluid is no longer flowing through the tissue. In contrast, both the ramp modulus and the dynamic modulus are dependent on the level of fluid pressurization generated in the tissue during loading and the associated flow of fluid. The extent of fluid pressurization during loading of cartilage depends on the permeability of the tissue (Gannon et al., 2012), with lower permeability leading to higher levels of fluid pressurization and hence stiffer tissues during dynamic loading.

While the dynamic mechanical properties of the fibre-reinforced IPNs increased with time in culture, approaching that of the meniscus, the equilibrium (flow-independent) mechanical properties of these constructs were notably higher than that of the native tissue.

This suggests that the solid phase of meniscal tissue is inherently less stiff than that of the fibre-reinforced IPN. The fact that the dynamic properties are comparable suggests that the permeability of meniscus is lower than that of the hereby engineered tissue. Further studies are required to better understand the physiological relevance of these subtle differences in structure-function relations.

4.5. Conclusion

To summarize, this chapter successfully identified an IPN of alginate and GelMA as a favourable bioink for meniscus tissue engineering due to its shear thinning

properties. In addition, BMSCs encapsulated within this IPN bioink can secrete a cartilaginous matrix, improving the mechanical properties of the construct such that they better mimic the dynamic properties or the native meniscus. Thus, this research further closes a knowledge gap in the literature in the development of materials for 3D bioprinting of cartilage and fibrocartilage. However, the secreted matrix has been found to undergo slight calcification as well as to mainly consist of collagen II in contrast to native meniscus tissue which consists predominantly of Col I. Chapter 5 will therefore focus on tailoring the composition of the IPN bioink further in order to increase Col I production and hence the development of a tissue more representative of the normal meniscus.

Chapter 5

CREATION OF ZONAL SPECIFIC BIOINKS OF THE MENISCUS BASED ON SOLUBILIZED ECM

5.1. Introduction

In chapter 4 a shear thinning bioink was developed which was capable of supporting the robust chondrogenic differentiation of BMSCs. However, meniscus tissue has a more fibro-cartilaginous composition, with higher levels of Col I in its matrix. Bioengineered meniscal tissues/implants typically fail to accurately mimic the complex composition and structure of the matrix of native meniscus tissue. This chapter will therefore focus on the development of meniscus-specific bioinks, with the goal of developing printable hydrogels with biochemical compositions that mimic the different regions of the meniscus.

The meniscus consists of an inner white zone and an outer red zone which differ in vascularization, innervation, biochemical properties, ECM composition, and cell population among others (Makris et al., 2011b). In recent years it has been demonstrated that ECM derived biomaterials can direct the tissue-specific differentiation of stem cells. For example, it has been demonstrated that solubilised tendon can promote tendogenic differentiation of MSCs, while solubilised AC promotes the chondrogenic differentiation of MSCs (Yang et al., 2013). In the context of meniscus tissue engineering, it has been demonstrated that ECM from the inner regions of meniscus enhances expression of Col II and aggrecan, while ECM for the outer region of the meniscus promotes the expression of Col I (Romanazzo et al., 2017; Rothrauff et al., 2017; Shimomura et al., 2017). These finding can be attributed, at least in part, to the unique compositions of the different regions of the meniscus.

Specifically, the outer zone has shown to be composed of mostly Col I as well as a low sGAG content. The inner zone, however, has been reported to consist of only 40% Col I and 60% type II as well as a higher degree of sGAGs (Makris et al., 2011a). Col II hydrogels have been shown to promote a more chondrogenic phenotype in MSCs compared to Col I hydrogels. A limitation of ECM derived hydrogels for tissue engineering applications is their poor mechanical properties. This motivates the development of new ECM functionalised hydrogels and bioinks that retain their biological activity whilst simultaneously being capable of supporting the challenging mechanical environment within the knee.

The objective of this chapter is two-fold. Firstly, recognising that the outer meniscus zone is populated by cells with a more fibroblast-like phenotype, while the inner zone is populated by more chondrocyte-like cells, this chapter will first explore how the relative levels of alginate and GelMA within an IPN will influence the fibro-chondrogenic differentiation of BMSCs. Different materials have been used in the past in meniscus tissue engineering to reflect that through the use of gels with a varying amount of cells-binding motifs or gels with different degrees of stiffness which promotes or prohibits cell spreading or migration (G Bahcecioglu et al., 2019; Gokhan Bahcecioglu et al., 2018). Alginate lacks cell-binding domains and MSCs typically adopt a round morphology upon encapsulation, whiles cells typically bind and spread within GelMA hydrogels. The following study will therefore analyse the effects of differing amounts of alginate (which promotes a more rounded, chondrogenic phenotype) and GelMA (which allows for cell-matrix interaction and allows for a more spread cell phenotype) on BMSC differentiation within an alginate-GelMA IPN.

However, a more direct approach in tissue engineering is to stimulate cell differentiation through decellularized meniscus ECM components (Pati et al., 2014; Rothrauff et al., 2017; Shimomura et al., 2017). The second objective of this study was therefore to create two solubilized meniscus ECM based bioinks based on a protocol

previously established for growth plate and AC (Almeida et al., 2014; Browe et al., 2019), with a view to further enhancing meniscus region specific differentiation of BMSCs. In order to create a biomaterial based on native tissue, the targeted tissue has to be treated with physical and/or chemical means in order to create a material which can be rendered printable. Furthermore, the material has to undergo decellularization steps in order to remove cellular material (e.g. DNA) which causes an immunological response upon implantation of the material, whilst retaining the matrix proteins responsible for promoting a specific cell response (Visser, Levett, et al., 2015). Following solubilization of ECM isolated from the inner and outer regions of porcine meniscus, a rheological characterization of the resulting biomaterials was carried out with the aim of analysing their shear thinning properties. IPNs of alginate and GelMA, combined with the solubilized ECM fractions, were then engineered with the aim of investigating their capacity to promote fibrochondrogenic differentiation of MSCs.

5.2. Methods

5.2.1 Tissue solubilisation

A protocol established by my colleagues previously (Dudurych, 2015) was used to decellularize and solubilize porcine meniscus tissue. To summarize, porcine menisci from 3 months old female pigs were circumferentially cut from horn to horn into two zones of equal thickness(Fig.5.1 a). The zones were then cut into pieces < 1 mm, freeze dried for 24 hrs at -10°C and 0.2 mbar vacuum and cryo-milled (freezer mill 6770, SPEX sample Prep) in liquid N2. Consecutively, the powder was then dissolved in 0.2 M NaOH (1 ml/ 50 mg wet tissue) for 24 hours at 4°C. After centrifugation at 2500 G at 4°C for 10 minutes, the pellet was twice washed with ultra pure water and centrifuged under the same conditions. Furthermore, the pellet was digested in pepsin (1500 U / 1 ml 0.5 M acetic acid (HAc) / 50 mg wet tissue, Sigma Aldrich) for 24 hours under agitation at room temperature. After a centrifugation step at 2500 G for 1 hour at

4°C the supernatant was subject to a salt precipitation step. 5M NaCl was added so the salt concentration was adjusted to 0.8 M for the outer meniscus zone and 0.9 M for the inner zone and equilibrated over night at 4°C and consecutively centrifuged for 1 hour with 2500 G at 4°C. The pellet was then resuspended in 0.5 M HAc and the salt precipitation step was repeated. In the next step the precipitated pellet was dialyzed against 0.02 M Na_2HPO_4 (pH 9.4) through a membrane of 12-14 kDa pore size for 24 h at 4 °C before freeze drying it for 20 hrs again at -10°C and 0.2 mbar vacuum.

5.2.2 Rheology

Rheological analysis of the used materials was conducted as described in **chapter 4.**

5.2.3 Preparation of constructs

Solubilized and freeze dried inner and outer ECM was first cut into pieces < 1 mm before being sterilized via ETO gas for 12 hours and left to evaporate for 1 day. All further steps were then conducted under sterile conditions. Next, 1.3% [w/V] of inner and outer ECM was dissolved in sterile filtered 0.12M HAc (pH 4) with 0.15 mg/ml phenol red under constant rotation at 4°C for 48 hours. After completely dissolving the pH of the ECM was adjusted to 7 using sterile 5M NaOH. Next 12% [w/V] LVG sodium alginate (Pronova) in DMEM was mixed with the dissolved ECM and 0.5% irgacure 2959 (Sigma) in a ratio of 3:3:1 using syringes connected with a luer-lock adapter. BMSC were isolated and cultured as described in chapter 3. After trypsinization and centrifugation cells were then dissolved in 17% [w/V] GelMA in a cell density of $67*10^6$ cells/ml. The mixture of GelMA and cells was then mixed with the mixture of ECM, alginate and irgacure in a ratio of 3:3:3:1 to receive a bioink with final concentrations of 3.5% GelMA, 5% alginate, 0.4% inner or outer ECM, 0.05% irgacure 2959 and a cell density of $20*10^6$ cells/ml. The bioink was then pipetted through a cylindrical 23G needle into moulds of 3% agarose and 45 mM $CaCl_2$ and crosslinked as described in **chapter 4.**

IPN gels of 3.5% alginate and 5% GelMA were prepared as described in **chapter 4**. IPN gels of 1% alginate and 10% GelMA were prepared by dissolving 2.2% LVG alginate in DMEM and 22% GelMA in DMEM, then dissolving cultured BMSCs in GelMA at a cell density of $44*10^6$ cells/ml. GelMA with cells, alginate and 0.5% irgacure 2959 were then mixed in a ratio 4.5:4.5:1. The mixed bioink was then pipetted into agarose and $CaCl_2$ moulds and crosslinked as described in **chapter 4.**

5.2.4 Scanning Electron Microscopy (SEM)

Samples were dehydrated in a graded ethanol series with concentrations of 50% (2 x 10 min), 70% (2 x 10 min), 90% (2 x 10 min) and 100% (2 x 15 min). They were then immersed in hexamethyldisilazane (HMDS) (2 x 15 min) and allowed to dry overnight. Samples were then mounted on SEM stubs and coated with gold/palladium for 90s at a current of 40mA using a Cressington 208HR sputter coater. SEM imaging was conducted at 5kV in a Zeiss ULTRA plus.

5.2.5 Cell culture

Cell culture was conducted as described in **chapter 4.**

5.2.6 Biochemical analysis

Biochemical analysis was conducted as described in chapter 4. Furthermore, a calcium assay was conducted on samples without papain digest. Samples were first digested in 1M HCl at 60°C under constant rotation for 4 days before analysing them using a calcium liquid colorimetric assay (Alpha laboratories, Sentinel Diagnostics). Values were normalized by gel weights.

5.2.7 Histological analysis

Histological analysis was conducted as described in **chapter 4**

5.2.8 Mechanical characterization

Mechanical characterization was conducted as described in chapter 4 with the exception that gels were cut to cylinders with flat bases in order to ensure contact with compression platens.

5.2.9 Statistical analysis

Data was expressed as mean and standard error of the mean. Significance was calculated using the student t-test with Welch's correction or ANOVA and Tukey's post-hoc test. Differences were considered to be statistically different at $p \leq 0.05$ (*), $p \leq 0.001$ (**), $p \leq 0.0005$ (***) and $p \leq 0.0001$ (****), $n = 6$

5.3. Results

5.3.1 Solubilized ECM from the inner and outer zone of meniscus tissue improves the shear thinning properties of IPN based bioinks

The inner and outer region of porcine meniscus tissue was first solubilized and then incorporated into the IPN based bioink developed in chapter 4. A picogreen assay demonstrated a significant reduction in DNA levels within solubilized tissue, below 50 ng/mg dry weight in both the inner and outer ECM. Furthermore, the levels of sGAGs and collagen within the ECM were reduced by the solubilization treatment, however the ratio of their levels in the inner and outer zone remained unchanged (Fig. 5.1).

Following solubilization, the ECMs were mixed with the IPN (3.5% alginate and 5% GelMA), at a concentration of an additional 0.4% inner (termed *inECM*) or outer ECM (termed *outECM*). A rheological characterization of the bioinks was then conducted in order to assess the effect which the addition of ECM had on their rheology and shear thinning properties. An analysis of the viscosity as the function of shear stress revealed that the viscosity of the solubilised ECM alone was very low, but still showed high shear thinning properties. However, when mixed with the IPN of 3.5%

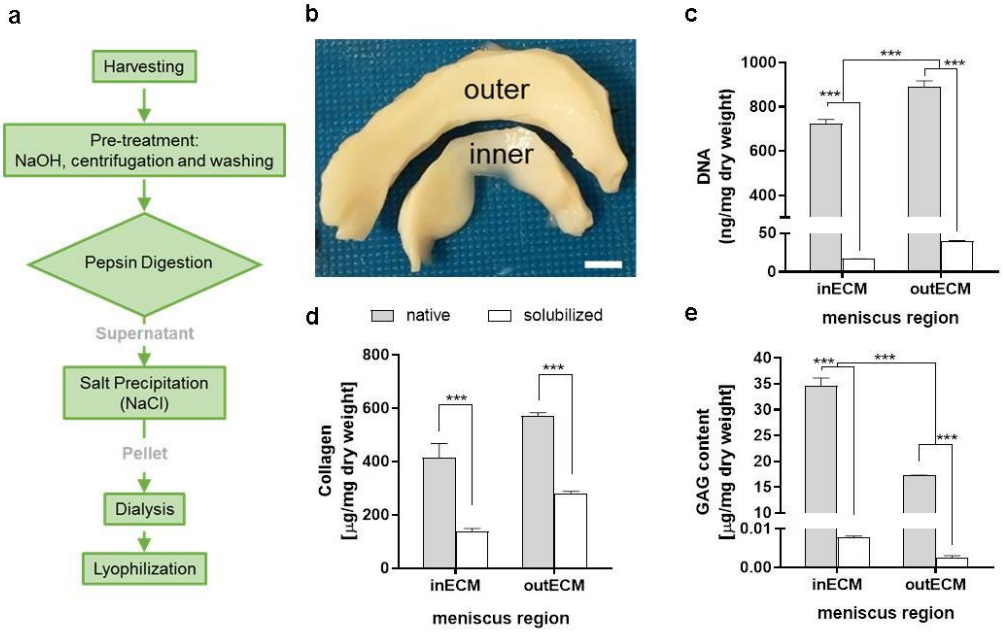

Fig. 5.1 Meniscus solubilization: Porcine menisci were dissected into inner and outer regions and solubilized (a-b), before analyzing native and solubilized DNA content(c), collagen content (d) and sGAG content(e). Scale bar 5 mm. $p \leq 0.05$ (*), $p \leq 0.001$, n = 3

alginate and 5% GelMA, the resulting bioinks showed a significant increase in both viscosity and shear thinning properties (Fig. 5.2 a-b). Specifically, when fitting the data to the Herschel-Bulkely model Eq. 4.1) the flow index n decreased further compared to the IPN alone, indicating a higher shear thinning effect (Fig. 5.2 c). Furthermore, an increase in yield stress τ_0 and consistency index k was also observed (Fig. 5.2 d-e). Specifically, when adding *outECM* to the IPN of alginate and GelMA, the shear thinning behaviour and consistency further increased compared to adding *inECM*, as seen through the lower flow index, as well as increased yield stress and consistency index (Table 5.1).

Table 5.1 Herschel-Bulkley model of rheological analysis

	n	k [Pa*s^n]	τ_0 [Pa]	R^2
0.4% outECM	0.475	0.314	0.091	0.992
0.4% inECM	0.510	0.277	0.092	0.998
3.5% Alg/	0.594	20.600	8.851	0.997
3.5% Alg/ 5% GelMA /	0.305	87.852	49.433	0.991
3.5% Alg/ 5% GelMA /	0.444	39.997	14.672	0.998

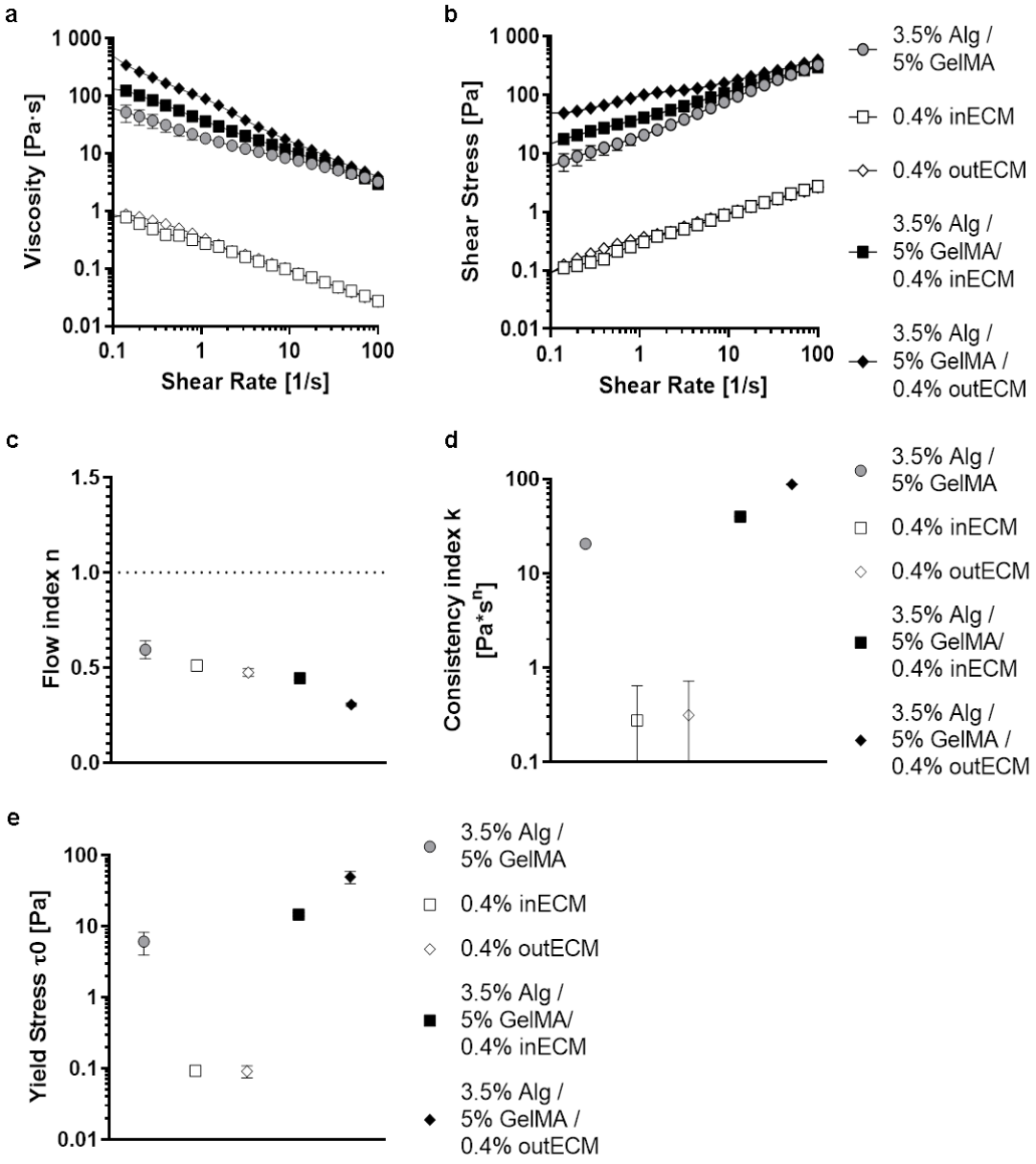

Fig. 5.2 Rheological analysis: A rheological analysis to assess the viscosity (a) and shear stress (b) as a function of shear rate was fitted to the Herschel-Bulkely model to calculate the flow index (c), consistency index (d) and yield stress (e). n = 3 in triplicates

5.3.2 Solubilized ECM increases tissue calcification in chondrogenic analysis

After mixing the four different bioinks of 1% alginate / 10% GelMA, 3.5% alginate / 5% GelMA, 0.5% alginate / 5% GelMA / 0.4% inECM and 0.5% alginate / 5% GelMA / 0.4% *outECM* with BMSCs they were crosslinked via UV light and $CaCl_2$ and

cultivated in chondrogenic media with TGF-β3 and physioxic culture conditions for 42 days.

An SEM analysis of the mixed and cross-linked bioinks showed a smoother surface of the IPN of 1% alginate and 10% GelMA compared to 3.5% alginate and 5% GelMA. Furthermore, the addition of 0.4% ECM of inner or outer meniscus zone revealed a surface with a deeper network of pores compared to alginate and GelMA alone (Fig. 5.3 a). Macroscopical observation of the MSC laden constructs after 42 days of culture revealed the development of large white sections of tissue being formed in the inside of constructs of all groups (Fig. 5.3 b). However, Live/Dead staining revealed a decrease in viability after 3 weeks of culture in all groups, which slightly recovered by day 42. (Fig. 5.4).

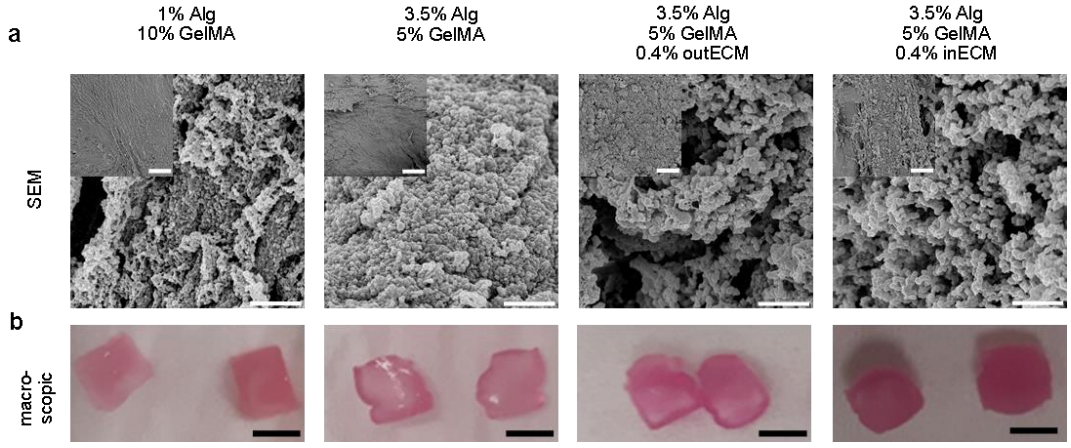

Fig. 5.3 Macroscopic and SEM imaging: SEM imaging was conducted before (a) and a microscopical analysis after 42 days of culture scale (b) scale bars. 1 mm, 100 µm, Work has been done in conjunction with Kian Eichholz, PhD.

A pico-green assay to measure DNA levels in the cultured constructs revealed a significant decrease in the DNA content of all bioinks except for the IPN of 1% alginate and 10% GelMA. DNA levels remained constant in the bioink of 1% alginate / 10% GelMA, as were sGAGs and collagen levels, but an increase in calcification was detected. The bioinks of 3.5% alginate / 5% GelMA, as well as those functionalised with 0.4% *inECM* or *outECM*, showed a significant decrease in DNA levels. Total

collagen and sGAG levels in the gels remained constant, but increased when matrix levels were normalized to DNA levels. Calcium accumulation also increased after 42 days of culture in these constructs (Fig. 5.5).

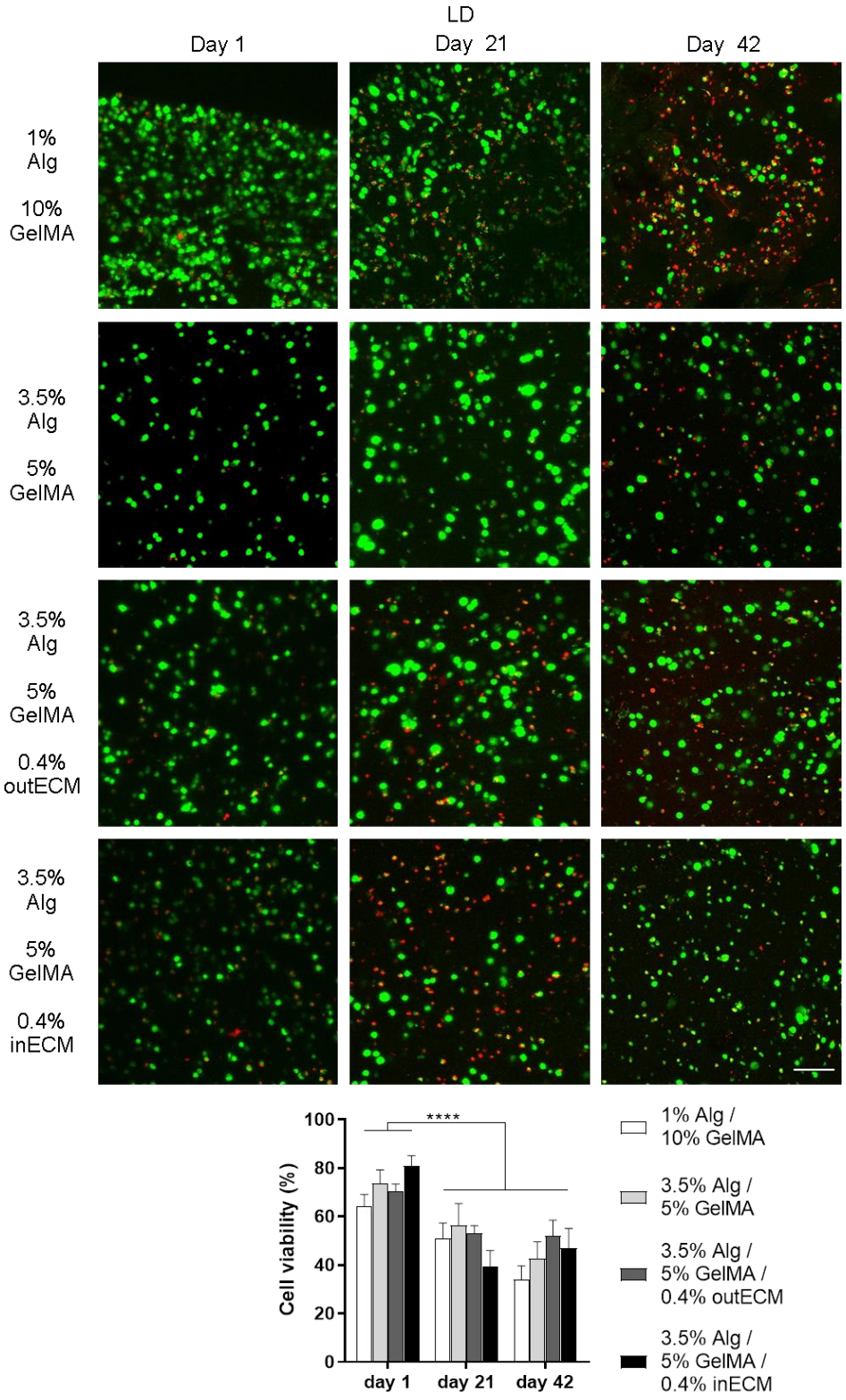

Fig. 5.4 Live/Dead imaging and quantification: Cultured constructs were stained via Live/Dead assay to quantify their viability. Scale bar 100 µm. $p \leq 0.05$ (*), $p \leq 0.001$ (**), $p \leq 0.0005$ (***) and $p \leq 0.0001$ (****). n = 3

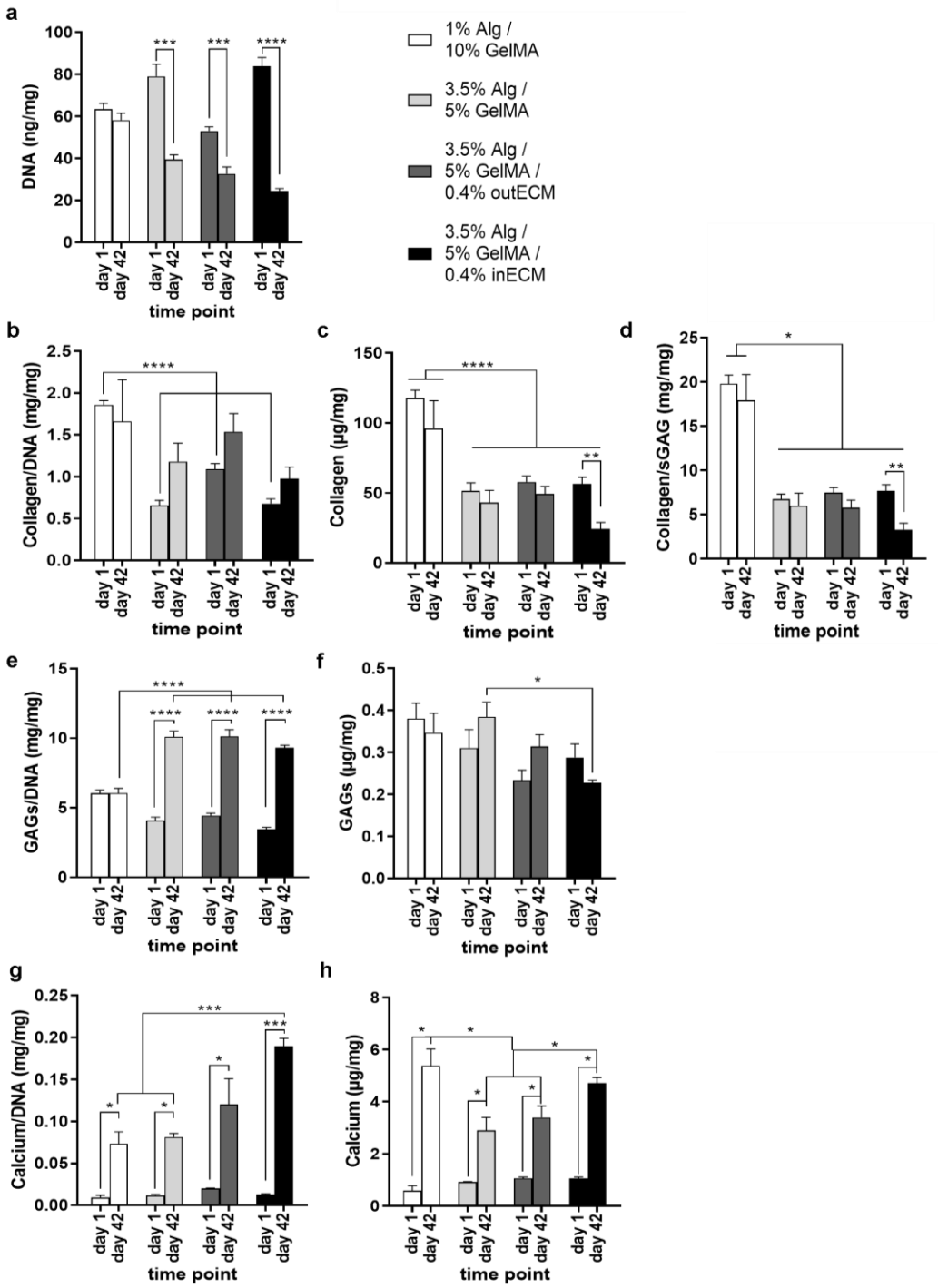

Fig. 5.5 Biochemical analysis: A biochemical analysis of DNA(a), collagen(b-c), sGAG(d-e) and calcium levels (f-g) of BMSCs in IPN and IPN + PCL was conducted. $p \leq 0.05$ (*), $p \leq 0.001$ (**), $p \leq 0.0005$ (***) and $p \leq 0.0001$ (****). n = 3

Histological analysis revealed only low and mostly pericellular secretion of sGAGs in all gels through an Aldehyde Fuchsin/Alcian Blue staining (Fig. 5.6). The Picrosirius Red staining revealed only a slight increase in collagen secretion in those 3 groups as well as a layered pattern in gels containing *inECM* and *outECM*, which had disappeared at the time point of 3 weeks (Fig. 5.7). Furthermore, the Alizarin Red staining showed a distinct increase in calcification in those three bioinks by day 42, especially in the bioink mixed with *outECM* (Fig. 5.8). In contrast, the bioink of 1% alginate and 10% GelMA showed a very different internal structure to the other three gels as seen through Aldehyde Fuchsin/Alcian Blue and Picrosirius Red stainings. While the outer layer of the gels seemed to be of a homogenous composition, their cores showed a heterogeneous separation of two materials with differently intense staining as well as hollow sections in between them (Fig. 5.5).

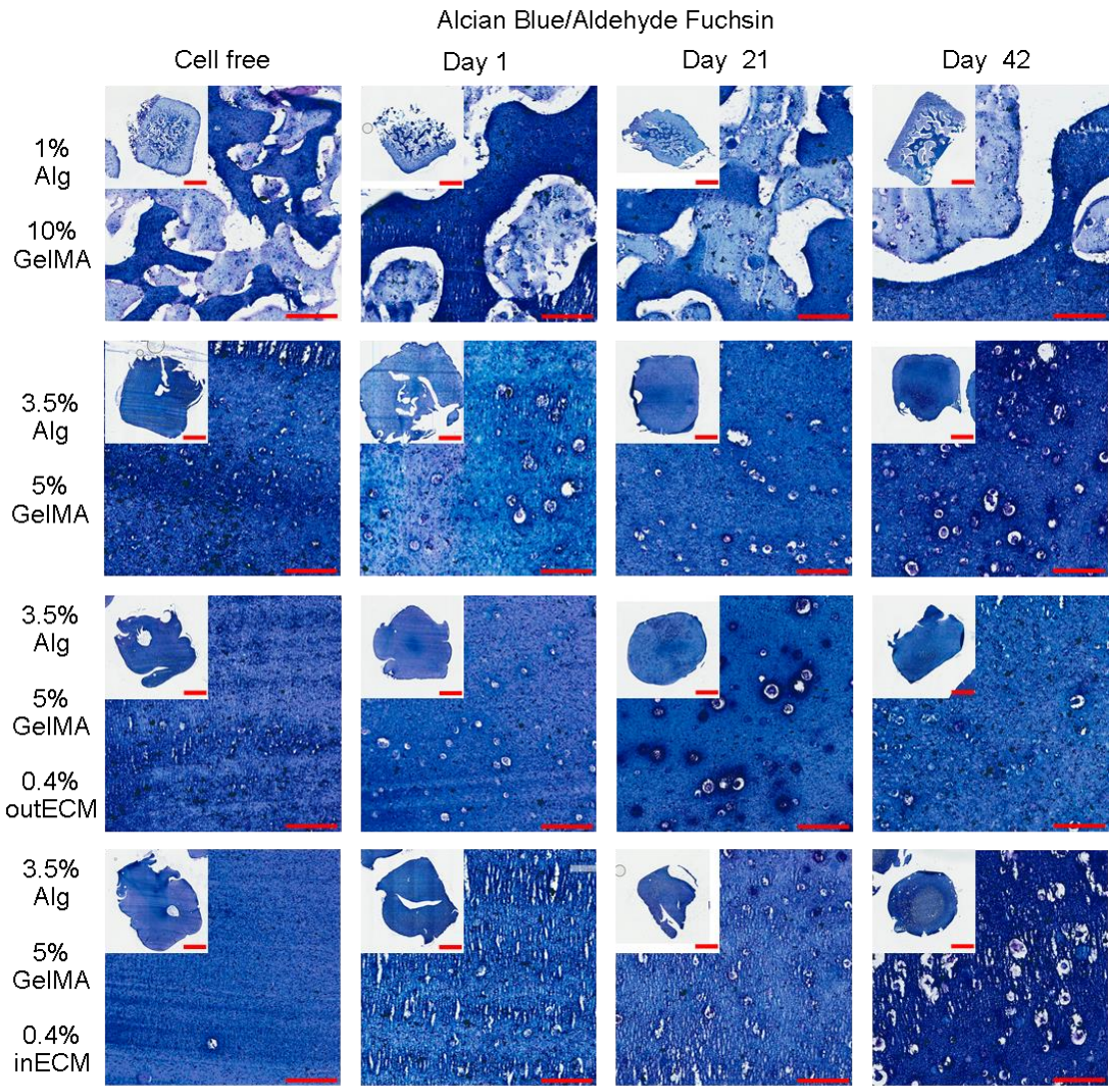

Fig. 5.6 Histologcal staining via Alcian Blue/Aldehyde Fuchsin: Histological analysis of cultured scaffolds over the course of 42 days via Alcian Blue/Aldehyde Fuchsin. Scale bars: 1 mm and 100 µm. n = 3

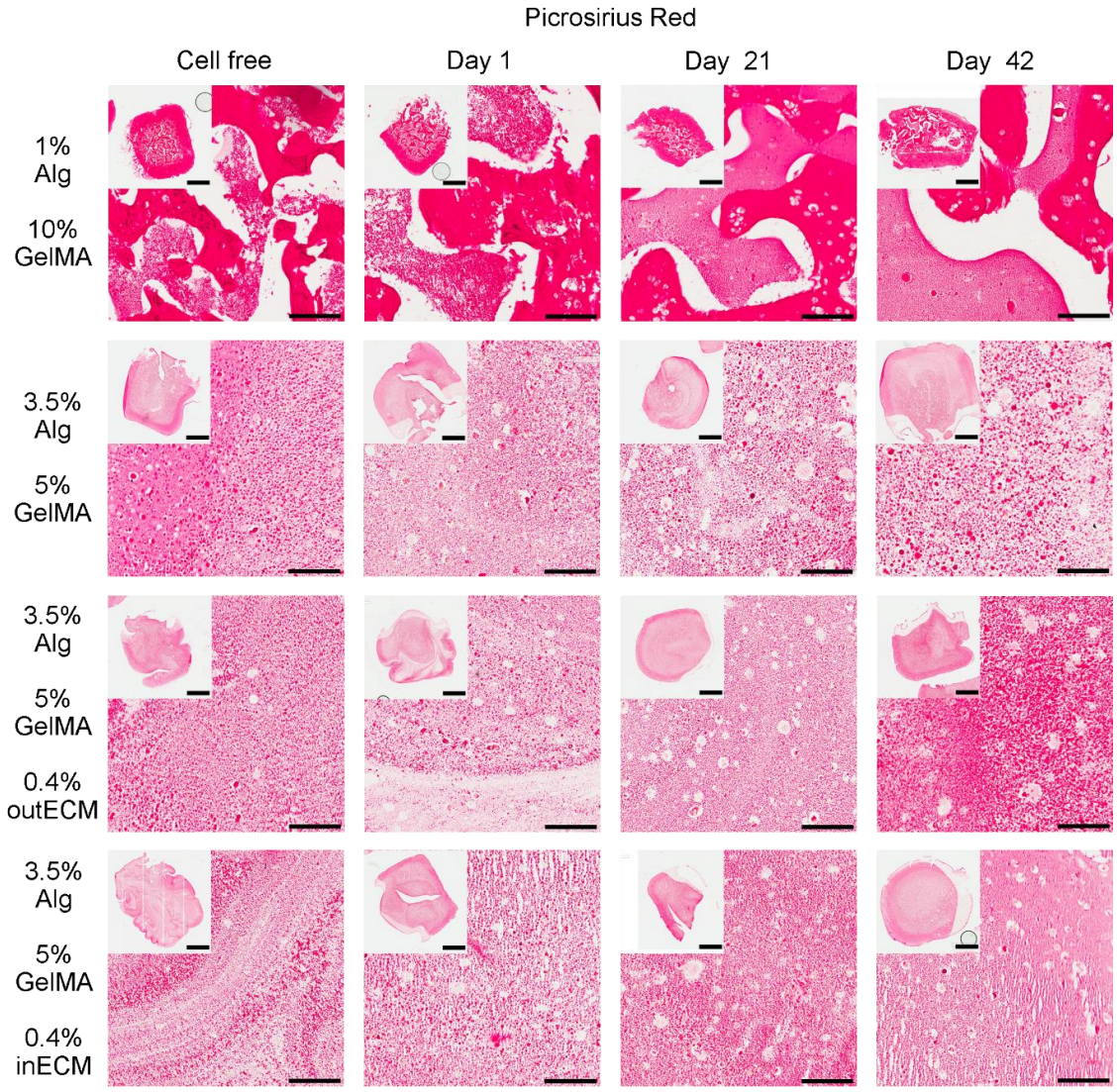

Fig. 5.7 Histological staining via Picrosirius Red: Histological analysis of cultured scaffolds over the course of 42 days via Picrosirius Red. Scale bars: 1 mm and 100 µm. n = 3

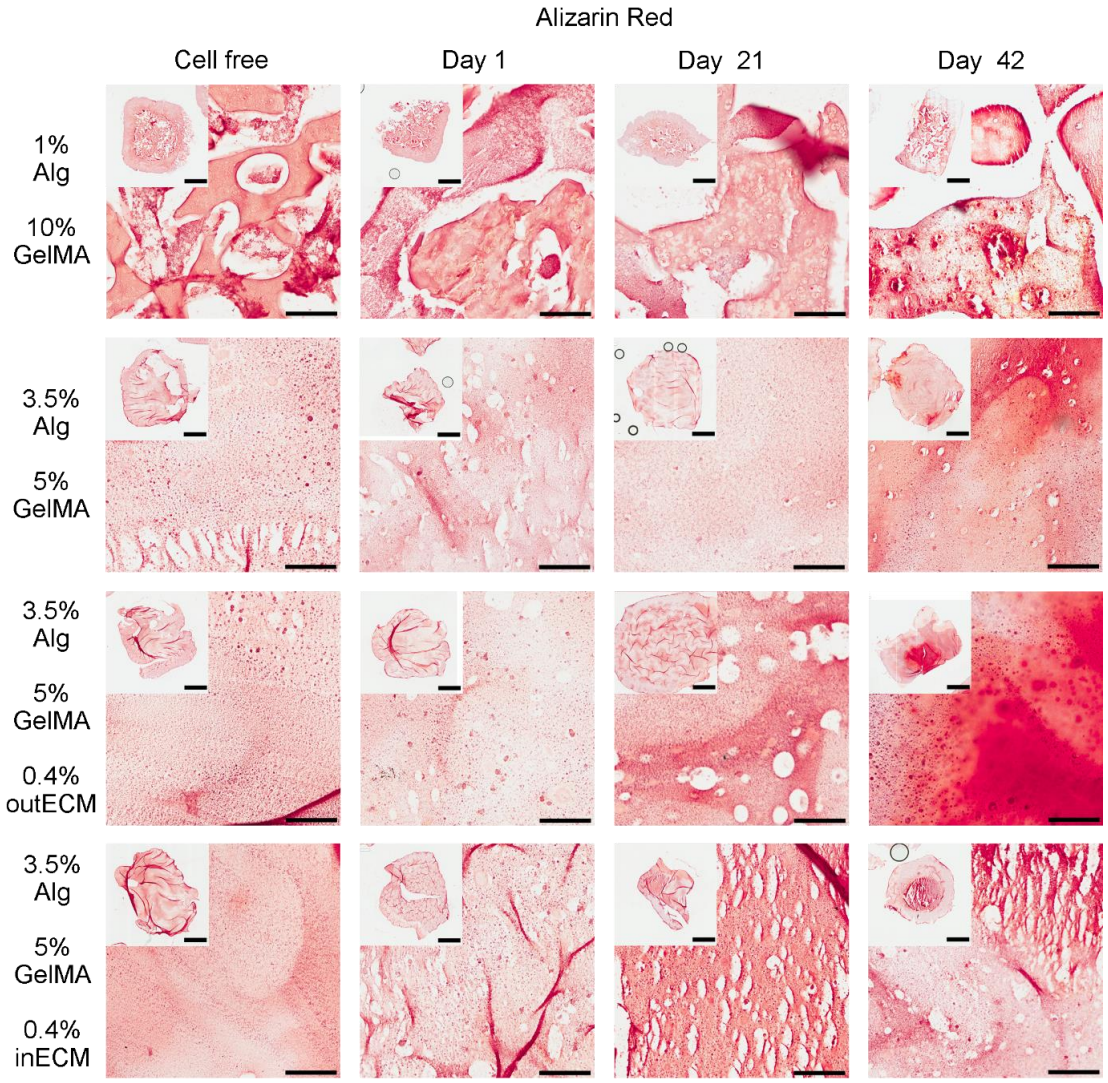

Fig. 5.8 Histological staining via Alizarin Red: Histological analysis of cultured scaffolds over the course of 42 days via Alizarin Red. Scale bars: 1 mm and 100 µm. n = 3

An increase in elastic, dynamic and equilibrium modulus in bioinks of 3.5% alginate, 5% GelMA and 0.4% inner or outer ECM was observed after 42 days of culture. The bioink of 1% alginate and 10% GelMA was shown to be the softest of all groups (Fig. 5.9).

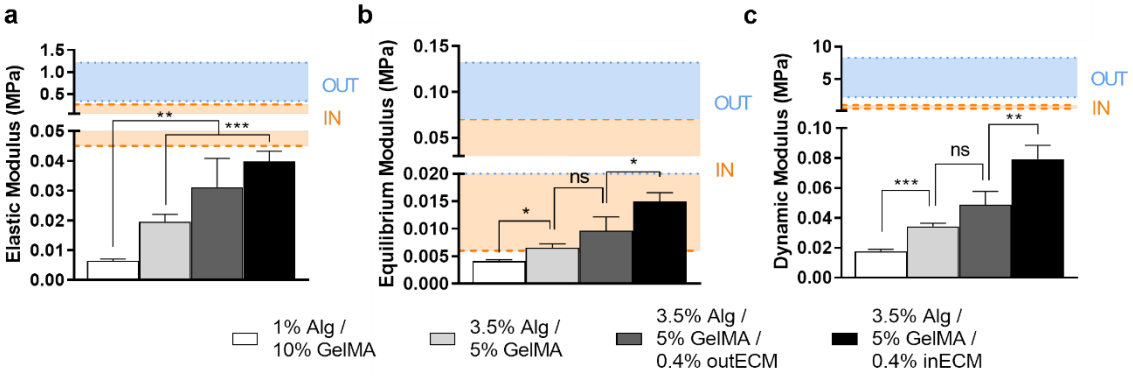

Fig. 5.9 Mechanical testing of gels: A compressive testing regime was employed to test the elastic (a), equilibrium (b) and dynamic modulus (c) after 42 days of culture as well as the moduli of native porcine meniscus samples of the inner and outer zone. $p \leq 0.05$ (*), $p \leq 0.001$ (**), $p \leq 0.0005$ (***). n = 4

To summarize, inner and outer meniscus tissue were successfully solubilized and their viscoelastic properties were demonstrated to further increase the shear thinning properties of a developed bioink of alginate and GelMA. However, a cell study with BMSCs in chondrogenic media over 6 weeks showed low cell viability and relatively poor cartilagenous matrix production as well as increased construct calcification.

5.4. Discussion

Chapter 4 demonstrated the IPN of alginate and GelMA as a suitable bioink for meniscus tissue engineering due to its shear thinning properties and its capacity to support robust chondrogenesis of BMSCs. The overall goal of this current chapter was to further develop the alginate and GelMA based bioink to promote more meniscus-specific matrix secretion. Specifically, the aim was to mimic the specific collagen types and sGAG of the inner and outer region of the meniscus within ECM functionalised

bioinks, based on the belief that this would enhance their capacity to support meniscus-specific differentiation of BMSCs (C H Lee et al., 2014; Rothrauff et al., 2017; Shimomura et al., 2017). This was achieved through both the variation of the IPN composition as well as through an addition of decellularized meniscus ECM components. To summarize, inner and outer meniscus tissue were successfully solubilized and their viscoelastic properties were demonstrated to further increase the shear thinning properties of a developed bioink of alginate and GelMA. However, a cell study with BMSCs in chondrogenic media over 6 weeks showed low cell viability and relatively poor cartilaginous matrix production as well as increased construct calcification.

The success of the solubilization protocol for efficiently decellularizing the ECM was confirmed by demonstrating a reduction in DNA content to below 50 ng/mg, which has been suggested as the threshold necessary to avoid immune responses upon implantation of an ECM derived material (Crapo, Gilbert, & Badylak, 2011b). Furthermore, the collagen and sGAG contents were also reduced by the solubilization treatment, but the collagen:sGAG ratio for the solubilised ECMs was comparable to that of the native tissue. This retained ratio suggests a maintenance of the relative number of binding sites for specific growth factors and cell binding sites which have been associated with promoting chondrogenesis (Rutgers et al., 2012)(Schneiderbauer, Dutton, & Scully, 2004). Moreover, the solubilized ECM fractions, which were rich in collagenous proteins, were found to possess low viscosities alone but strong shear thinning properties, as assessed by fitting the rheology data to the Herschel-Bulkley model. Consequently, when combined with the previously developed IPN of 3.5% alginate and 5% GelMA, a significant increase in both viscosity and shear thinning behaviour was observed, especially for the outer meniscus ECM. This improvement rheological properties (for bioprinting applications) through the incorporation of collagen into bioinks has been explained through a change

in their fibre orientation under shear forces during extrusion (Malda et al., 2013). To summarize, the solubilized ECM fractions were developed into highly shear thinning bioinks, retaining ratios of sGAG:collagen that may prove beneficial for promoting either an inner or outer meniscus phenotype.

To assess the capacity of these ECM functionalised IPN bioinks to support chondrogenesis, they were loaded with BMSCs and maintained in culture for 42 days. During this time period, no increase in sGAG or collagen levels were detected. Furthermore cell viability was low and the engineered constructs calcified in culture. These negative findings were also observed in the IPN control group (3.5% alginate and 5% GelMA), which in chapter 4 was shown to support robust chondrogenesis of BMSCs. This suggests that the specific batch of BMSCs used in this experiment may have possessed a limited capacity for chondrogenesis. Calcification of cartilaginous tissues engineered using BMSCs is a well documented limitation of this cell source (Rathan et al., 2019). Alternative cell sources could be explore in the future, including fat-pad derived MSCs which have shown to be less prone to calcification and tend to produce tissue rich in both Col I and II, which would be ideal for meniscus tissue engineering (Browe et al., 2019; Luo, Thorpe, Buckley, & Kelly, 2015; Romanazzo et al., 2017)(Almeida et al., 2014). Furthermore, employing a different solubilization protocol based on alternative strategies which are being discussed in the field at the moment could further improve the bioink. For example, a protocol based on urea as it has been reported, which could avoid calcification while driving a differentiation response distinguishable between inner and outer phenotype (Shimomura et al., 2017)(Y. Zhang et al., 2009). In addition, avoiding a pepsin-digestion step has been reported to increase the fraction of low to moderate molecular weight proteins in the ECM fraction, which improved the fibroinductive signals conveyed by the biomaterial (Visser, Levett, et al., 2015). A further challenge in engineering tissues with phenotypical differences representative of the inner and outer meniscus zones is the

common use of TFG-β3 to support MSC differentiation. This growth factor is necessary to promote a robust chondrogenic response, but has also been shown to dilute phenotypically different responses between two zones (Rothrauff et al., 2017).

To summarize, the bioinks developed for the different anatomical meniscus zones based on alginate, GelMA and solubilized ECM showed a high degree of shear thinning. However, no evidence was found to support the hypothesis that meniscus ECM functionalization promotes a more fibrochondrogenic response over the IPN only developed in chapter 4, which showed a stable chondrogenic response when loaded with BMSCs. The improvement in shear thinning characteristics of the two developed bioinks motivates further investigation into the printability of such materials. Given the concerns related to the specific batch of BMSCs used in this study, further studies are warranted to investigate the fibro-chondrogenic potential of solubilised meniscus ECM. Finally, additional studies are required towards scaling up of bioprinted tissues to produce an anatomically correct tissue engineered meniscus construct.

5.5. Conclusion

The solubilized ECM fractions of inner and outer meniscus failed to improve the fibrochondrogenic potential of the developed IPN based bioinks but significantly improved their shear thinning and viscoelastic behaviour. Next, chapter 6 was then focused on scaling up the printing process and to create an anatomically shaped and sized meniscus construct based on the scaffold parameters and bioinks, which had been developed in the previous chapters.

Chapter 6

3D BIOPRINTING OF SCALED UP, BIOMIMETIC MENISCUS CONSTRUCTS

6.1. Introduction

Partial meniscectomies are still widely performed when surgically treating damaged meniscal tissue, despite the fact that this procedure is associated with a 4-fold increase in the risk of developing OA (M Englund, Roos, & Lohmander, 2003). Similarly, in case of severe meniscal damage, total meniscectomies are conducted despite a 14-fold associated increase in risk of development of OA (H. Roos et al., 1998). Total meniscectomies are then followed by allograft transplants, which are still commonly considered the gold standard to replace the removed meniscus tissue. However, shortages of health donor menisci and a technically challenging surgical procedure have limited its widespread use. A number of implants to replace tissue following partial meniscectomies (Actifit™ and CMI®) are also in clinical use, however they do not restore normal meniscal tissue anatomy and joint function and clinical results are mixed (Leroy et al., 2016; Makris et al., 2011a; Monllau et al., 2011).

This is partially due to a number of limitations associated with such biomaterial scaffolds, in particular their failure to mimic the gross anatomy, internal structure and biomechanical behaviour of the normal meniscus. Modern biomaterial fabrication techniques like electrospinning and 3D printing strategies enable the engineering of implantable biomaterials that mimic specific aspects of the internal architecture and biomechanics of soft biological tissues (B. M. Baker & Mauck, 2007; Levato, Visser, Planell, & Engel, 2014; W.-J. Li, Cooper, Mauck, & Tuan, 2006; Visser, Melchels, et al., 2015). In spite of this, engineering implants that mimic both the external geometry and

internal architecture of the meniscus remains a challenge. More biomimetic tissue engineered meniscus implants could offer alternatives to allograft transplants for total meniscectomies and alternative approaches to existing constructs for treating partial meniscal defects.

In recent years, 3D bioprinting has been utilized to engineer biological constructs that mimic certain aspects of the structure, composition and biomechanics of native meniscus tissue (G Bahcecioglu et al., 2019; Gokhan Bahcecioglu et al., 2018; Chang H Lee et al., 2014; Szojka et al., 2017). For example, Szojka et al demonstrated an anatomically accurate 3D printed meniscus scaffold with PCL fibres mimicking circumferential collagen fibre directionality and explored offset fibre pattern to modulate the compressive properties of the construct. Lee et al and their follow-up study by Nakagawa et al printed an anatomically accurate PCL scaffold with PLA/PGA microspheres which contained CTGF and TGF-β3 to create a spatio-temporal release profile to recreate inner and outer zones. *In vitro* studies with human synovial cells showed increased levels of col I in the outer zone and col II and sGAG in the inner zone as well as mechanical reinforcement through the secreted matrix after 6 weeks in a mixture of chondrogenic and fibrogenic media. *In vivo* studies in sheep for 3, 6 and 12 months showed meniscal tissue formation and no signs of synovial inflammation, however in combination with damages to the meniscus extrusion and subsequent damages to the AC due to a lack of fixation to the tibial plateau (C H Lee et al., 2014; Nakagawa et al., 2019a). A more recent study filled varying compositions of GelMA and agarose into the pores of a meniscus shaped PCL scaffold in order to create an inner and outer zone where the authors reported varying cell morphologies and ECM composition to some degree. (G Bahcecioglu et al., 2019) Similar zonally engineered constructs were also achieved through a combination of dynamic mechanical and biochemical stimulation through CTGF and TGF-β3 in vitro and led to promising tissue regeneration in rabbit studies *in vivo* (Z.-Z. Zhang et al., 2017; Zheng-zheng Zhang et

al., 2019). However, scaling-up the 3D bioprinting process to engineer anatomically accurate cell-laden constructs that mimic the biomechanics and external geometry of the entire meniscus remains a challenge.

The *in vitro* maturation of such scaled-up biological constructs is a particular challenge, as limitations in sufficient nutrient and gas exchange throughout the engineered tissue can lead to cell death and limited matrix deposition (Rouwkema et al., 2013). Sacrificial hydrogels (e.g. pluronics 127) have previously been used to create nutrient channels in printed constructs (Daly & Kelly, 2019; Daly, Pitacco, Nulty, & Kelly, 2018). While such strategies can support nutrient transfer *in vitro* and vascularization of engineered tissues *in vivo*, using multiple biomaterials in the printing process further increases the complexity of the final implant and therefore the required time and quality control during the manufacturing process and adds further logistical challenges (Oropallo & Piegl, 2016). Multistage 3D printing processes are subject to variations at each stage and therefore require a high amount of quality control through feedback loops to minimize the propagation of errors during the printing process (Gibson, Rosen, & Stucker, 2010; Shi & Zhou, 2009)(Gibson et al., 2010; Shindo, Nurani, & Strojwas, 1998). Therefore consideration of the complexity of the printing process, as well as the time required for bioprinting of live cells, must be considered in the design of emerging 3D bioprinting strategies to produce scaled-up biological implants.

In previous chapters of this thesis, PCL printing patterns have been identified which are capable of mimicking the anisotropic and heterogenous mechanical properties of native meniscus. Moreover, chondrogenic bioinks which support a (fibro)chondrogenic phenotype were developed and combined with 3D printed PCL networks to develop composites believed compatible with implantation into load bearing environments. The aim of this study was to leverage these outputs and use 3D bioprinting to engineer a cell-laden meniscal construct that mimics the biomechanics

and the overall anatomical size and shape of the human meniscus. To this end, a rheological analysis and a series of 3D printing tests were conducted to identify the optimal temperature and extrusion pressure settings for each bioinks. Next, a recently developed 3D bioprinting technique, herein termed *z-printing*, was utilised in order to overcome some of the current challenges in printing complex, large-scale constructs. Lastly, 3D printing was utilised to produce MSC-laden implants mimicking the anatomy of the human meniscus, incorporating zone specific bioinks, channels to enhance nutrient transport and region specific biomechanics.

6.2. Methods

6.2.1 Preparation of bioinks

Bioinks of 3.5% alginate, 5% GelMA and 0.4% *inECM* or 0.4% *outECM* were produced as described in chapter 5.

6.2.2 Rheological analysis

Rheological analysis was performed in order to determine the gelation kinetics of the developed bioinks as a function of temperature using a MCR 102 Rheometer (Anton Paar, Austria) with a PP25 rotating plate and a measuring gap of 0.5 mm. Samples were allowed to equilibrate for 20 minutes at 4°C before the start of each measurement. Storage modulus (G'), loss modulus (G'') and the complex viscosity (η) were determined through a temperature sweep from 4°C to 37ºC with a temperature increase of 1°/min, a constant oscillating shear strain (γ) of 5% and an angular frequency (ω) of 10/s. Finally, the loss factor ($tan\ \delta$) was determined by calculating the ratio of G'' to G' Eq. 6.1. All measurements were conducted in triplicates.

$$tan\ \delta = \frac{G''}{G'}$$

Eq. 6.1

6.2.3 Spreading ratio

A 3D bioprinter from RegenHU (3D Discovery) was used to evaluate the printability of the developed bioinks. Materials were extruded through a cylindrical 23G needle (inner diameter = 337 mm) using a feed rate of 10 mm/s and a series of pressure settings into a pattern of 4 mm fibre spacing and 90° orthogonal orientation. The printability was then determined through a calculation of the spreading ratio as previously described (Daly, Critchley, Rensock, & Kelly, 2016b)Eq. 6.2. All measurements were conducted in triplicates.

$$Spreading\ ratio = \frac{Printed\ diameter}{Inner\ needle\ diameter}$$

Eq. 6.2

6.2.4 Z-printing

Z-printing and conventional 3D bioprinting technique were compared through a printed scaffold of PCL and two gels of Pluronics F127 (Sigma) with food coloring with 5 mm height as well as versions scaled to 10 and 15 height. The PCL scaffold of 1.5 mm edge length, 2 mm fibre spacing, aligned and double layered pattern was printed using a 3D Discovery printer (RegenHU, Switzerland) with parameters described in chapter 3. For conventional 3D bioprinting gel 1 and gel 2 were printed alternating with the extrusion of the PCL fibres in a commonly used and previously described pattern (Daly, Cunniffe, et al., 2016), as shown in figure 6.2 a. Extrusion settings for gel 1 and 2 were chosen at 13°C with cylindrical 23G needles, 1.75 bar and 10 mm/s speed. To conduct *z-printing* gel 1 and 2 were printed while moving along the z-axis through the pores of the PCL scaffold after the completion of all PCL layers. In contrast to conventional printing technique, where materials are alternated at each layer and extruded while moving along the x and y-axis (Fig. 6.2 a). First, the coordinates of each

pore were determined by manually finding positions on the x, y and z-axis of the 3D Discovery printer (Fig. 6.2 b). Then all coordinates were put into an algorithm written in visual basic (Table 6.1) to generate a G-code. This enabled the printing needle to vertically move into the selected pores and extrude gel 1 and 2 while exiting the pores through the top along the z-axis (Table 6.2). Gels were extruded at 13°C with 1.75 bar pressure through cylindrical 23G needle with 1/2 inch length to create the scaffold seen in Fig. 6.2 c. Printing times were measured for the full process as well as the duration of automatic changes of printheads in case of conventional 3D printing and manual changes for *z-printing*, as well as the printing times of each separate material. Printing times of scaffolds with the selected volumes were then fitted to a linear regression equation (Fig. 6.3 a-c).

6.2.5 Multistage process analysis of z-printing

Printing processes were described as multistage processes using simplified state space models(Shi & Zhou, 2009). Briefly explained, the key quality characteristics of the printed construct at stage *k* (e.g. hydrogel extrusion) can be represented by state vector x_k which depends on state specific process variables like input u_k (e.g. extrusion pressure) and error w_k (e.g. needle blockage). The output *y* (e.g. construct of PCL and bioink) of each printing stage was subject to quality control via visual evaluation through a feedback loop *Fy* followed by possible adjustment of stage specific process variable u_k. Furthermore, evaluation of state vectors was conducted through intermediate feedback loops *Fx*. Pre-printing stages were defined as preparational working steps before any printing takes place, like the creation of a 3D model or the design of a printing pattern. Printing stages were defined as the extrusion of a single material in a single layer, the changing of a printhead or the extrusion of a single material into a single pore via *z-printing*. Feedback loops were defined as quality control processes of a state vector x_k or output *y.* Printing stages and feedback loops

were then quantified. Post-printing stages were defined as finishing working steps taking place after printing, such as cross-linking. Intermittent modification steps were defined as steps taking place between the completion of one printing stage and the beginning of another.

6.2.6 3D printing meniscus PCL scaffold

A digital file was created by 3D scanning a porcine meniscus using a LPX-250 Picza 3D laser scanner (Roland, UK). The STL file was then scaled to adult human size, sliced into 120 µm thick layers and imported into the software BioCAD (RegenHU, Switzerland). Using BioCAD the file was filled in with the previously investigated infill patterns in order to reflect the mechanical properties of the native tissue (Fig. 6.5 a). The posterior and central region was filled with an infill pattern of 120 µm fibres in double layered offset pattern in 2 mm spacing. The anterior region was filled with the same pattern but with a 1.5 mm spacing, in order to stiffen this region, as observed in normal human meniscus tissue. The fibres were oriented orthogonally, but additionally in circumferential and radial directions in order to reflect the anisotropy of the fibre orientation in the native meniscus tissue (Makris et al., 2011b) (Fig. 6.5 b). The infill pattern was then adapted to the entire meniscus and scaled up slightly to be printed in human size (Fig. 6.5 c).

6.2.7 Z-printing to 3D bioprint meniscus

A mould was created using a Form 3 3D printer (Formlabs, USA) in order to position the printed meniscus construct upside down on the printing platform of the RegenHU printer so all pores could be accessed during the *z-printing* process. In the following step, the printing coordinates were written into a G-code program using the algorithm displayed in Table 6.1 and Table 6.2. Pluronics F127 was then z-printed into pores in approximately 2 mm distance with 3 bars pressure through a cylindrical 23G needle (Fig. 6.5 d-e). This distance between pluronics filled pores was reported to allow nutrient and gas exchange to BMSCs after the sacrificial gel would have been

removed (Grayson et al., 2008). Bioinks of 3.5% alginate, 5% GelMA and 0.4% *inECM* or *outECM* with $20*10^6$ BMSCs/ml in as described in chapter 5 were then z-printed into the pores of the inner and outer zone of the meniscus, respectively, with printing settings described above. The bioink filled pores were chosen in approximately 1.5 mm distance from each other since the gels were observed to flow over from the pore they were originally extruded into and close that distance (Fig. 6.5 e-d). The construct was then lifted from the mould and cross-linked in $CaCl_2$ and UV light as described above and incubated over night at 37°C in physioxic conditions in XPAN media as described in chapter 2.

6.2.8 Assessment of cell viability

Analysis of viability was conducted through staining with a Live/Dead kit and confocal imaging, as described in chapter 4. Furthermore, constructs were separated into cross-sections as well as anterior, central and posterior sections to facilitate imaging.

Table 6.1 Algorithm to program z-printing G-code: Algorithm written in Visual Basic to write G-code for z-printing. Work was done in conjunction with Simon Carrol, PhD.

```
Sub compile_GCode()
Dim i, j, x, y, z, lrow As Double
Dim Line1, Line2, Line3, Line4, Line5, Line6, Line7, Line8,
Line9 As String
lrow        =        Worksheets("Coords").Cells(Rows.Count,
1).End(xlUp).Row
i = 1
j = 1
Do Until i = lrow * 9 + 1

    With Worksheets("Coords")
        x = .Cells(j, 1).Value
        y = .Cells(j, 2).Value
        z = .Cells(j, 3).Value
    End With

    Line1 = "G0 X" & x & " Y" & y
    Line2 = "G0 Z" & z + 0.2
    Line3 = "M97"
    Line4 = "G91"
    Line5 = "F5 G1 Z" & z + 1
    Line6 = "G90"
    Line7 = "F10 G1 Z" & z
    Line8 = "M96"
    Line9 = "G0 Z" & 15

    With Worksheets("Code")
        .Cells(i, 1).Value = Line1
        i = i + 1
        .Cells(i, 1).Value = Line2
        i = i + 1
        .Cells(i, 1).Value = Line3
        i = i + 1
        .Cells(i, 1).Value = Line4
        i = i + 1
        .Cells(i, 1).Value = Line5
        i = i + 1
        .Cells(i, 1).Value = Line6
        i = i + 1
        .Cells(i, 1).Value = Line7
        i = i + 1
        .Cells(i, 1).Value = Line8
        i = i + 1
        .Cells(i, 1).Value = Line9
        i = i + 1
    End With
    ' increment x, y, z by the required amount
    j = j + 1

Loop

End Sub
```

Table 6.2 Z-printing G-code commands: G-code commands used to write an algorithm for Z-printing in table 6.1.

G-code command	Translation
G0 XxYy	Move with max speed to coordinates xy of pore
G0 Z0.2	Move with max speed to 0.2 mm from the bottom of the pore
M97	Start extrusion via air pressure
G91	Switch to incremental positioning
F5 G1 Z1	Move 1 mm up with speed of 5 mm/s
G90	Switch to absolute positioning
F10 G1 Zz	Move to z mm height of scaffold
M96	Stop extrusion via air pressure
G0 Z15	Move with maximum speed to 15mm above base

6.2.9 Histological characterization

After confocal imaging, sections of the printed constructs were fixed, encased in 3% agarose, dehydrated and embedded in paraffin wax. Due to the bigger size of the sections of the printed construct, the xylene and paraffin wax embedding steps were extended from 1 hour twice to 3 hours twice to ensure complete removal of air pockets and homogenous dehydration. Finally, constructs were sliced and stained in Alcian Blue/Aldehyde Fuchsin, Alizarin Red and Picrosirius Red as described in chapter 4.

6.3. Results

6.3.1 Bioinks of IPN and ECM show good printability

The printability of the bioinks developed in chapter 5 (IPN of 3.5% alginate and 5% GelMA with or without solubilized inner and outer zone meniscus ECM) was first evaluated. Viscosity was analysed as a function of temperature in order to determine the optimum printing temperature. A temperature sweep under oscillation revealed a significant difference between the viscosity of the IPN alone (30 Pa*s) compared to the ECM functionalised IPNs (100 Pa*s) at 4°C. However, the differences in viscosity decreased with increasing temperature and all displayed lower viscosity of approximately 10 Pa*s at 37°C (Fig. 6.1 a). Furthermore, the value for Tan Delta (the ratio of loss G'' and storage moduli G') for the IPN alone was >1, demonstrating that the bioink behaves like a viscous liquid and increased with increasing temperature. In contrast, the IPN bioinks containing *inECM* and *outECM* showed a value of Tan Delta <1 at lower temperatures, indicating that the material behaves like an elastic solid, but this increased to ~ 1 at temperatures of 32°C and higher (Fig. 6.1 b). At 13°C the viscosities of all three bioinks were sufficiently high that based on previous experience meant that they should be printable. To further assess the printability, a spreading ratio assay was conducted at 13°C under different extrusion pressure settings. The spreading ratio decreased with lower pressure settings for all bioinks. Higher spreading ratios were observed for IPN bioinks containing *inECM* and *outECM* (Fig. 6.1 c). To summarize, the printability of IPN bioinks containing 3.5% alginate and 5% GelMA, with and without 0.04% *inECM* and *outECM*, were characterized and 13°C was determined as a suitable printing temperature.

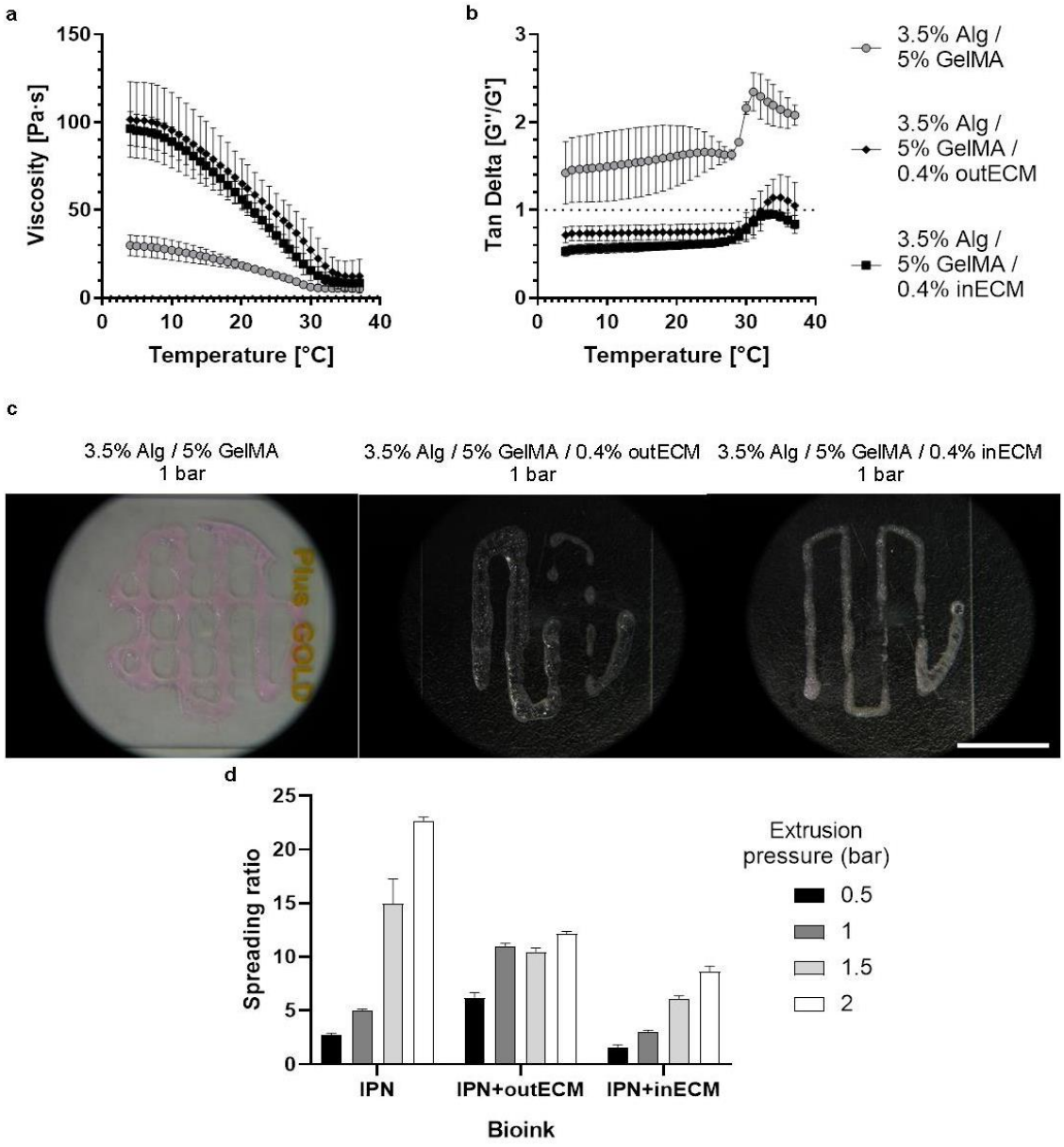

Fig. 6.1 Printability characterization of bioinks: rheological analysis of viscosity as a function of temperature (a-b) and spreading ratio assay(c-d). Scale bar 10 mm, n = 3 in triplicates

6.3.2 Z-printing accelerates the 3D bioprinting of complex large scale constructs

The emerging concept of '*z-printing*' was next explored as a novel 3D printing technique that facilitates accelerated bioprinting of complex, large scale cell-laden constructs. The concept of *z-printing* involves linearly moving the depositing needle into the spaces/channels of a pre-existing biomaterial and then extruding a bioink while

exiting the construct from the bottom to the top along the z-axis of the printing platform (Fig. 6.2 a). First, the time to print a scaffold with a width of 1.5 mm and a height of either 5, 10 and 15 mm, consisting of PCL and 2 different inks, was compared for *z-printing* and conventional x-y printing (Fig. 6.2 b-c). Z-printing was found to be faster than conventional x-y printing for each scaffold size by 20 - 35% and printing times increased with increasing scaffold volume on a linear scale by a factor of 2.2, whereas printing times for conventional printing methods scaled with a factor of 3.2 (Fig. 6.3 a-b). Upon closer inspection of the duration of the individual printing steps, it was shown that the total duration necessary to change printheads was shortened through the z-printing approach. Furthermore, the technique of *z-printing* allowed a segmentation of the various printing steps of extruding different materials as well as switching between them into separate working steps, whereas conventional 3D printing required all working steps to be performed in a singular uninterrupted process (Fig. 6.3 c).

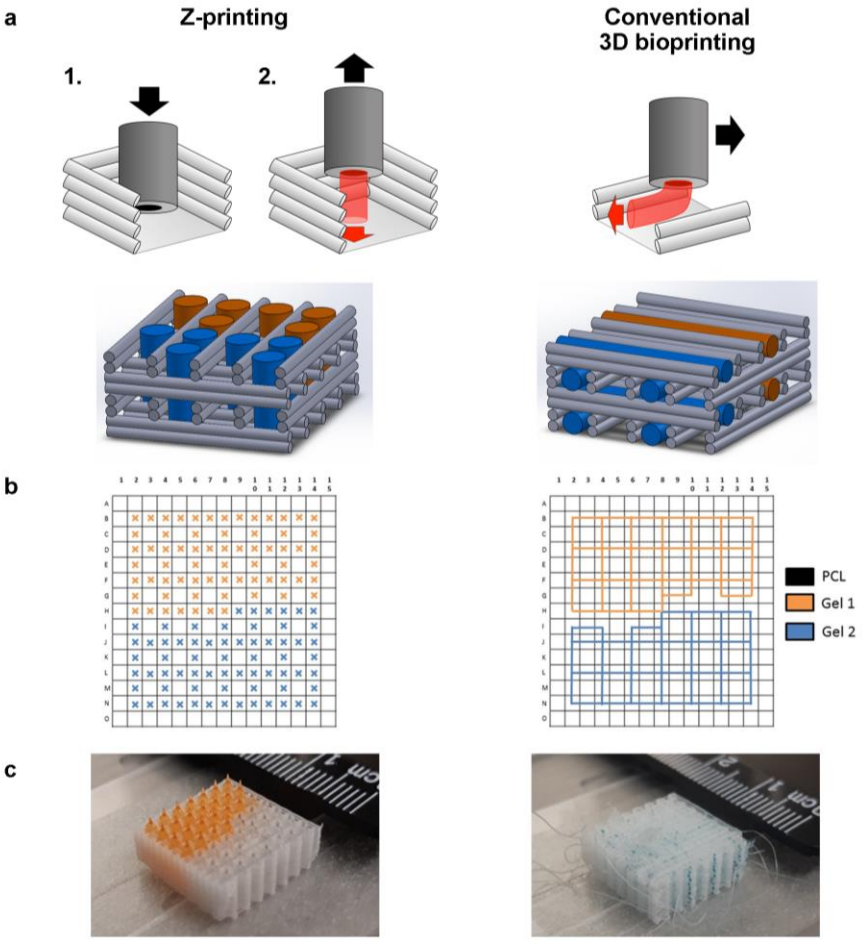

Fig. 6.2 Z-printing compared to conventional 3D bioprinting: Two constructs were either designed for with *z-printing* or conventional 3D bioprinting using PCL via FDM and two hydrogels via air pressure extrusion (a). Infill patterns to print a scaffold and as finished prints of 5 mm height(c).

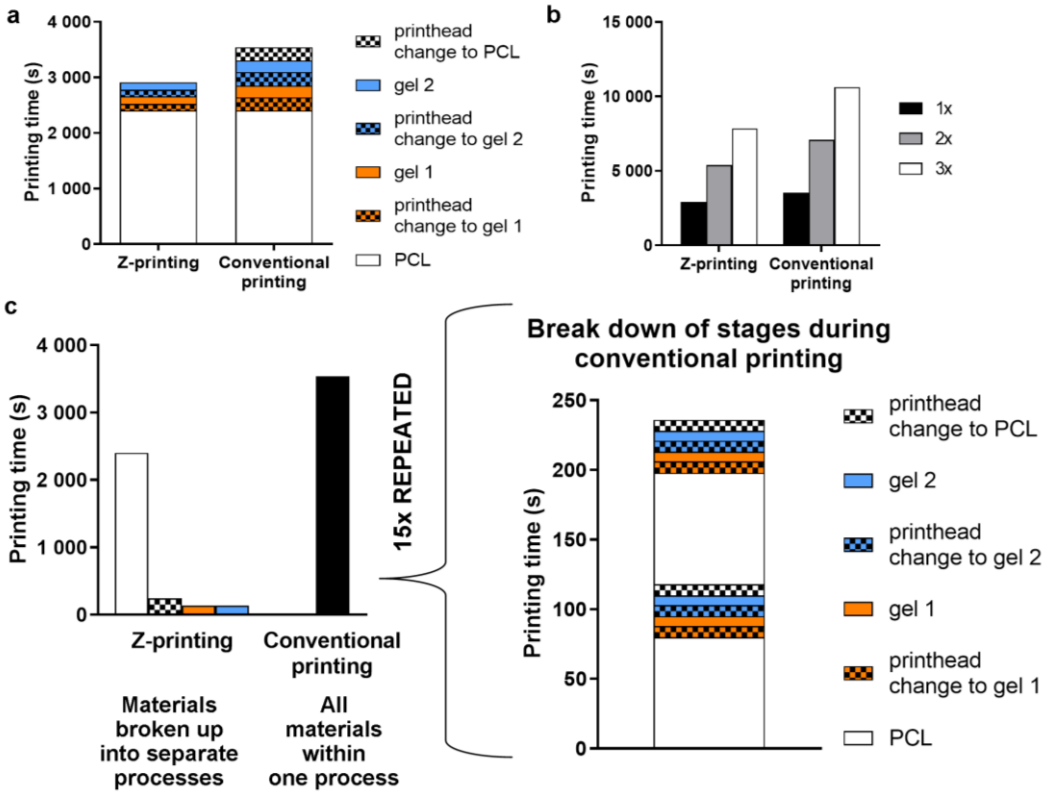

Fig. 6.3 Quantification of printing processes: Duration to print each scaffold for each action of the printer (a) and further compared when the scaffolds were scaled up to bigger volumes (b). The printing times of the separate stages of each printing technique were broken down to gain insight into the details of the different processes (c).

6.3.3 Z-printing allows a higher ratio of printing stages to feedback loops

Next, conventional printing and *z-printing* were described as multistage manufacturing process using a state space model (Fig. 6.4 a-d). A quantification of the amount of printing stages and feedback loops revealed that the number of printing stages associated with a conventional 3D bioprinting process scaled faster with increasing scaffold size compared to a z-printing process (Table 6.3) (Fig. 6.5 a). Moreover, z-printing is characterised by a lower ratio of printing stages per feedback loops compared to a conventional 3D bioprinting technique, which also scaled slower with increasing scaffold size (Fig. 6.5 b).

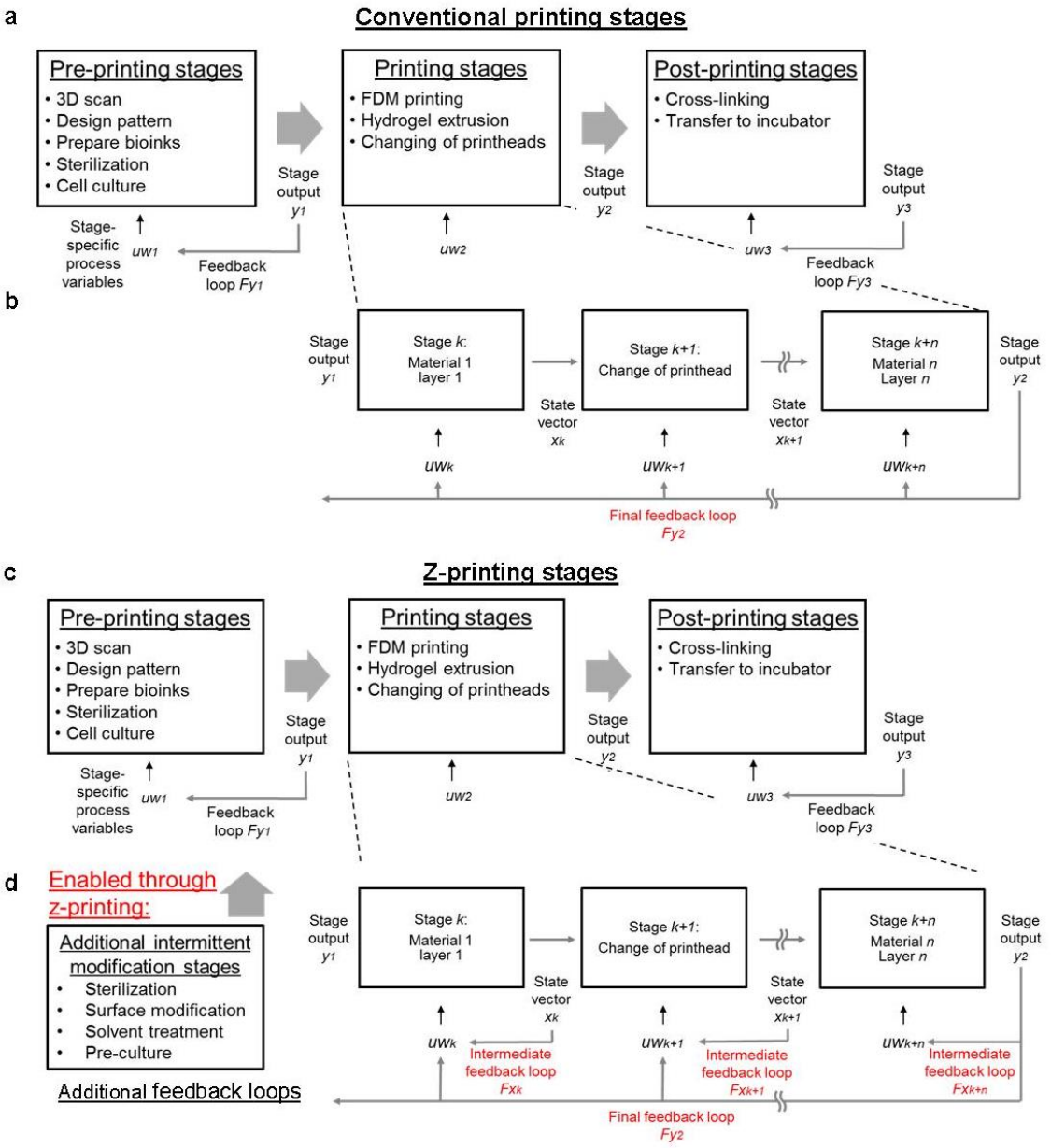

Fig. 6.4 State space models of 3D printing as multistage manufacturing process: 3D bioprinting can be described as a state space model of multistage manufacturing process with pre-printing stages, post-printing stages and several printing sub-stages (a).

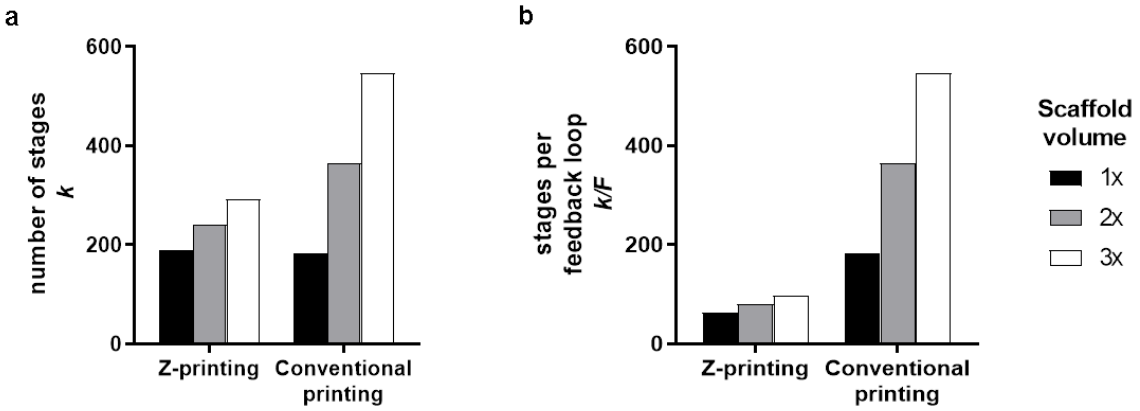

Fig. 6.5 Quantification of number of stages and stages per feedback loops: The number of printing stages used in conventional printing processes increases faster with scaffold volume compared to the number of stages in a *z-printing* process (a), as does the number of stages per feedback loop (b).

Table 6.3: Quantification of printing stages and feedback loops

Conventional 3D bioprinting				Z-printing			
5	10	15	height (mm)	5	10	15	height (mm)
amount of stages			stage k	amount of stages			stage k
52	104	156	PCL layers	52	104	156	PCL layers
26	52	78	gel 1 layers	67	67	67	gel 1 pores
26	52	78	gel 2 layers	66	66	66	gel 2 pores
26	52	78	change printhead to PCL	1	1	1	change printhead to PCL
26	52	78	change printhead to gel 1	1	1	1	change printhead to gel 1
26	52	78	change printhead to gel 2	1	1	1	change printhead to gel 2
182	364	546	sum of stages k	188	240	292	sum of stages k
amount of feedback loops F			feedback loop F	amount of feedback loops F			feedback loop F
		1	end of printing stage Fy2	1	1	1	end of PCL printing stages Fxk1
	-	-	-	1	1	1	end of gel 1 printing stages Fxk2
-	-	-	-	1	1	1	end of gel 2 printing stages Fxk3 = end of printing stage Fy2
1	1	1	sum of feedback loops F	3	3	3	sum of feedback loops F
182	364	546	ratio of stages to feedback loops k/F	62.6	80	97.3	ratio of stages to feedback loops k/F

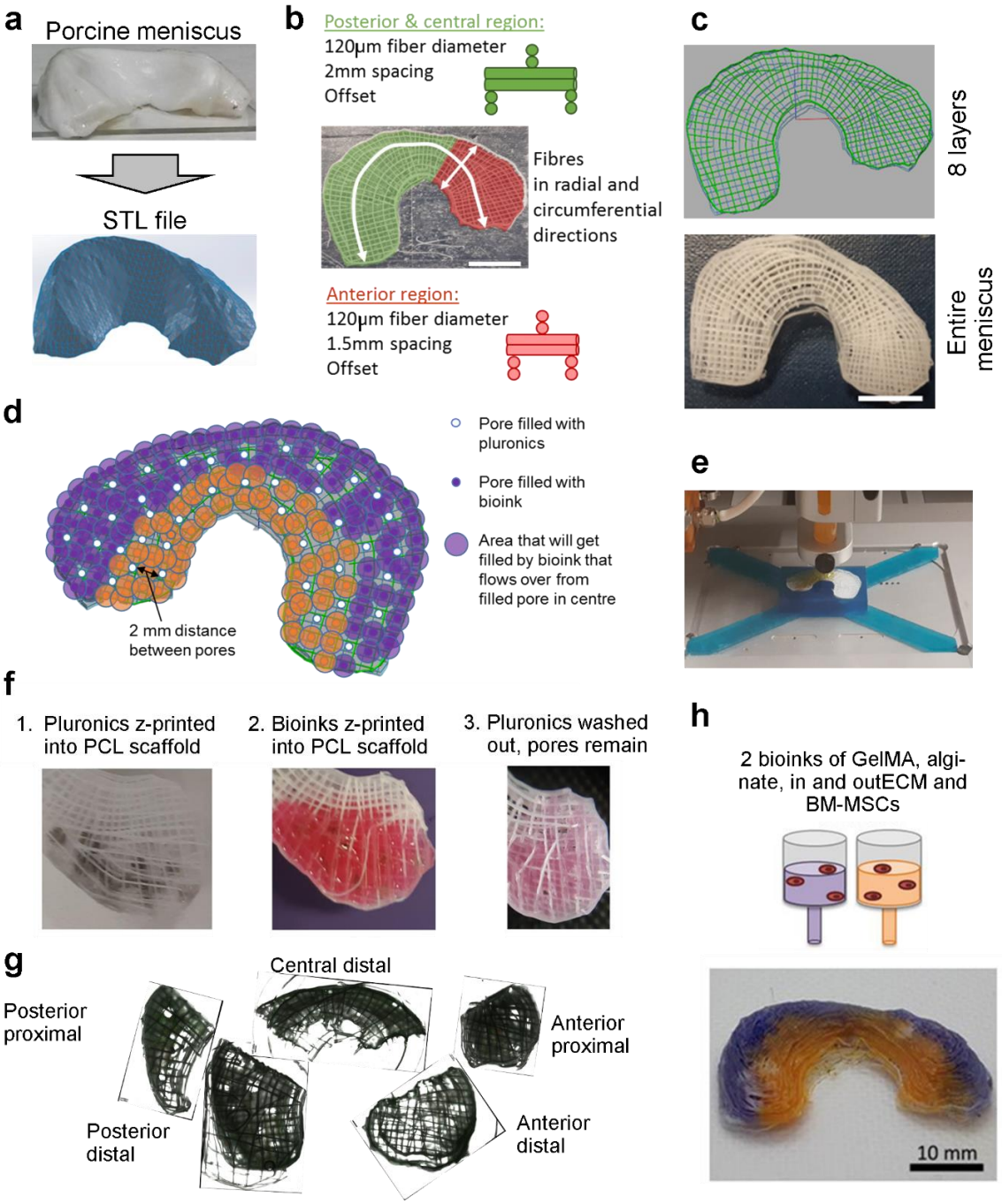

Fig. 6.6 Multiple-tool biofabrication of an anatomically accurate meniscal graft mimicking the anisotropic and heterogeneous properties of the native tissue: Schematics of how a porcine meniscus was 3D scanned and converted into an STL file (a), and subsequently further converted into a printable file with infill pattern of circumferentially and radially orientated fibres with 120 µm, double layer, offset and 1.5 mm spacing in the anterior or 2 mm in the central and posterior region. Scale bar 10 mm (b). Schematics of scaling up the infill pattern to 3D print a meniscus of anatomical size and shape. Scale bar 10 mm (c). Schematics in top view of pores of meniscus construct (d) and utilization of *z-printing* with pluronics and bioinks for inner and outer zone (e). Application of pluronics as sacrificial hydrogel to create pores after washing out (f) and confirmation of pores via confocal microscopy (g). Printed construct with distinct inner and outer zones using bioinks of alginate, GelMA, *inECM* or *outECM* with BMSC (h).

6.3.4 Multiple-tool biofabrication of an anatomically accurate meniscal graft mimicking the anisotropic and heterogeneous properties of the native tissue

After printing a PCL scaffold mimicking the anatomical size and shape of a human meniscus, the spaces between PCL filaments (i.e. the scaffold pores) were filled with an alginate-GelMA IPN bioink functionalised with either *inECM* or *outECM* (Fig. 6.6 a-e). After crosslinking the construct and swelling over night at 37°C, the sacrificial pluronics bioink had washed out leaving behind a network of nutrient channels (Fig. 6.6 f). To demonstrate the capacity to spatially locate different bioinks within the inner and outer zones of the printed meniscus, each bioink was loaded with either purple or yellow food colouring (Fig. 6.6 g). Live/Dead imaging of cells encapsulated in the bioinks showed a viability of ~80%, with a relatively homogenous distribution of cells in the cross sectional as well as the transversal view. Furthermore, after maintaining these MSC laden constructs for 24 hours in chondrogenic culture conditions, a histological analysis revealed a homogenous accumulation of extracellular matrix throughout the printed meniscus construct (Fig. 6.7).

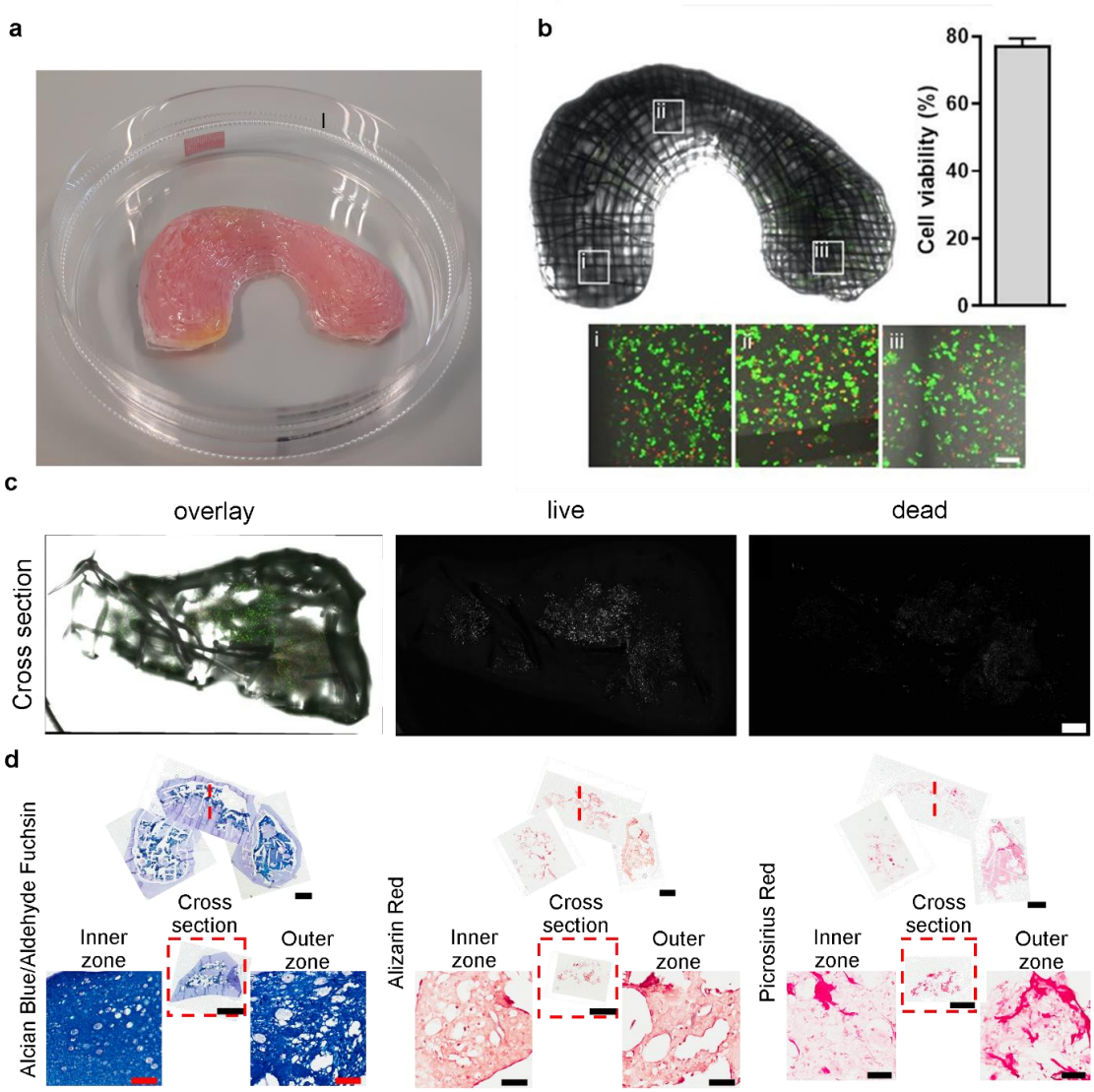

Fig. 6.7: 3D bioprinted meniscus of bioinks seeded with BMSCs: anatomically shaped and sized meniscus construct printed from PCL and bionks of alginate, GelMA and *inECM* or *outECM* (a), cell viability analysis in the transverse plane (scale bar 100 µm) (b) and cross sectional view (scale bar 1 mm) (c). Histological assessment via Alcian Blue/Aldehyde Fuchsin, Alizarin Red and Picrosirius Red staining. Scale bars 4 mm and 100 µm (d).

6.4. Discussion

In the previous chapters, PCL printing patterns and IPN bioinks were developed which enabled the engineering of cell-laden bi-phasic constructs mimicking key aspects of the non-linear, heterogeneous biomechanical properties of native meniscal tissue. The aim of this chapter was to further analyse the printability of these bioinks and to develop a printing technique which facilitates accelerated 3D bioprinting of complex large scale constructs. To demonstrate the utility of this approach, an anatomically accurate meniscus construct was fabricated, which mimicked key aspects of composition and biomechanical properties of the native tissue.

Viscosity and spreading ratio analyses of the developed bioinks revealed favourable printability at 13°C using a print pressure of 1-1.75 bar with a 23G needle. The IPN of GelMA and alginate assumed a Tan Delta value > 1 throughout the measured temperature range, which indicates that the material can primarily be described as a viscous liquid. Tan Delta increased further with increasing temperature which can be attributed to the melting point of GelMA at 37°C. In contrast, the addition of solubilized *inECM* or *outECM* to the IPN based bioink showed significantly increased its viscosity at lower temperatures. Furthermore, the Tan Delta values < 1 indicate that the ECM containing bioinks can be described as elastic gels. At 37°C, however, the decreased viscosity and increased Tan Delta values suggest a similar behaviour as observed in the IPN alone. Consequently, 13°C was chosen as optimal printing temperature since increased viscosity at lower temperatures provides better printability while the temperature remained in a range in which viability of encapsulated cells would not be diminished (J. Wang et al., 2017). It should be noted, however, that the spreading ratio was found to be relatively high, even at lower extrusion pressure or 1 bar, even when solubilized ECMs were incorporated into the bioink. Further tuning of the developed bioinks in the future could be achieved for example by partially pre-crosslinking the alginate component of the IPN bioink prior to printing (Freeman &

Kelly, 2017). In summary, rheology and spreading ratio assays of developed bioinks were conducted successfully in order to determine printing conditions to scale up a bioprinted meniscus construct.

Next, a novel 3D bioprinting technique was utilised to accelerate the biofabrication of complex, large scale tissues like a meniscus. The described *z-printing* technique has three advantages: the printing process takes less time, it allows the whole process to be broken up into separate stages for more quality control, and finally it enables additional intermittent material modification stages. These features are especially beneficial when creating complex, large scale constructs. The term *z-printing* describes the movement of printheads along the z-axis instead of the x and y-axis as usually done in conventional 3D printing techniques. In short, instead of completing a layer with each material before printing the next layer as in conventional methods, *z-printing* completes the extrusion of all layers with one material before extruding another material. After printing of all PCL layers, the needle of the hydrogel bioink printhead is translated through pores or channels within the exiting PCL structure, extruding a specific bioink while upwards in a z-direction. This technique is, therefore, not a strict layer-by-layer process, similar to other recently developed printing technologies, enabled by novel printing devices like six axis printers for example (Y. Chen, Zhou, & Lao, 2011; Choudhury, Anand, & Naing, 2018; Keating & Oxman, 2013; Zhu et al., 2018) or volumetric printing (Bernal et al., 2019). Similarly to *z-printing*, hydrogels have been bioprinted in the z-direction into the pores of scaffolds fabricated via MEW recently as well, however, without applying the technique to larger construct which was here enabled through FDM printed scaffolds (de Ruijter et al., 2018). Despite numerous developments in the field of 3D bioprinting, decreasing the duration of the printing processes is still considered a major challenge (Oropallo & Piegl, 2016), especially when printing cell-laden constructs sensitive to the length of the overall printing process. The *z-printing* process required less time to produce large,

multi-material constructs compared to conventional 3D bioprinting. This was shown to mainly be due to a decrease in necessary changes of printheads required when using multiple materials. Furthermore, when using state space models to display 3D bioprinting as a multistage process, it was shown that z-printing increases the opportunities for quality control due to a higher number of feedback loops. Due to its layer-by-layer approach, conventional printing processes can suffer from errors which accumulate from stage to stage, but typically only offer one opportunity for quality control at the end of the process (Gibson et al., 2010). Since the *z-printing* process is broken up into stages dedicated to each material separately, additional feedback loops are introduced, which enable oversight and corrections of common errors like clogged needles, software or human errors. Lastly, *z-printing* introduces additional intermittent material modification steps which allow a further increase in construct complexity. Processes like surface treatment of printed PCL fibres, that would otherwise be cytotoxic if performed on cell containing constructs (J. S. Park et al., 2007; Qi et al., 2016), or indeed simple sterilization steps can be easily introduced into the bioprinting workflow. Furthermore, sequential cell seeding is enabled through *in vitro* culture of a construct before transferring it back onto the printer to add another cell-carrying bioink (Baldwin et al., 2014; Iyer, Chiu, Vunjak-Novakovic, & Radisic, 2012). Like every technique, *z-printing* has limitations such as the restriction of the outer needle diameter by the channel/pore size of an existing scaffolds, or where the full volume cannot be accessed via pores due to overhangs. In addition, it is difficult to alter the bioink composition through the depth of the construct. In spite of these limitations, it is the contention of this thesis that the developed *z-printing* technique offers a number of advantages compared to conventional 3D bioprinting when bio-fabricating large, multi-material constructs.Finally, an MSC-laden construct mimicking the shape and size of the human meniscus was 3D bioprinted, which considered the non-linear and heterogenous biomechanics and spatial composition of the native meniscus tissue. Both FDM and MEW have been used in the past for tissue engineering of

cartilagenous constructs. MEW has similar strengths as FDM like printing highly detailed structures via a layer-by-layer process in addition to a higher resolution with fibre diameters as low as 2 µm. Furthermore, the mechanical properties of both FDM and MEW constructs are highly tunable and show compressive properties similar to the ones of native meniscus tissue when in the form of fibre reinforced IPN as demonstrated in this study (Bas et al., 2015; Visser, Melchels, et al., 2015). Despite much recent progress however, the main disadvantage of the emerging technology of MEW is still its lack in scalability (Dalton, n.d.; Robinson, Hutmacher, & Dalton, 2019; Wunner, Wille, et al., 2018a). Only very recently have MEW scaffolds been created in a height sufficient for meniscus tissue engineering for the size of human tissue or larger (Wunner, Wille, et al., 2018b). Furthermore, the long duration of printing large scale constructs like the one presented in this thesis when using MEW compared to FDM was another reason why FDM was chosen to print this meniscus construct (Dalton, n.d.; Wunner, Eggert, et al., 2018). Similarly to other meniscus tissue engineering papers (Gokhan Bahcecioglu et al., 2019; C H Lee et al., 2014; Szojka et al., 2017; Zheng-zheng Zhang et al., 2019) FDM was used instead due to its ability to print complex structures that can withstand the biomechanical forces in the knee joint. Often used in bone tissue engineering, FDM printed PCL shows the advantage of high mechanical strength essential for load bearing tissues (Daly, Cunniffe, et al., 2016; Hutmacher, 2000). Furthermore, the developed offset pattern in combination with IPNs make it possible to create constructs with bi-phasic mechanical properties close to one of meniscus tissue. The approach described in this chapter offers therefore a number of advantages over the small number of earlier attempts to 3D print meniscal constructs. Zone-specific tissue engineered meniscus constructs have previously been fabricated using a 3D printed PCL scaffold loaded with CTGF and TGF-β3 encapsulated in microspheres within the outer and inner zones of the construct, with the goal of creating a spatio-temporal growth factor release profile (Chang H Lee et al., 2014). A more recent study combined tailored PCL scaffolds with GelMA and agarose

hydrogels (G Bahcecioglu et al., 2019; Gokhan Bahcecioglu et al., 2018). Unlike the printed construct in this study, they utilised a broadly orthogonal fibre pattern, failing to recapitulate the circumferentially and radially orientated fibres observed in native meniscus (G Bahcecioglu et al., 2019). In contrast, Zhang et al and Szojka et al developed scaffold designs with circumferential and radially oriented PCL fibres which mimic the directionality of the native meniscus collagen architecture (Szojka et al., 2017; Z.-Z. Zhang et al., 2017). The design used in the current study also mimics the biomechanical differences between heterogeneous anterior, central and posterior regions of the native tissue, which was not taken into account in the above-mentioned studies. Moreover, the reported inclusion of pores in this study to enable gas and nutrient exchange through diffusion (Grayson et al., 2008; Rouwkema et al., 2013) as well as cell migration into the centre of the construct represents another novelty in printing large scale meniscus tissue engineering constructs.

Moreover, the studies above also report successful simulation of rounded and spread cell morphology in inner and outer zones respectively (G Bahcecioglu et al., 2019) and secretion of zone specific ECM through biochemical and/or biomechanical stimulation through CTGF and TGF-β3 *in vitro* or *in vivo* studies in rabbits or sheep (G Bahcecioglu et al., 2019; Chang H Lee et al., 2014; Nakagawa et al., 2019b; Z.-Z. Zhang et al., 2017; Zheng-zheng Zhang et al., 2019). However, the construct reported in this current study was not subject to long term *in vitro* culture or implanted *in vivo.* Future work should be carried out in order to assess the zone-specific fibrochondrogenic and chondrogenic differentiation potential of the developed construct.

6.5. Conclusion

This chapter describes the development of a 3D bioprinted meniscus construct which mimics the external size and shape of the human meniscus as well as its

internal heterogeneous structure. The print patterns employed in this study were also previously shown (Chapter 3) to mimic key aspects of the biomechanics of the normal meniscus. Furthermore, the creation of this large, multi-material biological constructs was facilitated through the development of a novel 3D bioprinting technique which successfully addresses several key challenges of 3D printing as a manufacturing process.

Chapter 7
DISCUSSION

7.1. Summary and discussion of key findings

The objective of this thesis was to 3D bioprint a cell-laden and anatomically accurate engineered meniscus construct with (i) heterogeneous and anisotropic mechanical properties and (ii) spatially defined regulatory cues in the form of meniscus ECM components, thereby mimicking key features of the native meniscus. This bioprinted construct was also required to have the potential to continue to mature either *in vitro* or *in vivo*. This required the development of polymer scaffolds and bioinks with specific biomechanical properties and the potential to support fibro-cartilaginous tissue deposition by encapsulated cells. Chapter 3 therefore explored the mechanical properties PCL scaffolds produced using FDM, varying the fibre diameter, spacing and print pattern. Using this approach is was possible to produce scaffolds with axial compressive properties and radial tensile properties similar to human meniscus tissue. Chapter 4 described the development of a composite construct consisting of an MSC laden hydrogel reinforced with a 3D printed PCL fibre network. This composite biomaterial displayed biomechanical behaviour similar to bi-phasic soft tissues like the meniscus. Furthermore, the developed hydrogel showed shear thinning properties making it suitable for putative 3D bioprinting applications, and supported robust chondrogenesis of MSCs *in vitro*. Chapter 5 then sought to functionalise the alginate and GelMA IPNs with solubilized ECM fractions from the inner and outer zones of porcine meniscus. While the addition of ECMs improved the shear thinning properties of the developed hydrogel bioinks, it did not dramatically alter the capacity of the inks to support the fibrochondrogenic differentiation of MSCs. Finally, in chapter 6 of the thesis a novel 3D bioprinting technique was described which was used to create

large scale tissue engineered constructs. Using this approach a meniscus construct with a size and shape similar to that of the human meniscus was produced, using printing parameters that were previously shown to produce composites with anisotropic and bi-phasic biomechanical properties.

The thesis began with the aim of engineering materials with compressive and tensile properties similar to the native human meniscus tissue by 3D printing composite constructs consisting of IPN hydrogels reinforced with networks of PCL fibres (chapter 3). First, the effect of the variation of fibre diameters and spacing on the compressive and tensile properties was investigated. Mechanical properties decreased with decreasing PCL content, with a scaffold consisting of a 120 μm fibre diameter and a 2 mm fibre spacing best mimicking the axial compressive properties of the native tissue. While PCL scaffolds with a tensile modulus mimicking that of the radial direction of the meniscus could be readily achieved, reaching values observed in the circumferential direction of the meniscus required printing scaffolds with almost 50% PCL content. However these scaffold possessed an axial compressive modulus at least one order of magnitude higher than that observed int eh native tissue, and hence could not be considered biomimetic of the native tissue. Next the influence of fibre print pattern was explored by 3D printing consecutive parallel layers of fibres either directly ‘aligned’ with the underlying parallel layer or ‘offset’ to the underlying parallel layer. This design reduced the compressive modulus of 3D printed samples more than its tensile modulus, without altering the PCL content, and therefore increased the ratio of the tensile to compressive modulus to native tissue-like values. These PCL networks were then used to mechanically reinforce IPN hydrogels, producing highly hydrated composites with soft tissue-like biomechanical behaviour.

Chapter 4 of the thesis explored then the potential of the IPN to support chondrogenesis in MSCs and further investigated the bi-phasic mechanical properties of such constructs. First, through a rheological characterization of the IPN and its

components, the viscosity as function of shear rate was fitted to Herschel-Bulkley model. The shear thinning properties of an IPN of 3.5% alginate and 5% GelMA were hereby found to be in the range of other reported bioinks and considered suitable for biofabrication (Chimene et al., 2018; Melchels et al., 2016). Next, the chondrogenesis of BMSCs within the fibre reinforced IPN was investigated through histological, immunohistological and biochemical analysis after a 6 week *in vitro* study in physioxic conditions where the encapsulated cells were stimulated with TGF-β3. The IPN supported robust chondrogenesis of BMSCs, however, some evidence of calcification was observed, and the cartilage tissue was dominated by Col II, in contrast to native meniscus tissue which consists predominantly of Col I (Makris et al., 2011a). A complex compressive testing protocol was employed next to analyze the effect of the cell secreted ECM on both the flow dependent and flow independent mechanical properties of the engineered tissues. The flow independent equilibrium moduli of the constructs were notably higher than that of the native tissue, which suggests that the solid phase of meniscal tissue is inherently less stiff than that of the fibre-reinforced IPN. Meanwhile, the dynamic mechanical properties of the composite increased with time in culture, only approaching that of the meniscus, which suggests that the permeability of meniscus is lower than that of the hereby engineered tissue and therefore better able to generate fluid load support (Gannon et al., 2012). In conclusion, It was demonstrated that an IPN of alginate and GelMA has shear thinning properties, that BMSCs secrete a cartilaginous matrix within this hydrogel and that this secreted matrix improves the mechanical properties of the PCL reinforced IPN, resulting in tissues with dynamic mechanical properties closer to native meniscal tissue.

The goal of chapter 5 was to further develop the alginate and GelMA IPN bioinks by functionalising them with solubilised ECM isolated from the inner and outer region of the meniscus, based on the belief that this would enhance their capacity to

support meniscus-specific differentiation of BMSCs (C H Lee et al., 2014; Romanazzo et al., 2017; Rothrauff et al., 2017; Shimomura et al., 2017). The success of the solubilization protocol for efficiently decellularizing the ECM was confirmed by demonstrating a reduction in DNA content to below 50 ng/mg, which has been suggested as the threshold necessary to avoid immune responses upon implantation of an ECM derived material (Crapo et al., 2011b). Furthermore, the collagen and sGAG contents were also reduced by the solubilization treatment, but the collagen:sGAG ratio for the solubilised ECMs was comparable to that of the native tissue. This suggested a maintenance of the relative number of binding sites for specific growth factors and cell binding sites that may be important for promoting chondrogenesis (Rutgers et al., 2012)(Schneiderbauer et al., 2004). Moreover, the solubilized ECM fractions were found to possess low viscosities alone but strong shear thinning properties, as assessed by fitting the rheology data to the Herschel-Bulkley model in a rheological analysis. Consequently, when combined with the previously developed IPN of 3.5% alginate and 5% GelMA, a significant increase in both viscosity and shear thinning behaviour was observed, especially for the outer meniscus ECM. This improvement rheological properties (for bioprinting applications) through the incorporation of matrix components into bioinks has been explained through a change in the collagen fibre orientation under shear forces during extrusion (Malda et al., 2013). To assess the capacity of these ECM functionalised IPN bioinks to support chondrogenesis, they were loaded with BMSCs and maintained in culture for 42 days. The solubilized ECM fractions of inner and outer meniscus failed to improve the fibrochondrogenic potential of the developed IPN based bioinks, but significantly improved their shear thinning and viscoelastic behaviour.

The aim of chapter 6 was to further analyse the printability of these bioinks, develop a printing technique which facilitates accelerated and scaleable 3D bioprinting of complex large scale constructs and finally to fabricate an anatomically accurate

meniscus construct, which mimicked key aspects of the composition and biomechanical properties of the native tissue. Viscosity and spreading ratio analyses of the previously developed bioinks identified the optimal printing conditions. At lower temperatures, the bioinks displayed elastic solid behaviour and increased viscosity, which supported better printability in a temperature range in which viability of encapsulated cells would not be diminished (J. Wang et al., 2017). Next, *z-printing*, a novel 3D bioprinting technique was developed, which describes the movement of printheads along the z-axis instead of the x and y-axis as usually done in conventional 3D printing techniques. After printing of all PCL layers, the needle of the hydrogel bioink printhead is translated through pores or channels within the exiting PCL structure, extruding a specific bioink upwards in a z-direction. The described technique has three advantages: the printing process takes less time, it allows the whole process to be broken up into separate stages for more quality control, and finally it enables additional intermittent material modification stages. These features are especially beneficial when creating complex, large scale constructs. Finally, an MSC-laden construct mimicking the shape and size of the human meniscus was 3D bioprinted, which considered the non-linear and heterogenous biomechanics and spatial composition of the native meniscus tissue, similarly to a small number of earlier attempts to 3D print meniscal constructs (G Bahcecioglu et al., 2019; Lee et al., 2014; Nakagawa et al., 2019; Z. Zhang et al., 2019)(Szojka et al., 2017; Z.-Z. Zhang et al., 2017). Moreover, the reported inclusion of pores into the bioprinted construct supported nutrient transport and waste removal (Grayson et al., 2008; Rouwkema et al., 2013), providing further benefits in printing large scale meniscal constructs.

In summary, this thesis describes the development of a 3D bioprinted meniscus construct which mimics the external size and shape of the human meniscus as well as its internal heterogenous structure. The fibre reinforced IPN constructs employed in this study were shown to mimic key bi-phasic biomechanical attributes of the normal

meniscus. Moreover, the developed bioink showed its potential for 3D bioprinting in the field of cartilaginous tissue engineering, being both shear thinning and supportive of a chondrogenic phenotype. Furthermore, the creation of this large, multi-material biological constructs was facilitated through the development of a novel 3D bioprinting technique which successfully addresses several key challenges of 3D printing as a manufacturing process.

7.2. Limitations

The PCL patterns developed in chapter 3 mimic a number of biomechanical properties of the native meniscus tissue, but still have a number of shortcomings, particularly the inability to mimic the circumferential tensile properties of the meniscus without dramatically reducing the overall porosity of the printed scaffold. This can be attributed to the limitations of PCL as material of choice. Possible alternative design solutions for future studies are to combine 3D-printing with other manufacturing methods and biomaterials such as silk fibre (Warnecke et al., 2018) or Ultra High Weight Polyethylene (NUsurface®, AIC, Memphis, Tennessee)(Active Implants, 2018; Balint et al., 2012; Elsner & Linder-ganz, 2010) to provide greater tensile strength in the backbone of the construct. Moreover, a further increase of the tensile properties of printed PCL fibres could be achieved through the secreted matrix of BMSCs over an extended *in vitro* culture period (C H Lee et al., 2014). The created construct does not fully mimic the native biomechanical properties but addresses many of the problems of currently available products.

Chapter 4 demonstrated chondrogenesis of the BMSCs when cultured in the fibre reinforced IPN constructs, but some cartilage calcification observed after 42 days of *in vitro* culture, which suggests progression along an endochondral pathway. Previous studies have demonstrated that $CaCl_2$ crosslinked alginate can support

spontaneous calcification (Liberski, Latif, Raynaud, Bollensdorff, & Yacoub, 2016), which could potentially have been prevented by using bisphosphatate or barium chloride to crosslink the IPN (C. S. D. Lee et al., 2010). Furthermore, calcification of cartilaginous tissues engineered using BMSCs is a well documented limitation of this cell source when exposed to TGF-β3 (Rathan et al., 2019), related to the inherent tendency of chondrogenically primed MSCs to become hypertrophy and progress along an endochondral pathway (Makris et al., 2011b) (Bracht et al., 2007). Tissue calcification could be prevented by using a different cell source like synovium (C H Lee et al., 2014; Shirasawa et al., 2006) or fat pad derived stem cells (Romanazzo et al., 2017)(Buckley et al., 2010; Luo et al., 2015). However, in this thesis porcine BMSCs were used due to the simplicity of their isolation in high numbers and the doubling speed during the expansion phase, as 3D bioprinting large constructs requires a comparatively high amount of cells. Going forward a co-culture approach incorporating meniscal derived fibrochondrocytes and stem cells could be used as an alternative cell population suitable for such applications. Furthermore, using human cells instead of porcine would have shown more clinical relevance, due to the possibility of using allograft or autograft cells in a cell therapy. However, as described in chapter 2, human autograft BMSCs often show low chondrogenic potential due to the advanced age of many patients.

While the *in vitro* study presented in chapter 4 showed promising chondrogenesis and secretion of type II collagen, native menisci (and particularly the outer zone) consist of more fibrocartilage-like tissue rich in collagen type I. However, chapter 5 failed to induce a more fibrochondrogenic response in the MSCs. The increased cell death observed in this study could be related to the use of irgacure 2959 and UV light to crosslink the IPN, which has been associated with higher levels of cytotoxicity (Billiet, Gevaert, De Schryver, Cornelissen, & Dubruel, 2014)(Mironi-harpaz, Yingquan, Venkatraman, & Seliktar, 2012)(Bahney et al., 2016)(Rouillard et

al., 2011). Alternative catalysts like LAP or VA-086 which crosslink using less harmful optical light or less cytotoxic crosslinkers like genipin instead could improve cell viability within the constructs (Pahoff, Klein, Meinert, Bas, & Hutmacher, 2019; Rouillard et al., 2011). Unlike previous studies (Rothrauff et al., 2017; Shimomura et al., 2017), the use of solubilized ECM failed to induce a zone-specific meniscal phenotype. Alternative approaches that could be explored in future studies include the spatio-temporal release of factors such as CTGF and TGF-β3, which have previously been used in successful meniscus tissue engineering studies (C H Lee et al., 2014; Nakagawa et al., 2019a; Z.-Z. Zhang et al., 2017; Zheng-zheng Zhang et al., 2019).

Chapter 6 demonstrated the creation of a 3D bioprinted construct mimicking the external and internal structure of the human meniscus based on the fibre reinforced IPNs developed in chapter 3 and 4. However, it lacks further verification if the biomechanical properties also translate to the more irregular fibre design of the meniscus shaped construct. The biomechanical properties of the developed fibre reinforced IPN constructs were analyzed through uniaxial testing in the shape of cylinders or dogbone structures in chapters 3 and 4. A more complex testing setup through indentation testing (Q. Li et al., 2017) or cut-out studies would be required to assess the mechanical properties of the scale-up construct (Peloquin, Santare, & Elliott, 2015). Equally, a multidirectional testing rig would be necessary in order to analyse the tensile properties of the circumferentially orientated fibres (Dienst et al., 2007; R. S. Jones et al., 1996; Kahlon, Hurtig, & Gordon, 2015). This would also enable a more accurate mechanical testing of native porcine meniscus tissue presented in chapter 4. Here the varying heights of biopsies between the inner and the outer zones, the wedge-shaped form of the tissue, and the variation in ECM between surface layers compared to deeper ones led to difficulties in sample preparation and large differences in the results.

7.2.1 Conclusions

- It is possible to 3D bioprint a meniscus construct which mimics the external size and shape of the human meniscus as well as its internal heterogeneous structure.

- The fibre reinforced IPN constructs employed in this study were shown to mimic key aspects of the bi-phasic biomechanics of the normal meniscus.

- This thesis successfully developed bioinks of alginate, GelMA and solubilized meniscus ECM for 3D bioprinting applications in the field of cartilage tissue engineering, as demonstrated by their shear thinning properties and chondrogenic potential.

- The creation of large, cell-laden and multi-material biological constructs was facilitated through the development of *z-printing*, a novel 3D bioprinting technique which successfully addresses several key challenges of 3D printing as a manufacturing process.

7.2.2 Future work

This thesis developed a series of bioinks based on alginate, GelMA and solubilized porcine meniscus ECM that were characterised by rheology, spreading ratio analysis and biochemical analysis of the solubilized tissue fractions. Future work could see further development and in depth analysis of the created bioinks. Additional tuning of the developed bioinks in the future could be achieved, for example, by partially pre-crosslinking the alginate component of the IPN bioink prior to printing (Freeman & Kelly, 2017). Moreover, the solubilized meniscus ECM fractions could be further

categorized through proteomic analysis (western blot or mass spectrometry) in order to gain insight into the retained growth factors and binding sites (Cunniffe et al., 2019). Lastly, future work could employ additional analysis methods of the bioinks like filament deflection assay or injectability tests (Barki, Bocquet, & Stevenson, 2017; Ribeiro et al., 2018).

Comparable published meniscus tissue engineered constructs saw tissue maturation through *in vitro* or *in vivo* studies in long term bioreactor studies. Dynamic compressive stimulation of MSCs growing on 3D printed PCL constructs in combination with a spatio-temporal growth factor application of CTGF and TGF-β3 showed gene expression and tissue maturation similar to the inner and outer zones of the native meniscus tissue (G Bahcecioglu et al., 2019; Gokhan Bahcecioglu et al., 2018; C H Lee et al., 2014; Nakagawa et al., 2019a; Puetzer & Bonassar, 2016; Z.-Z. Zhang et al., 2017; Zheng-zheng Zhang et al., 2019). The scaled-up meniscus construct developed in this thesis, however, was only analysed after short-term culture. Future work could therefore be to culture the construct developed in this thesis inside a bioreactor under dynamic compression or media agitation and spatio-temporal stimulation via CTGF and TGF-β3 in order to study long-term tissue maturation. Through such a study, the developed construct could be compared more closely to the other recently tissue engineered menisci reported in the literature mentioned above.

Tissue engineered meniscus constructs are designed with the application in mind to replace patient tissue, which has been torn and removed via partial or total meniscectomy. Hereby, the implant needs to be sutured to the remainder of the meniscus tissue of the patient and over time integrate into the surrounding host tissue. Future work could therefore be to conduct pull out tests to assess the ability of the construct to resist forces through the sutures after implantation (Szojka et al., 2017). Furthermore, an explant study could assess the cells and ECM bridging the gap between the construct and the surrounding meniscus tissue as well as the resistance

of the construct against being physically separated from its surrounding host tissue (Hennerbichler, Moutos, Hennerbichler, Centers, & Carolina, 2007). Future studies like these would therefore confirm the design of the scaffold in a more clinically relevant setting.

Chapter 8

BIBLIOGRAPHY

Abdel-hamid, M., Hussein, M. R., Ahmad, A. F., & Elgezawi, E. M. (2005). Enhancement of the repair of meniscal wounds in the red – white zone (middle third) by the injection of bone marrow cells in canine animal model. *International Journal of Experimental Pathology*, *86*, 117–123.

Abedalwafa, M., Wang, F., Wang, L., & Li, C. (2013). Biodegradable Poly-Epsilon-Caprolactone (PCL)for Tissue Engineering Applications: A Review. *Rev Adv MAter Sci*, *34*, 123–140.

Active Implants. (2018). The VENUS Clinical Study (Verifying the Effectiveness of the NUsurface® System) (VENUS). Retrieved from https://clinicaltrials.gov/ct2/show/NCT02136901

Almeida, H. V, Liu, Y., Cunniffe, G. M., Mulhall, K. J., Matsiko, A., Buckley, C. T., … Kelly, D. J. (2014). Controlled release of transforming growth factor- b 3 from cartilage- extra-cellular-matrix-derived scaffolds to promote chondrogenesis of human-joint-tissue-derived stem cells. *Acta Biomaterialia*, *10*(10), 4400–4409. http://doi.org/10.1016/j.actbio.2014.05.030

Anderson, D. R., Gershuni, D. H., Nakhostine, M., & Danzig, L. A. (1993). The effects of non-weight-bearing and limited motion on the tensile properties of the meniscus. *Arthroscopy : The Journal of Arthroscopic & Related Surgery : Official Publication of the Arthroscopy Association of North America and the International Arthroscopy Association*, *9*(4), 440–445. http://doi.org/10.1016/s0749-8063(05)80319-6

Ansari, S., Sarrion, P., Hasani-sadrabadi, M. M., Aghaloo, T., Wu, B. M., & Moshaverinia, A. (2017). Regulation of the fate of dental-derived mesenchymal stem cells using engineered alginate-GelMA hydrogels, 2957–2967. http://doi.org/10.1002/jbm.a.36148

Arnoczky, S. P., & Warren, R. F. (1982). Microvasculature of the human meniscus. *The American Journal of Sports Medicine*, *10*(2), 90–95. http://doi.org/10.1177/036354658201000205

Athanasiou, K. A., & Eswaramoorthy, R. (2013). Self-Organization and the Self-Assembling Process in Tissue Engineering. *Annu. Rev. Biomed. Eng.*, *15*, 115–136. http://doi.org/10.1146/annurev-bioeng-071812-152423

Aufderheide, A. C., & Athanasiou, K. A. (2006). A direct compression stimulator for articular cartilage and meniscal explants. *Annals of Biomedical Engineering*, *34*(9), 1463–1474. http://doi.org/10.1007/s10439-006-9157-x

Bahcecioglu, G., Bilgen, B., Hasirci, N., & Hasirci, V. (2019). Anatomical meniscus construct with zone specific biochemical composition and structural organization. *Biomaterials*,

218(June), 119361. http://doi.org/10.1016/j.biomaterials.2019.119361

Bahcecioglu, G., Hasirci, N., Bilgen, B., & Hasirci, V. (2018). A 3D printed PCL/hydrogel construct with zone-specific biochemical composition mimicking that of the meniscus.

Bahcecioglu, G., Hasirci, N., Bilgen, B., & Hasirci, V. (2019). International Journal of Biological Macromolecules Hydrogels of agarose , and methacrylated gelatin and hyaluronic acid are more supportive for in vitro meniscus regeneration than three dimensional printed polycaprolactone scaffolds. *International Journal of Biological Macromolecules*, *122*, 1152–1162. http://doi.org/10.1016/j.ijbiomac.2018.09.065

Bahney, C. S., Lujan, T. J., Hsu, C. W., Bottlang, M., West, J. L., & Johnstone, B. (2016). Visible Light Photoinitiation of Mesenchymal Stem Cell-laden Bioresponsive Hydrogels. *Eur Cell Mater*, *22*, 43–55.

Baker, B. E., Peckham, A., Puparo, F., & Sanborn, J. C. (1985). Review of meniscal injury and associated sports. *The American Journal of Sports Medicine*, *13*(1).

Baker, B. M., & Mauck, R. L. (2007). The effect of nanofiber alignment on the maturation of engineered meniscus constructs. *Biomaterials*, *28*(11), 1967–1977. http://doi.org/10.1016/j.biomaterials.2007.01.004

Baker, B. M., Shah, R. P., Huang, A. H., & Mauck, R. L. (2011). Dynamic tensile loading improves the functional properties of mesenchymal stem cell-laden nanofiber-based fibrocartilage. *Tissue Engineering. Part A*, *17*(9–10), 1445–1455. http://doi.org/10.1089/ten.TEA.2010.0535

Baldwin, J., Antille, M., Bonda, U., De-juan-pardo, E. M., Khosrotehrani, K., Ivanovski, S., … Hutmacher, D. W. (2014). In vitro pre-vascularisation of tissue-engineered constructs A co-culture perspective, 1–16. http://doi.org/10.1186/2045-824X-6-13

Balint, E., Gatt, C. J., & Dunn, M. G. (2012). Design and mechanical evaluation of a novel fiber-reinforced scaffold for meniscus replacement. *Journal of Biomedical Materials Research - Part A*, *100 A*(1), 195–202. http://doi.org/10.1002/jbm.a.33260

Ballyns, J. J., Gleghorn, J. P., Niebrzydowski, V., Rawlinson, J. J., Potter, H. G., Maher, S. A., … Bonassar, L. J. (2008). Image-guided tissue engineering of anatomically shaped implants via MRI and micro-CT using injection molding. *Tissue Engineering. Part A*, *14*(7), 1195–1202. http://doi.org/10.1089/ten.tea.2007.0186

Baratz, M. E., Fu, F. H., & Mengato, R. (1986). Meniscal tears : The effect of meniscectomy and of repair on intraarticular contact areas preliminary report *. *The American Journal of Sports Medicine*, *14*(4), 270–275.

Barki, A. M., Bocquet, L., & Stevenson, A. (2017). Linking Rheology and Printability for Dense and Strong Ceramics by Direct Ink Writing, (July), 1–10. http://doi.org/10.1038/s41598-

017-06115-0

Barrett, G. R. (1998). Clinical results of meniscus repair in patients 40 years and older. *Arthroscopy: The Journal of Arthroscopic & Related Surgery*, *14*(8), 824–829. http://doi.org/https://doi.org/10.1016/S0749-8063(98)70018-0

Bas, O., Angella, D. D., Baldwin, J. G., Castro, N. J., Wunner, F. M., Saidy, N. T., … Hutmacher, D. W. (2017). An Integrated Design, Material, and Fabrication Platform for Engineering Biomechanically and Biologically Functional Soft Tissues. *Applied Materials & Interfaces*, *9*, 29430–29437. http://doi.org/10.1021/acsami.7b08617

Bas, O., De-Juan-Pardo, E. M., Chhaya, M. P., Wunner, F. M., Jeon, J. E., Klein, T. J., & Hutmacher, D. W. (2015). Enhancing structural integrity of hydrogels by using highly organised melt electrospun fibre constructs. *European Polymer Journal*, *72*, 451–463. http://doi.org/10.1016/j.eurpolymj.2015.07.034

Bernal, P. N., Delrot, P., Loterie, D., Li, Y., Malda, J., Moser, C., & Levato, R. (2019). Volumetric Bioprinting of Complex Living-Tissue Constructs within Seconds, *1904209*. http://doi.org/10.1002/adma.201904209

Billiet, T., Gevaert, E., De Schryver, T., Cornelissen, M., & Dubruel, P. (2014). The 3D printing of gelatin methacrylamide cell-laden tissue-engineered constructs with high cell viability. *Biomaterials*, *35*(1), 49–62. http://doi.org/10.1016/j.biomaterials.2013.09.078

Blache, U., Stevens, M. M., & Gentleman, E. (2020). Harnessing the secreted extracellular matrix to engineer tissues. *Nature Biomedical Engineering*. http://doi.org/10.1038/s41551-019-0500-6

Bracht, H. Van der, Verdonk, R., Verbruggen, G., Elewaut, D., & Verdonk, P. (2007). Cell-Based Meniscus Tissue Engineering. *Topics in Tissue Engineering*, *3*.

Bray, R. C., Smith, J. A., Eng, M. K., Leonard, C. A., Sutherland, C. A., & Salo, P. T. (2001). Vascular response of the meniscus to injury: effects of immobilization. *Journal of Orthopaedic Research : Official Publication of the Orthopaedic Research Society*, *19*(3), 384–390. http://doi.org/10.1016/S0736-0266(00)00037-1

Browe, D. C., Kelly, D. J., Mahon, O. R., & Díaz-payno, P. J. (2019). Glyoxal cross-linking of solubilized extracellular matrix to produce highly porous , elastic , and chondro-permissive scaffolds for orthopedic tissue engineering, (January), 2222–2234. http://doi.org/10.1002/jbm.a.36731

Browner, B. (2009). *Skeletal trauma: basic science, management, and reconstruction.* London: Elsevier Health Sciences.

Bryant, S. J., Chowdhury, T. T., Lee, D. A., Bader, D. L., & Anseth, K. S. (2004). Crosslinking density influences chondrocyte metabolism in dynamically loaded photocrosslinked

poly(ethylene glycol) hydrogels. *Annals of Biomedical Engineering*, *32*(3), 407–417. http://doi.org/10.1023/b:abme.0000017535.00602.ca

Buckley, C. T., Vinardell, T., Thorpe, S. D., Haugh, M. G., Jones, E., McGonagle, D., & Kelly, D. J. (2010). Functional properties of cartilaginous tissues engineered from infrapatellar fat pad-derived mesenchymal stem cells. *Journal of Biomechanics*, *43*(5), 920–926. http://doi.org/10.1016/j.jbiomech.2009.11.005

Bulgheroni, P., Murena, L., Ratti, C., Bulgheroni, E., Ronga, M., & Cherubino, P. (2010). Follow-up of collagen meniscus implant patients: clinical, radiological, and magnetic resonance imaging results at 5 years. *The Knee*, *17*(3), 224–229. http://doi.org/10.1016/j.knee.2009.08.011

Bullough, P. G., Munuera, L., Murphy, J., & Weinstein, A. M. (1970). the Strength of the Menisci of the Knee As It Relates To Their Fine Structure. *J Bone Joint Surg Br*, *52–B*(3), 564–570. Retrieved from http://www.bjj.boneandjoint.org.uk/content/52-B/3/564.short

Burr, D. B., Frederickson, R. G., Pavlinch, C., Sickles, M., & Burkart, S. (1984). Intracast muscle stimulation prevents bone and cartilage deterioration in cast-immobilized rabbits. *Clinical Orthopaedics and Related Research*, (189), 264–278.

Caplan, A. I. (2017). New MSC : MSCs as Pericytes Are Sentinels and Gatekeepers. *J Orthop Res*, *35*(April), 10–13. http://doi.org/10.1002/jor.23560

Caplan, A. I., & Dennis, J. E. (2006). Mesenchymal Stem Cells as Trophic Mediators, *1084*, 1076–1084. http://doi.org/10.1002/jcb.20886

Castilho, M., Hochleitner, G., Wouter, W., Rietbergen, B. Van, & Paul, D. (2018). Mechanical behavior of a soft hydrogel reinforced with three- dimensional printed microfibre scaffolds. *Scientific Reports*, *8*, 1–10. http://doi.org/10.1038/s41598-018-19502-y

Chatain, F., Robinson, A. H. N., Adeleine, P., Chambat, P., Livet, C., Margnolles, D., … Charial, R. A. (2001). The natural history of the knee following arthroscopic medial meniscectomy. *Knee Surg, Sports Traumatol, Arthrosc*, *9*, 15–18. http://doi.org/10.1007/s001670000146

Chen, G.-Q., & Wu, Q. (2005). The application of polyhydroxyalkanoates as tissue engineering materials. *Biomaterials*, *26*(33), 6565–6578. http://doi.org/10.1016/j.biomaterials.2005.04.036

Chen, J., & Cheng, T. (2006). Thermo-Responsive Chitosan- graft -poly (N - isopropylacrylamide) Injectable Hydrogel for Cultivation of Chondrocytes and Meniscus Cells. *Macromolecular Bioscience*, *6*, 1026–1039. http://doi.org/10.1002/mabi.200600142

Chen, X., Zhou, Y., Wang, L., Santare, M. H., Wan, L. Q., Lucas, X., & Lu1. (2017). Determining Tension-Compression Nonlinear Mechanical Properties of Articular Cartilage from Indentation Testing, *44*(4), 1148–1158. http://doi.org/10.1007/s10439-015-1402-

8.Determining

Chen, Y.-C., Chen, R.-N., Jhan, H.-J., Liu, D.-Z., Ho, H.-O., Mao, Y., … Sheu, M.-T. (2015). Development and characterization of acellular extracellular matrix scaffolds from porcine menisci for use in cartilage tissue engineering. *Tissue Engineering Part C: Methods*, *21*(9), 971–986.

Chen, Y. X., Cain, B., & Soman, P. (2017). Gelatin methacrylate-alginate hydrogel with tunable viscoelastic properties, *4*(December 2016), 363–369. http://doi.org/10.3934/matersci.2017.2.363

Chen, Y., Zhou, C., & Lao, J. (2011). A layerless additive manufacturing process based on CNC accumulation, *3*(November 2010), 218–227. http://doi.org/10.1108/13552541111124806

Chiari, C., Koller, U., Dorotka, R., Eder, C., Plasenzotti, R., Lang, S., … Nehrer, S. (2006). A tissue engineering approach to meniscus regeneration in a sheep model. *Osteoarthritis and Cartilage*, *14*(10), 1056–1065. http://doi.org/10.1016/j.joca.2006.04.007

Chimene, D., Kaunas, R., & Gaharwar, A. K. (2020). Hydrogel Bioink Reinforcement for Additive Manufacturing : A Focused Review of Emerging Strategies, *1902026*, 1–22. http://doi.org/10.1002/adma.201902026

Chimene, D., Lennox, K. K., Kaunas, R. R., & Gaharwar, A. K. (2016). Advanced Bioinks for 3D Printing: A Materials Science Perspective. *Annals of Biomedical Engineering*, *44*(6), 2090–2102. http://doi.org/10.1007/s10439-016-1638-y

Chimene, D., Peak, C. W., Gentry, J. L., Carrow, J. K., Cross, L. M., Mondragon, E., … Gaharwar, A. K. (2018). Nanoengineered Ionic − Covalent Entanglement (NICE) Bioinks for 3D Bioprinting. http://doi.org/10.1021/acsami.7b19808

Choudhury, D., Anand, S., & Naing, M. W. (2018). The arrival of commercial bioprinters – Towards 3D bioprinting revolution !, (June). http://doi.org/10.18063/IJB.v4i2.139

Collier, S., & Ghosh, P. (1995). Effects of transforming growth factor beta on proteoglycan synthesis by cell and explant cultures derived from the knee joint meniscus. *Osteoarthritis and Cartilage*, *3*(2), 127–138. http://doi.org/10.1016/S1063-4584(05)80045-7

Colosi, C., Shin, S. R., Manoharan, V., Massa, S., Costantini, M., Barbetta, A., … Khademhosseini, A. (2016). Microfl uidic Bioprinting of Heterogeneous 3D Tissue Constructs Using Low-Viscosity Bioink, 677–684. http://doi.org/10.1002/adma.201503310

Costantini, M., Onofrillo, C., Duchi, S., Daly, A. C., & Critchley, S. E. (n.d.). 3D bioprinting of BM-MSCs-loaded ECM biomimetic hydrogels for in vitro neocartilage formation 3D bioprinting of BM-MSCs-loaded ECM biomimetic hydrogels for in vitro neocartilage formation.

Crapo, P. M., Gilbert, T. W., & Badylak, S. F. (2011a). An overview of tissue and whole organ

decellularization processes. *Biomaterials*, *32*(12), 3233–3243. http://doi.org/https://doi.org/10.1016/j.biomaterials.2011.01.057

Crapo, P. M., Gilbert, T. W., & Badylak, S. F. (2011b). An overview of tissue and whole organ decellularization processes. *Biomaterials*, *32*(12), 3233–3243. http://doi.org/10.1016/j.biomaterials.2011.01.057

Cunniffe, G. M., Díaz-payno, P. J., Sheehy, E. J., Critchley, S. E., Almeida, H. V, Pitacco, P., … Kelly, D. J. (2019). Biomaterials Tissue-specific extracellular matrix scaffolds for the regeneration of spatially complex musculoskeletal tissues. *Biomaterials*, *188*(September 2018), 63–73. http://doi.org/10.1016/j.biomaterials.2018.09.044

Dalton, P. D. (n.d.). ScienceDirect Melt electrowriting with additive manufacturing principles. *Current Opinion in Biomedical Engineering*, *2*, 49–57. http://doi.org/10.1016/j.cobme.2017.05.007

Daly, A. C., Critchley, S. E., Rensock, E. M., & Kelly, D. J. (2016a). A Comparison of Different Bioinks for 3D Bioprinting of Fibrocartilage and Hyaline Cartilage, 1–25.

Daly, A. C., Critchley, S. E., Rensock, E. M., & Kelly, D. J. (2016b). A Comparison of Different Bioinks for 3D Bioprinting of Fibrocartilage and Hyaline Cartilage. *Biofabrication*, *8*(4), 1–25. http://doi.org/10.1088/1758-5090/8/4/045002

Daly, A. C., Cunniffe, G. M., Sathy, B. N., Jeon, O., Alsberg, E., & Kelly, D. J. (2016). 3D Bioprinting of Developmentally Inspired Templates for Whole Bone Organ Engineering. *Advanced Healthcare Materials*, *5*(18), 2353–2362. http://doi.org/10.1002/adhm.201600182

Daly, A. C., & Kelly, D. J. (2019). Biomaterials Biofabrication of spatially organised tissues by directing the growth of cellular spheroids within 3D printed polymeric microchambers. *Biomaterials*, *197*(January), 194–206. http://doi.org/10.1016/j.biomaterials.2018.12.028

Daly, A. C., Pitacco, P., Nulty, J., & Kelly, D. J. (2018). Biomaterials 3D printed microchannel networks to direct vascularisation during endochondral bone repair, *162*, 34–46. http://doi.org/10.1016/j.biomaterials.2018.01.057

Darling, E. M., & Athanasiou, K. A. (2005). Rapid phenotypic changes in passaged articular chondrocyte subpopulations, *23*, 425–432. http://doi.org/10.1016/j.orthres.2004.08.008

de Groot, J. (2010). Actifit, Polyurethane meniscus implant: basic science. In *The Meniscus* (pp. 383–387). Berlin, Heidelberg: Springer Berlin Heidelberg. http://doi.org/10.1007/978-3-642-02450-4_48

de Ruijter, M., Hrynevich, A., Haigh, J. N., Hochleitner, G., Castilho, M., Groll, J., … Dalton, P. D. (2018). Out-of-Plane 3D-Printed Microfibers Improve the Shear Properties of Hydrogel Composites. *Small*, *14*(8), 1702773. http://doi.org/10.1002/smll.201702773

Dehaven, K. E., & Arnoczky, S. P. (1994). Meniscal Repair, Part 1: Basic Science. Indications for repair and open repair. *J Bone Joint Surg [Am]*, *76–A*, 140–152.

Dienst, M., Greis, P. E., Ellis, B. J., Bachus, K. N., & Burks, R. T. (2007). Effect of Lateral Meniscal Allograft Sizing on Contact Mechanics of the Lateral Tibial Plateau An Experimental Study in Human Cadaveric Knee Joints, 34–42. http://doi.org/10.1177/0363546506291404

Djurasovic, M., Aldridge, J. W., Grumbles, R., Rosenwasser, M. P., Howell, D., & Ratcliffe, A. (1998). Knee joint immobilization decreases aggrecan gene expression in the meniscus. *The American Journal of Sports Medicine*, *26*(3), 460–466. http://doi.org/10.1177/03635465980260032101

Do, J. T., Hong, K., Cha, J. M., Shin, S. R., & Bae, H. (2018). Marine Biomaterial-Based Bioinks for Generating 3D Printed Tissue Constructs. *Marine Drugs*, *16*(12). http://doi.org/10.3390/md16120484

Dowdy, P. A., Miniaci, A., Arnoczky, S. P., Fowler, P. J., & Boughner, D. R. (1995). The effect of cast immobilization on meniscal healing. An experimental study in the dog. *The American Journal of Sports Medicine*, *23*(6), 721–728. http://doi.org/10.1177/036354659502300615

Driscoll, T. P., Nerurkar, N. L., Jacobs, N. T., Elliott, D. M., & Mauck, R. L. (2011). Fiber angle and aspect ratio influence the shear mechanics of oriented electrospun nanofibrous scaffolds. *Journal of the Mechanical Behavior of Biomedical Materials*, *4*(8), 1627–1636. http://doi.org/10.1016/j.jmbbm.2011.03.022

Dudurych, I. (2015). Fabrication and In Vitro Characterisation of Glyoxal Cross-linked Collagen Type II Scaffolds and Hydrogels By, (August).

Elsner, J. J., & Linder-ganz, E. (2010). Design of a Free-Floating Implant Using Finite Element Modeling and Experimental Validation. *Journal of Biomechanical Engineering*, *132*(September), 1–8. http://doi.org/10.1115/1.4001892

Englund, M., Guermazi, A., Roemer, F. W., Aliabadi, P., Yang, M., Lewis, C. E., … Felson, D. T. (2009). Meniscal tear in knees without surgery and the development of radiographic osteoarthritis among middle-aged and elderly persons: The multicenter osteoarthritis study. *Arthritis & Rheumatism*, *60*(3), 831–839. http://doi.org/10.1002/art.24383

Englund, M., Niu, J., Guermazi, A., Roemer, F. W., Hunter, D. J., Lynch, J. A., … Felson, D. T. (2007). Effect of meniscal damage on the development of frequent knee pain, aching, or stiffness. *Arthritis & Rheumatism*, *56*(12), 4048–4054. http://doi.org/10.1002/art.23071

Englund, M., Roos, E. M., & Lohmander, L. S. (2003). Impact of type of meniscal tear on radiographic and symptomatic knee osteoarthritis: A sixteen-year followup of meniscectomy with matched controls. *Arthritis & Rheumatism*, *48*(8), 2178–2187. http://doi.org/10.1002/art.11088

Englund, M., Roos, E. M., Roos, H. P., & Lohmander, L. S. (2001). Patient-relevant outcomes fourteen years after meniscectomy: influence of type of meniscal tear and size of resection. *Rheumatology*, *40*, 631–639.

Fairbank, T. (1947). Knee Joint Changes after Meniscectomy. *The Journal of Bone and Joint Surgery*, *30–B*(4).

Ferretti, M., Srinivasan, A., Deschner, J., Gassner, R., Baliko, F., Piesco, N., … Agarwal, S. (2005). Anti-inflammatory effects of continuous passive motion on meniscal fibrocartilage. *Journal of Orthopaedic Research : Official Publication of the Orthopaedic Research Society*, *23*(5), 1165–1171. http://doi.org/10.1016/j.orthres.2005.01.025

Fithian, D., Kelly, M., & Mow, V. C. (1990). Material properties and structure-function relationships in the menisci. *Clinical Orhtopaedics and Related Research*, *252*.

Forriol, F. (2009). Growth factors in cartilage and meniscus repair. *Injury*, *40*, S12–S16. http://doi.org/https://doi.org/10.1016/S0020-1383(09)70005-1

Freeman, F. E., & Kelly, D. J. (2017). Tuning Alginate Bioink Stiffness and Composition for Controlled Growth Factor Delivery and to Spatially Direct MSC Fate within Bioprinted Tissues. *Scientific Reports*, (November), 1–12. http://doi.org/10.1038/s41598-017-17286-1

Gannon, A., Nagel, T., & Kelly, D. J. (2012). The role of the superficial region in determining the dynamic properties of articular cartilage. *Osteoarthritis and Cartilage*, *20*(June).

Ghadially, F. N., Thomas, I., Yong, N., & Lalonde, J. M. (1978). Ultrastructure of rabbit semilunar cartilages. *Journal of Anatomy*, *125*(Pt 3), 499–517.

Ghosh, P., & Taylor, T. (1987). The knee joint meniscus: A fibrocartilage of some distinction. *Clin Orthop Relat Res.*, *224*.

Gibson, I., Rosen, D., & Stucker, B. (2010). *Additive Manufacturing Technologies* (2nd ed.). New York, Heidelberg, Dordrecht, London: Springer.

Grayson, W. L., Bhumiratana, S., Cannizzaro, C., Chao, P.-H. G., Lennon, D. P., Caplan, A. I., & Vunjak-Novakovic, G. (2008). Effects of Initial Seeding Density and Fluid Perfusion Rate on Formation of Tissue-Engineered Bone. *Tissue Engineering Part A*, *14*(11), 1809–1820. http://doi.org/10.1089/ten.tea.2007.0255

Greis, P. E., Bardana, D. D., Holmstrom, M. C., & Burks, R. T. (2002). Meniscal Injury : I . Basic Science and Evaluation, 168–176.

Gunja, N. J., & Athanasiou, K. A. (2007). Passage and reversal effects on gene expression of bovine meniscal fibrochondrocytes. *Arthritis Research & Therapy*, *9*(5), R93–R93. http://doi.org/10.1186/ar2293

Gunja, N. J., Huey, D. J., James, R. A., & Athanasiou, K. A. (2009). Effects of agarose mould

compliance and surface roughness on self-assembled meniscus-shaped constructs, (August), 521–530. http://doi.org/10.1002/term

Gupta, T., Zielinska, B., McHenry, J., Kadmiel, M., & Haut Donahue, T. L. (2008). IL-1 and iNOS gene expression and NO synthesis in the superior region of meniscal explants are dependent on the magnitude of compressive strains. *Osteoarthritis and Cartilage*, *16*(10), 1213–1219. http://doi.org/10.1016/j.joca.2008.02.019

Hall, M., Wrigley, T. V, Metcalf, B. R., Hinman, R. S., Dempsey, A. R., Mills, P. M., … Bennell, K. L. (2014). A longitudinal study of impact and early stance loads during gait following arthroscopic partial meniscectomy. *Journal of Biomechanics*, *47*(12), 0–18.

Harston, A., Nyland, J., Brand, E., Mcginnis, M., & Caborn, D. N. M. (2012). Collagen meniscus implantation : a systematic review including rehabilitation and return to sports activity, 135–146. http://doi.org/10.1007/s00167-011-1579-9

Hatsushika, D., Muneta, T., Nakamura, T., Horie, M., Koga, H., Nakagawa, Y., … Sekiya, I. (2014). Repetitive allogeneic intraarticular injections of synovial mesenchymal stem cells promote meniscus regeneration in a porcine massive meniscus defect model. *Osteoarthritis and Cartilage*, *22*(7), 941–950. http://doi.org/https://doi.org/10.1016/j.joca.2014.04.028

Hede, A., Larsen, E., & Sandberg, H. (1992). The long term outcome of open total and partial meniscectomy related to the quantity and site of the meniscus removed. *International Orthopaedics*, *16*, 122–125.

Heijkants, R. G. J. C., van Calck, R. V, De Groot, J. H., Pennings, A. J., Schouten, A. J., van Tienen, T. G., … Veth, R. P. H. (2004). Design, synthesis and properties of a degradable polyurethane scaffold for meniscus regeneration. *Journal of Materials Science. Materials in Medicine*, *15*(4), 423–427. http://doi.org/10.1023/b:jmsm.0000021114.39595.1e

Hellio Le Graverand, M. P., Ou, Y., Schield-Yee, T., Barclay, L., Hart, D., Natsume, T., & Rattner, J. B. (2001). The cells of the rabbit meniscus: their arrangement, interrelationship, morphological variations and cytoarchitecture. *Journal of Anatomy*, *198*(Pt 5), 525–535. http://doi.org/10.1046/j.1469-7580.2000.19850525.x

Hennerbichler, A., Moutos, F. T., Hennerbichler, D., Centers, D. M., & Carolina, N. (2007). Repair Response of the Inner and Outer Regions of the Porcine Meniscus In Vitro. *The American Journal of Sports Medicine*, *35*(5), 754–762. http://doi.org/10.1177/0363546506296416

Henning CE, Lynch MA, Yearout KM, Vequist SW, Stallbaumer RJ, D. K. (1990). Arthroscopic meniscal repair using an exogenous fibrin clot. *Clinical Orthopaedics and Related Research*, *252*, 64–72.

Herwig, J., Egner, E., & Buddecke, E. (1984). Chemical changes of human knee joint menisci in

various stages of degeneration, 635–640.

Higashioka, M. M., Chen, J. A., Hu, J. C., & Athanasiou, K. A. (2014). Building an Anisotropic Meniscus with Zonal Variations, *20*, 294–302. http://doi.org/10.1089/ten.tea.2013.0098

Hoben, G. M., Hu, J. C., Ph, D., James, R. A., Athanasiou, K. A., & Ph, D. (2007). Self-Assembly of Fibrochondrocytes and Chondrocytes for Tissue Engineering of the Knee Meniscus*, *13*(5). http://doi.org/10.1089/ten.2006.0116

Hugh, C., & MacNab, I. (1972). The Structure of the Meniscus of the Human Knee joint. *Clinical Orhtopaedics and Related Research*, *89*.

Hutchinson, I. D., Moran, C. J., Potter, H. G., Warren, R. F., & Rodeo, S. a. (2014). Restoration of the meniscus: form and function. *The American Journal of Sports Medicine*, *42*(4), 987–98. http://doi.org/10.1177/0363546513498503

Hutmacher, D. W. (2000). Scaffolds in tissue engineering bone and cartilage. *Biomaterials*, *21*(24), 2529–43. Retrieved from http://www.ncbi.nlm.nih.gov/pubmed/11071603

Iyer, R. K., Chiu, L. L. Y., Vunjak-Novakovic, G., & Radisic, M. (2012). Biofabrication enables efficient interrogation and optimization of sequential culture of endothelial cells , fibroblasts and cardiomyocytes for formation of vascular cords in cardiac tissue engineering. *Biofabrication*, *4*(3). http://doi.org/10.1088/1758-5082/4/3/035002

Izuta, Y., Ochi, M., Adachi, N., Deie, M., Yamasaki, T., & Shinomiya, R. (2005). Meniscal repair using bone marrow-derived mesenchymal stem cells : experimental study using green fluorescent protein transgenic rats. *The Knee*, *12*, 217–223. http://doi.org/10.1016/j.knee.2001.06.001

Jeon, O., Shin, J.-Y., Marks, R., Hopkins, M., Kim, T.-H., Park, H.-H., & Alsberg, and E. (2017). Highly Elastic and Tough Interpenetrating Polymer Network- Structured Hybrid Hydrogels for Cyclic Mechanical Loading- Enhanced Tissue Engineering. *Chemistry of Materials*, *29*, 8425–8432. http://doi.org/10.1021/acs.chemmater.7b02995

Johannah Sanchez-A, & Athanasiou, K. A. (2009). The Knee Meniscus : A Complex Tissue of Diverse Cells. *Cellular and Molecular Bioengineering*, *2*(3), 332–340. http://doi.org/10.1007/s12195-009-0066-6

Jones, D. S., Mclaughlin, D. W. J., Mccoy, C. P., & Gorman, S. P. (2005). Physicochemical characterisation and biological evaluation of hydrogel-poly (e -caprolactone) interpenetrating polymer networks as novel urinary biomaterials. *Biomaterials*, *26*, 1761–1770. http://doi.org/10.1016/j.biomaterials.2004.06.002

Jones, R. S., Keene, G. C. R., Learmonth, D. J. A., Nawana, N. S., Costi, J. J., & Pearcy, M. J. (1996). Direct measurement of hoop strains in the intact and torn human medial meniscus, *1*. http://doi.org/10.1016/0268-0033(96)00003-4

Jr, C. T. V., Ii, J. F., Boyd, J., Dellaero, D. T., Mills, C. R., & Leroux-williams, M. (2014). Adult Human Mesenchymal Stem Cells Delivered via, 90–98.

Kahlon, A., Hurtig, M. B., & Gordon, K. D. (2015). Regional and depth variability of porcine meniscal mechanical properties through biaxial testing. *Journal of the Mechanical Behavior of Biomedical Materials*, *41*, 108–14. http://doi.org/10.1016/j.jmbbm.2014.10.008

Keating, S., & Oxman, N. (2013). Robotics and Computer-Integrated Manufacturing Compound fabrication : A multi-functional robotic platform for digital design and fabrication. *Robotics and Computer Integrated Manufacturing*, *29*(6), 439–448. http://doi.org/10.1016/j.rcim.2013.05.001

Kendall, K., & Fuller, K. (1987). J-shaped stress / strain curves and crack resistance of biological materials.

Killian, M. L., Haut, R. C., & Haut Donahue, T. L. (2014). Acute cell viability and nitric oxide release in lateral menisci following closed-joint knee injury in a lapine model of post-traumatic osteoarthritis. *BMC Musculoskeletal Disorders*, *15*, 297. http://doi.org/10.1186/1471-2474-15-297

Kim, Y. M., Rhee, K. J., Lee, J. K., Hwang, D. S., Yang, J. Y., & Kim, S. J. (2006). Arthroscopic Pullout Repair of a Complete Radial Tear of the Tibial Attachment Site of the Medial Meniscus Posterior Horn. *Arthroscopy - Journal of Arthroscopic and Related Surgery*, *22*(7), 1–4. http://doi.org/10.1016/j.arthro.2005.12.040

Klein, L., Heiple, K. G., Torzilli, P. A., Goldberg, V. M., & Burstein, A. H. (1989). Prevention of ligament and meniscus atrophy by active joint motion in a non-weight-bearing model. *Journal of Orthopaedic Research : Official Publication of the Orthopaedic Research Society*, *7*(1), 80–85. http://doi.org/10.1002/jor.1100070111

Klein, L., Player, J. S., Heiple, K. G., Bahniuk, E., & Goldberg, V. M. (1982). Isotopic evidence for resorption of soft tissues and bone in immobilized dogs. *The Journal of Bone and Joint Surgery. American Volume*, *64*(2), 225–230.

Klompmaker, J., Jansen, H. W., Veth, R. P., de Groot, J. H., Nijenhuis, A. J., & Pennings, A. J. (1991). Porous polymer implant for repair of meniscal lesions: a preliminary study in dogs. *Biomaterials*, *12*(9), 810–816. http://doi.org/10.1016/0142-9612(91)90066-j

Kon, E., Chiari, C., Marcacci, M., Delcogliano, M., Salter, D. M., Martin, I., … Ph, D. (2008). Tissue Engineering for Total Meniscal Substitution : Animal Study in Sheep Model. *TISSUE ENGINEERING: Part A*, *14*(6). http://doi.org/10.1089/ten.tea.2007.0193

Kon, E., Filardo, G., Tschon, M., Sc, B., Ph, D., Fini, M., … Marcacci, M. (2012). Tissue Engineering for Total Meniscal Substitution : Animal Study in Sheep Model — Results at 12 Months. *TISSUE ENGINEERING: Part A*, *18*. http://doi.org/10.1089/ten.tea.2011.0572

Krishnamoorthy, S., & Zhang, Z. (2019a). Biofabrication of three-dimensional cellular structures based on gelatin methacrylate – alginate interpenetrating network hydrogel. *Journal of Biomaterials Applications*, *33*(8). http://doi.org/10.1177/0885328218823329

Krishnamoorthy, S., & Zhang, Z. (2019b). Biofabrication of three-dimensional cellular structures based on gelatin methacrylate – alginate interpenetrating network hydrogel. http://doi.org/10.1177/0885328218823329

Kwon, H., Brown, W. E., Lee, C. A., Wang, D., Paschos, N., Hu, J. C., & Athanasiou, K. A. (2019). Surgical and tissue engineering strategies for articular cartilage and meniscus. *Nature Reviews Rheumatology*, *15*, 550–570. http://doi.org/10.1038/s41584-019-0255-1

Lanzer, W. L., & Komenda, G. (1990). Changes in Articular Cartilage After Meniscectomy. *Clinical Orthopaedics and Related Research*, *252*, 41–48.

Lechner, K., Hull, M. L., & Howell, M. (2000). Is the Circumferential Tensile Modulus within a Human Medial Meniscus Affected by the Test Sample Location and Cross-Sectional Area ?, (6).

Lee, C. H., Moioli, E. K., & Mao, J. J. (2006). Fibroblastic differentiation of human mesenchymal stem cells using connective tissue growth factor. *Conference Proceedings : ... Annual International Conference of the IEEE Engineering in Medicine and Biology Society. IEEE Engineering in Medicine and Biology Society. Annual Conference*, *1*, 775–778. http://doi.org/10.1109/IEMBS.2006.259866

Lee, C. H., Rodeo, S. A., Fortier, L. A., Lu, C., Erisken, C., & Mao, J. J. (2014). Protein-releasing polymeric scaffolds induce fibrochondrocytic differentiation of endogenous cells for knee meniscus regeneration in sheep. *Sci Transl Med*, *6*(266), 266ra171. http://doi.org/10.1126/scitranslmed.3009696

Lee, C. H., Rodeo, S. A., Fortier, L. A., Lu, C., Erisken, C., & Mao, J. J. (2014). Protein-releasing polymeric scaffolds induce fibrochondrocytic differentiation of endogenous cells for knee meniscus regeneration in sheep. *Tissue Engineering*, *6*(266), 1–11.

Lee, C. S. D., Moyer, H. R., I, R. A. G., Williams, J. K., Boskey, A. L., Boyan, B. D., & Schwartz, Z. (2010). Regulating in vivo calcification of alginate microbeads. *Biomaterials*, *31*, 4926–4934. http://doi.org/10.1016/j.biomaterials.2010.03.001

Lee, S., Bin, S., Kim, J., Lee, B., Lee, C., Son, D., & Park, J. (2019). Long-term Outcomes of Meniscal Allograft Transplantation With and Without Extrusion. *The American Journal of Sports Medicine*, *4*, 815–821. http://doi.org/10.1177/0363546518825251

Lee, S. R., Kim, J. G., & Nam, S. W. (2012). The Tips and Pitfalls of Meniscus Allograft Transplantation, *24*(3), 137–145.

Leroy, A., Beaufils, P., Faivre, B., Steltzlen, C., Boisrenoult, P., & Pujol, N. (2016). Actifit®

polyurethane meniscal scaffold: MRI and functional outcomes after a minimum follow-up of 5 years. *Orthopaedics and Traumatology: Surgery and Research*, *103*(4), 609–614. http://doi.org/10.1016/j.otsr.2017.02.012

Levato, R., Visser, J., Planell, J. A., & Engel, E. (2014). Biofabrication of tissue constructs by 3D bioprinting of cell-laden microcarriers. *Biofabrication*, *6*. http://doi.org/10.1088/1758-5082/6/3/035020

Levett, P. A., Melchels, F. P. W., Schrobback, K., Hutmacher, D. W., Malda, J., & Klein, T. J. (2014). A biomimetic extracellular matrix for cartilage tissue engineering centered on photocurable gelatin , hyaluronic acid and chondroitin sulfate. *Acta Biomaterialia*, *10*(1), 214–223. http://doi.org/10.1016/j.actbio.2013.10.005

Li, Q., Qu, F., Han, B., Wang, C., Li, H., Mauck, R. L., & Han, L. (2017). Micromechanical anisotropy and heterogeneity of the meniscus extracellular matrix. *Acta Biomaterialia*, *54*. http://doi.org/10.1016/j.actbio.2017.02.043

Li, W.-J., Cooper, J. A. J., Mauck, R. L., & Tuan, R. S. (2006). Fabrication and characterization of six electrospun poly(alpha-hydroxy ester)-based fibrous scaffolds for tissue engineering applications. *Acta Biomaterialia*, *2*(4), 377–385. http://doi.org/10.1016/j.actbio.2006.02.005

Li, X., Lu, Z., Yang, Z., & Yang, C. (2018). Anisotropic in-plane mechanical behavior of square honeycombs under off-axis loading. *Materials & Design*, *158*, 88–97. http://doi.org/10.1016/j.matdes.2018.08.007

Liao, I.-C., Moutos, F. T., Estes, B. T., Zhao, X., & Guilak, F. (2013). Composite Three-Dimensional Woven Scaffolds with Interpenetrating Network Hydrogels to Create Functional Synthetic Articular Cartilage. *Advanced Functional Materials*, *23*(47), 5833–5839. http://doi.org/10.1002/adfm.201300483

Liberski, A., Latif, N., Raynaud, C., Bollensdorff, C., & Yacoub, M. (2016). Alginate for cardiac regeneration : From seaweed to clinical trials. *Global Cardiology Science & Practice*, *4*.

Loessner, D., Meinert, C., Kaemmerer, E., Martine, L. C., Yue, K., Levett, P. A., … Hutmacher, D. W. (2016). Functionalization , preparation and use of cell-laden gelatin methacryloyl – based hydrogels as modular tissue culture platforms. *Nature Protocols*, *11*(4), 727–746. http://doi.org/10.1038/nprot.2016.037

Longo, U. G., Campi, S., Romeo, G., Spiezia, F., Maffulli, N., & Denaro, V. (2012). Biological Strategies to Enhance Healing of the Avascular Area of the Meniscus. *Stem Cells International*, *2012*, 528359. http://doi.org/10.1155/2012/528359

Luo, L., Thorpe, S. D., Buckley, C. T., & Kelly, D. J. (2015). The effects of dynamic compression on the development of cartilage grafts engineered using bone marrow and infrapatellar fat pad derived stem cells The effects of dynamic compression on the development of cartilage grafts engineered using bone marrow and. *Biomedical Materials*, *10*.

http://doi.org/10.1088/1748-6041/10/5/055011

Maher, S. A., Rodeo, S. A., Doty, S. B., Brophy, R., Potter, H., Foo, L.-F., … Warren, R. F. (2010). Evaluation of a porous polyurethane scaffold in a partial meniscal defect ovine model. *Arthroscopy : The Journal of Arthroscopic & Related Surgery : Official Publication of the Arthroscopy Association of North America and the International Arthroscopy Association*, *26*(11), 1510–1519. http://doi.org/10.1016/j.arthro.2010.02.033

Majewski, M., & Susanne, H. (2006). Epidemiology of athletic knee injuries : A 10-year study, *13*, 184–188. http://doi.org/10.1016/j.knee.2006.01.005

Makris, E. A., Hadidi, P., & Athanasiou, K. A. (2011a). The knee meniscus : Structure, function, pathophysiology, current repair techniques, and prospects for regeneratio n. *Biomaterials*, *32*(30), 7411–7431. http://doi.org/10.1016/j.biomaterials.2011.06.037

Makris, E. A., Hadidi, P., & Athanasiou, K. A. (2011b). The knee meniscus: Structure-function, pathophysiology, current repair techniques, and prospects for regeneration. *Biomaterials*, *32*(30), 7411–7431. http://doi.org/10.1016/j.biomaterials.2011.06.037

Makris, E. A., Macbarb, R. F., Paschos, N. K., Hu, J. C., & Athanasiou, K. A. (2014). Biomaterials crosslinking agent lysyl oxidase to engineer functional neotissues for fi brocartilage repair. *Biomaterials*, *35*(25), 6787–6796. http://doi.org/10.1016/j.biomaterials.2014.04.083

Malda, J., Visser, J., Melchels, F. P., Jüngst, T., Hennink, W. E., Dhert, W. J. A., … Hutmacher, D. W. (2013). 25th anniversary article: Engineering hydrogels for biofabrication. *Advanced Materials*, *25*(36), 5011–5028. http://doi.org/10.1002/adma.201302042

Mandal, B. B., Park, S.-H., Gil, E. S., & Kaplan, D. L. (2011). Stem Cell-Based Meniscus Tissue Engineering. *Tissue Engineering Part A*, *17*(21–22), 2749–2761. http://doi.org/10.1089/ten.tea.2011.0031

Maroti, P., Varga, P., Abraham, H., Falk, G., Zsebe, T., & Meiszterics, Z. (2019). Printing orientation defines anisotropic mechanical properties in additive manufacturing of upper limb prosthetics Printing orientation de fi nes anisotropic mechanical properties in additive manufacturing of upper limb prosthetics. *Materials Research Express*, *6*.

Martinek, V., Ueblacker, P., Bräun, K., Nitschke, S., Mannhardt, R., Specht, K., … Imhoff, A. B. (2006). Second generation of meniscus transplantation: in-vivo study with tissue engineered meniscus replacement. *Archives of Orthopaedic and Trauma Surgery*, *126*(4), 228–234. http://doi.org/10.1007/s00402-005-0025-1

Matteo, B. Di, Tarabella, C. J. M. V, & Tomba, A. V. P. (2016). A history of meniscal surgery : from ancient times to the twenty - first century. *Knee Surgery, Sports Traumatology, Arthroscopy*, *24*(5), 1510–1518. http://doi.org/10.1007/s00167-015-3717-2

Mcdermott, I. D., & Amis, A. A. (2006). The consequences of meniscectomy. *The Journal of Bone and Joint Surgery. British Volume*, *88*(12), 1549–1556. http://doi.org/10.1302/0301-620X.88B12.18140

Mcdevitt, C. A., Mukherjee, S., Kambic, H., & Parker, R. (2002). Emerging concepts of the cell biology of the meniscus. *Current Opinion in Orthopaedics*, *13*, 345–350. http://doi.org/10.1097/01.BCO.0000030328.07427.B1

McDevitt, C. A., & Webber, R. J. (1990). The ultrastructure and biochemistry of meniscal cartilage. *Clinical Orthopaedics and Related Research*, (252), 8–18.

McHenry, J. A., Zielinska, B., & Donahue, T. L. H. (2006). Proteoglycan breakdown of meniscal explants following dynamic compression using a novel bioreactor. *Annals of Biomedical Engineering*, *34*(11), 1758–1766. http://doi.org/10.1007/s10439-006-9178-5

Mcnicholas, M. J., Rowley, D. I., Mcgurty, D., Adalberth, T., Abdon, P., Lindstrand, A., & Lohmander, L. S. (2000). Total meniscectomy in adolescence, A thirty-year follow-up. *THE JOURNAL OF BONE AND JOINT SURGERY. BRITISH VOLUME*, *82*(March).

Mcnulty, A. L., & Guilak, F. (2016). Mechanobiology of the Meniscus. *J Biomech.*, *48*(8), 1469–1478. http://doi.org/10.1016/j.jbiomech.2015.02.008.Mechanobiology

McNulty, A. L., Rothfusz, N. E., Leddy, H. A., & Guilak, F. (2013). Synovial fluid concentrations and relative potency of interleukin-1 alpha and beta in cartilage and meniscus degradation. *Journal of Orthopaedic Research : Official Publication of the Orthopaedic Research Society*, *31*(7), 1039–1045. http://doi.org/10.1002/jor.22334

Medlar, R. C., Mandiberg, J. J., & Lyne, E. D. (1980). Meniscectomies in children, Report of long-term results (mean, 8.3 years) of 26 children. *The American Journal of Sports Medicine*, *8*(2).

Melchels, F. P. W., Blokzijl, M. M., Levato, R., Peiffer, Q. C., Ruijter, M. de, Hennink, W. E., … Malda, J. (2016). Hydrogel-based reinforcement of 3D bioprinted constructs. *Biofabrication*, *8*.

Melrose, J., Smith, S., Cake, M., Read, R., & Whitelock, J. (2005). Comparative spatial and temporal localisation of perlecan, aggrecan and type I, II and IV collagen in the ovine meniscus: an ageing study. *Histochemistry and Cell Biology*, *124*(3–4), 225–235. http://doi.org/10.1007/s00418-005-0005-0

Mironi-harpaz, I., Yingquan, D., Venkatraman, S., & Seliktar, D. (2012). Acta Biomaterialia Photopolymerization of cell-encapsulating hydrogels : Crosslinking efficiency versus cytotoxicity. *Acta Biomaterialia*, *8*(5), 1838–1848. http://doi.org/10.1016/j.actbio.2011.12.034

Monllau, J. C., Gelber, P. E., Abat, F., Pelfort, X., Abad, R., Hinarejos, P., & Tey, M. (2011).

Outcome after partial medial meniscus substitution with the collagen meniscal implant at a minimum of 10 years' follow-up. *Arthroscopy - Journal of Arthroscopic and Related Surgery*, *27*(7), 933–943. http://doi.org/10.1016/j.arthro.2011.02.018

Moran, C. J., Atmaca, S., Declercq, H. A., Cornelissen, M. J., & Verdonk, P. C. (2014). Cell distribution and regenerative activity following meniscus replacement. *International Orthopaedics*, *38*(9), 1937–1944. http://doi.org/10.1007/s00264-014-2426-7

Moran, C. J., Barry, F. P., Maher, S. A., Shannon, F. J., & Rodeo, S. A. (2012). Advancing Regenerative Surgery in Orthopaedic Sports Medicine. *The American Journal of Sports Medicine*, *40*(4). http://doi.org/10.1177/0363546511426677

Moran, C. J., Busilacchi, A., Lee, C. A., Athanasiou, K. A., & Verdonk, P. C. (2015a). Biological augmentation and tissue engineering approaches in meniscus surgery. *Arthroscopy : The Journal of Arthroscopic & Related Surgery : Official Publication of the Arthroscopy Association of North America and the International Arthroscopy Association*, *31*(5), 944–955. http://doi.org/10.1016/j.arthro.2014.11.044

Moran, C. J., Busilacchi, A., Lee, C. A., Athanasiou, K. A., & Verdonk, P. C. (2015b). Biological Augmentation and Tissue Engineering Approaches in Meniscus Surgery. *Arthroscopy: The Journal of Arthroscopic & Related Surgery*, *31*(5), 944–955. http://doi.org/https://doi.org/10.1016/j.arthro.2014.11.044

Moran, C. J., Orth, F., Withers, D. P., Orth, F., Kurzweil, P. R., & Verdonk, P. C. (2015). Clinical Application of Scaffolds for Partial Meniscus Replacement. *Sports Med Arthrosc Rev*, *23*(3), 156–161.

Morgan, C. D., Wojtys, E. M., Casscells, C. D., & Casscells, S. W. (1991). Arthroscopic meniscal repair evaluated by second-look arthroscopy. *The American Journal of Sports Medicine*, *19*(6), 632–638. http://doi.org/10.1177/036354659101900614

Mouser, V. H. M., Melchels, F. P. W., Visser, J., Dhert, W. J. A., Gawlitta, D., & Malda, J. (2016). Yield stress determines bioprintability of hydrogels based on gelatin-methacryloyl and gellan gum for cartilage bioprinting Yield stress determines bioprintability of hydrogels based on gelatin- methacryloyl and gellan gum for cartilage bioprinting. *Biofabrication*, *18*.

Moutos, F., & Guilak, F. (2010). Functional Properties of Cell-Seeded Three-Dimensionally Woven Poly (e -Caprolactone) Scaffolds for Cartilage Tissue Engineering. *Tissue Engineering Part A*, *16*(4).

Moutos, F. T., Freed, L. E., & Guilak, F. (2007). A biomimetic three-dimensional woven composite scaffold for functional tissue engineering of cartilage. *Nature Materials*, *6*(2), 162–167. http://doi.org/10.1038/nmat1822

Mow, V. C., & Huiskes, R. (2005). *Basic Orthopaedic Biomechanics and Meacho-Biology, 3rd edition* (3rd ed.). Philadelphia: Lippincott Williams & Wilkins.

Myers, K. R., Sgaglione, N. A., & Kurzweil, P. R. (2013). A Current Update on Meniscal Scaffolds. *Operative Techniques in Sports Medicine*, *21*(2), 75–81. http://doi.org/https://doi.org/10.1053/j.otsm.2013.03.009

Nakagawa, Y., Fortier, L. A., Mao, J. J., Lee, C. H., Goodale, M. B., Koff, M. F., … Rodeo, S. A. (2019a). Long-term Evaluation of Meniscal Tissue Formation in 3-dimensional – Printed Scaffolds With Sequential Release of Connective Tissue Growth Factor and TGF- b 3 in an Ovine Model, 2596–2607. http://doi.org/10.1177/0363546519865513

Nakagawa, Y., Fortier, L. A., Mao, J. J., Lee, C. H., Goodale, M. B., Koff, M. F., … Rodeo, S. A. (2019b). Long-term Evaluation of Meniscal Tissue Formation in 3-dimensional – Printed Scaffolds With Sequential Release of Connective Tissue Growth Factor and TGF- b 3 in an Ovine Model. *The American Journal of Sports Medicine*, *47*(11), 2596–2607. http://doi.org/10.1177/0363546519865513

Nakata, K., Shino, K., Hamada, M., Mae, T., Miyama, T., Shinjo, H., … Yoshikawa, H. (2001). Human meniscus cell: characterization of the primary culture and use for tissue engineering. *Clinical Orthopaedics and Related Research*, (391 Suppl), S208-18.

Nerurkar, N. L., Han, W., Mauck, R. L., & Elliott, D. M. (2011). Homologous structure-function relationships between native fibrocartilage and tissue engineered from MSC-seeded nanofibrous scaffolds. *Biomaterials*, *32*(2), 461–468. http://doi.org/10.1016/j.biomaterials.2010.09.015

Nerurkar, N. L., Sen, S., Baker, B. M., Elliott, D. M., & Mauck, R. L. (2011). Dynamic culture enhances stem cell infiltration and modulates extracellular matrix production on aligned electrospun nanofibrous scaffolds. *Acta Biomaterialia*, *7*(2), 485–491. http://doi.org/10.1016/j.actbio.2010.08.011

Newman, A. P., Anderson, R. D., Daniels, A. U., & Dales, M. C. (1989). Mechanics of the healed meniscus in canine model *. *The American Journal of Sports Medicine*, *17*(2).

Niu, W., Guo, W., Han, S., Zhu, Y., Liu, S., & Guo, Q. (2016). Cell-Based Strategies for Meniscus Tissue Engineering, *2016*. http://doi.org/10.1155/2016/4717184

Noyes, F. R., & Barber-Westin, S. D. (2010). Repair of Complex and Avascular Meniscal Tears and Meniscal Transplantation. *The Journal of Bone and Joint Surgery*, *92–A*(4), 1011–1029.

Ochi, M., Kanda, T., Sumen, Y., & Ikuta, Y. (1997). Changes in the permeability and histologic findings of rabbit menisci after immobilization. *Clinical Orthopaedics and Related Research*, (334), 305–315.

OECD, & Chapter7EU. (2016). *Health at a Glance : Europe 2016*. OECD Publishing.

Olvera, D., Daly, A., & Kelly, D. J. (2015). Mechanical Testing of Cartilage Constructs. In

Cartilage Tissue Engineering. Methods in Molecular Biology (Vol. 1340, pp. 279–287). http://doi.org/10.1007/978-1-4939-2938-2

Oropallo, W., & Piegl, L. A. (2016). Ten challenges in 3D printing. *Engineering with Computers*, *32*(1), 135–148. http://doi.org/10.1007/s00366-015-0407-0

Pabbruwe, M. B., Kafienah, W., Tarlton, J. F., Mistry, S., Fox, D. J., & Hollander, A. P. (2010). Repair of meniscal cartilage white zone tears using a stem cell/collagen-scaffold implant. *Biomaterials*, *31*(9), 2583–2591. http://doi.org/10.1016/j.biomaterials.2009.12.023

Pahoff, S., Klein, T. J., Meinert, C., Bas, O., & Hutmacher, D. W. (2019). Effect of gelatin source and photoinitiator type on chondrocyte redifferentiation in gelatin constructs †. *Journal of Materials Chemistry B*, *7*, 1761–1772. http://doi.org/10.1039/c8tb02607f

Paletta, G. A., Manning, T., Snell, E., Parker, R., & Bergfeld, J. (1997). The Effect of Allograft Meniscal Replacement on Intraarticular Contact Area and Pressures in the Human Knee: A Biomechanical Study. *The American Journal of Sports Medicine*, *25*(5), 692–698. http://doi.org/10.1177/036354659702500519

Pangborn, C. A., & Athanasiou, K. A. (2005). Effects of growth factors on meniscal fibrochondrocytes. *Tissue Engineering*, *11*(7–8), 1141–1148. http://doi.org/10.1089/ten.2005.11.1141

Papalia, R., Franceschi, F., Balzani, L. D., D'Adamio, S., Maffulli, N., & Denaro, V. (2013). Scaffolds for partial meniscal replacement: An updated systematic review. *British Medical Bulletin*. http://doi.org/10.1093/bmb/ldt007

Park, J. S., Kim, J.-M., Lee, S. J., Lee, S. G., Jeong, Y.-K., Kim, S. E., & Lee, S. C. (2007). Surface hydrolysis of fibrous poly (ε-caprolactone) scaffolds for enhanced osteoblast adhesion and proliferation. *Macromolecular Research*, *15*(5), 424–429. http://doi.org/10.1007/BF03218809

Park, K. H., & Na, K. (2008). Effect of growth factors on chondrogenic differentiation of rabbit mesenchymal cells embedded in injectable hydrogels. *Journal of Bioscience and Bioengineering*, *106*(1), 74–79. http://doi.org/https://doi.org/10.1263/jbb.106.74

Parker, B. R., Hurwitz, S., Spang, J., Creighton, R., & Kamath, G. (2016). Surgical Trends in the Treatment of Meniscal Tears: Analysis of Data From the American Board of Orthopaedic Surgery Certification Examination Database. *The American Journal of Sports Medicine*, *44*, 1717–1723. http://doi.org/10.1177/0363546516638082

Pati, F., Jang, J., Ha, D., Kim, S. W., Rhie, J., Shim, J., … Cho, D. (2014). Printing three-dimensional tissue analogues with decellularized extracellular matrix bioink. *Nature Communications*, *5*, 1–11. http://doi.org/10.1038/ncomms4935

Peloquin, J. M., Santare, M. H., & Elliott, D. M. (2015). Advances in quantification of meniscus

tensile mechanics including nonlinearity, yield, and failure. *Journal of Biomechanical Engineering*, *138*(2), 21002. http://doi.org/10.1115/1.4032354

Petersen, W., & Tillmann, B. (1995). Age-related blood and lymph supply of the knee menisci : A cadaver study. *Acta Orthopaedica Scandinavica*, *66*(4), 308–312. http://doi.org/10.3109/17453679508995550

Pieter Buma, Tienen, T. Van, & Veth, R. (2007). The collagen meniscus implant. *Expert Rev Med Devices*, *4*(4), 507–516.

Proctor, C. S., Schmidt, M. B., Whipple, R. R., Kelly, M. A., & Mow, V. C. (1989). Material Properties of the Normal Medial Bovine Meniscus. *J Orthop Res*, *7*(29), 771–782.

Puetzer, J. L., & Bonassar, L. J. (2016). Physiologically Distributed Loading Patterns Drive the Formation of Zonally Organized Collagen Structures in Tissue-Engineered Meniscus, *22*, 907–916. http://doi.org/10.1089/ten.tea.2015.0519

Qi, X., Huang, Y., Han, D., Zhang, J., Cao, J., Jin, X., & Huang, J. (2016). Three-dimensional poly (ε-caprolactone)/hydroxyapatite/collagen scaffolds incorporating bone marrow mesenchymal stem cells for the repair of bone defects. *Biomedical Materials*, *11*(2), 25005. http://doi.org/10.1088/1748-6041/11/2/025005

Ramallal, M., Maneiro, E., Lopez, E., Fuentes-Boquete, I., Lopez-Armada, M. J., Fernandez-Sueiro, J. L., … Blanco, F. J. (2004). Xeno-implantation of pig chondrocytes into rabbit to treat localized articular cartilage defects: an animal model. *Wound Repair and Regeneration : Official Publication of the Wound Healing Society [and] the European Tissue Repair Society*, *12*(3), 337–345. http://doi.org/10.1111/j.1067-1927.2004.012309.x

Ramrattan, N. N., Heijkants, R. G. J. C., van Tienen, T. G., Schouten, A. J., Veth, R. P. H., & Buma, P. (2005). Assessment of tissue ingrowth rates in polyurethane scaffolds for tissue engineering. *Tissue Engineering*, *11*(7–8), 1212–1223. http://doi.org/10.1089/ten.2005.11.1212

Rathan, S., Dejob, L., Schipani, R., Haffner, B., Möbius, M. E., & Kelly, D. J. (2019). Fiber Reinforced Cartilage ECM Functionalized Bioinks for Functional Cartilage Tissue Engineering, *1801501*, 1–11. http://doi.org/10.1002/adhm.201801501

Ribeiro, A., Blokzijl, M. M., Levato, R., Visser, C. W., Castilho, M., Hennink, W. E., … Malda, J. (2018). Assessing bioink shape fidelity to aid material development in 3D bioprinting. *Biofabrication*, *10*(1). http://doi.org/10.1088/1758-5090/aa90e2

Riera, K. M., Rothfusz, N. E., Wilusz, R. E., Weinberg, J. B., Guilak, F., & McNulty, A. L. (2011). Interleukin-1, tumor necrosis factor-alpha, and transforming growth factor-beta 1 and integrative meniscal repair: influences on meniscal cell proliferation and migration. *Arthritis Research & Therapy*, *13*(6), R187. http://doi.org/10.1186/ar3515

Robinson, T. M., Hutmacher, D. W., & Dalton, P. D. (2019). The Next Frontier in Melt Electrospinning : Taming the Jet. *Advanced Functional Materials*, *29*. http://doi.org/10.1002/adfm.201904664

Rodeo, S. A. (2001). Meniscal allografts--where do we stand? *The American Journal of Sports Medicine*, *29*(2), 246–61. http://doi.org/0363-5465/101/2929-0246$02.00/0

Rodkey, W. G. D., Steadman, J. R. M., & Li, S.-T. P. (1999). A Clinical Study of Collagen Meniscus Implants to Restore th... : Clinical Orthopaedics and Related Research. *Clinical Orthopaedics & Related Research*, *367*, 281–292. Retrieved from http://journals.lww.com/corr/Abstract/1999/10001/A_Clinical_Study_of_Collagen_Meniscus_Implants_to.27.aspx

Rodkey, W. G., DeHaven, K. E., Montgomery, W. H., Baker, C. L., Beck, C. L., Hormel, S. E., … Briggs, K. K. (2008). Comparison of the Collagen Meniscus Implant with Partial Meniscectomy. *The Journal of Bone and Joint Surgery-American Volume*, *90*(7), 1413–1426. http://doi.org/10.2106/JBJS.G.00656

Romanazzo, S., S.Vedicherla, C. Moran, D. J. K. (2011). Meniscus ECM functionalized hydrogels containing joint derived stem cells for bioprinting of regionally defined meniscus tissue.

Romanazzo, S., Vedicherla, S., Moran, C., & Kelly, D. J. (2017). Meniscus ECM-functionalised hydrogels containing infrapatellar fat pad-derived stem cells for bioprinting of regionally defined meniscal tissue. *Journal of Tissue Engineering and Regenerative Medicine*, *12*(3), e1826–e1835. http://doi.org/10.1002/term.2602

Roos, E. M., Östenberg, A., Roos, H., Ekdahl, C., & Lohmander, L. S. (2001). Long-term outcome of meniscectomy: symptoms, function, and performance tests in patients with or without radiographic osteoarthritis compared to matched controls. *Osteoarthritis and Cartilage*, *9*(4), 316–324. http://doi.org/https://doi.org/10.1053/joca.2000.0391

Roos, H., Laurén, M., Adalberth, T., Roos, E. M., Jonsson, K., & Lohmander, L. S. (1998). Knee osteoarthritis after meniscectomy: Prevalence of radiographic changes after twenty-one years, compared with matched controls. *Arthritis & Rheumatism*, *41*(4), 687–693. http://doi.org/10.1002/1529-0131(199804)41:4<687::AID-ART16>3.0.CO;2-2

Rothrauff, B. B., Shimomura, K., Gottardi, R., Alexander, P. G., & Tuan, R. S. (2017). Anatomical region-dependent enhancement of 3-dimensional chondrogenic differentiation of human mesenchymal stem cells by soluble meniscus extracellular matrix. *Acta Biomaterialia*, *49*, 140–151. http://doi.org/10.1016/j.actbio.2016.11.046

Rouillard, A. D., Berglund, C. M., Lee, J. Y., Polacheck, W. J., Tsui, Y., Bonassar, L. J., … Ph, D. (2011). Methods for Photocrosslinking Alginate Hydrogel Scaffolds with High Cell Viability, *17*(2). http://doi.org/10.1089/ten.tec.2009.0582

Rouwkema, J., Koopman, B. F. J. M., Blitterswijk, C. A. Van, Dhert, W. J. A., Malda, J., Rouwkema, J., … Blitterswijk, C. A. Van. (2013). Supply of Nutrients to Cells in Engineered Tissues Supply of Nutrients to Cells in Engineered, *8725*. http://doi.org/10.5661/bger-26-163

Rowley, J. A., Madlambayan, G., & Mooney, D. J. (1999). Alginate hydrogels as synthetic extracellular matrix materials, *20*, 45–53.

Rubman, M. H., Noyes, F. R., & Barber-Westin, S. D. (1998). Arthroscopic Repair of Meniscal Tears that Extend into the Avascular Zone. *The American Journal of Sports Medicine*, *26*(1), 87–95. http://doi.org/10.1177/03635465980260013301

Rutgers, M., Saris, D. B., Vonk, L. A., Rijen, M. H. van, Akrum, V., Langeveld, D., … Creemers, L. B. (2012). Effect of Collagen Type I or Type II on Chondrogenesis. *TISSUE ENGINEERING: Part A*, *0*(0), 1–7. http://doi.org/10.1089/ten.tea.2011.0416

Salata, M. J., Gibbs, A. E., & Sekiya, J. K. (2010). The American Journal of Sports Medicine. http://doi.org/10.1177/0363546510370196

Schipani, R. (2019). *3D Bioprinting of Cartilage-mimetic Implans for Biological Joint Resurfacing*.

Schipani, R., Scheurer, S., E, C. S., & Kelly, D. J. (2020). Reinforcing interpenetrating network hydrogels with 3D printed polymeric frames to engineer cartilage mimetic composites. *(In Submission)*.

Schneiderbauer, M. M., Dutton, C. M., & Scully, S. P. (2004). Signaling "' cross-talk '" between TGF- h 1 and ECM signals in chondrocytic cells. *Cell Signalling*, *16*, 1133–1140. http://doi.org/10.1016/j.cellsig.2004.03.004

Schüttler, K. F., Haberhauer, F., Gesslein, M., Heyse, T. J., Figiel, J., Lorbach, O., … Roessler, P. P. (2016). Midterm follow - up after implantation of a polyurethane meniscal scaffold for segmental medial meniscus loss : maintenance of good clinical and MRI outcome. *Knee Surgery, Sports Traumatology, Arthroscopy*, *24*(5), 1478–1484. http://doi.org/10.1007/s00167-015-3759-5

Seedhom, B. B., & Hargreaves, D. J. (1979). Transmission of the Load in the Knee Joint with Special Reference to the Role of the Menisci: Part II: Experimental Results, Discussion and Conclusions. *Engineering in Medicine*, *8*(4), 220–228. http://doi.org/10.1243/emed_jour_1979_008_051_02

Setton, L. A., Guilak, F., Hsu, E. W., & Vail, T. P. (1999). Biomechanical factors in tissue engineered meniscal repair. *Clinical Orthopaedics and Related Research*, (367 Suppl), S254-72. http://doi.org/10.1097/00003086-199910001-00025

Shi, J., & Zhou, S. (2009). Quality control and improvement for multistage systems : A survey

Quality control and improvement for multistage systems : A survey. *IIE Transactions*, *41*, 744–753. http://doi.org/10.1080/07408170902966344

Shimomura, K., Rothrauff, B. B., & Tuan, R. S. (2017). Region-Specific Effect of the Decellularized Meniscus Extracellular Matrix on Mesenchymal Stem Cell–Based Meniscus Tissue Engineering. *The American Journal of Sports Medicine*, *45*(3), 604–611. http://doi.org/10.1177/0363546516674184

Shindo, W., Nurani, R. K., & Strojwas, A. J. (1998). Effects of Defect Propagation / Growth on In-Line Defect-Based Yield Prediction. *IEEE TRANSACTIONS ON SEMICONDUCTOR MANUFACTURING*, *11*(4), 546–551.

Shirasawa, S., Sekiya, I., Sakaguchi, Y., Yagishita, K., & Ichinose, S. (2006). In Vitro Chondrogenesis of Human Synovium-Derived Mesenchymal Stem Cells : Optimal Condition and Comparison With Bone Marrow-Derived Cells, *97*, 84–97. http://doi.org/10.1002/jcb.20546

Skaggs, D. L., Warden, W. H., & Mow, V. C. (1994). Radial tie fibers influence the tensile properties of the bovine medial meniscus. *Journal of Orthopaedic Research*, *12*(2), 176–185. http://doi.org/10.1002/jor.1100120205

Spencer, S. J., Saithna, A., Carmont, M. R., Dhillon, M. S., Thompson, P., & Spalding, T. (2012). Meniscal scaffolds: Early experience and review of the literature. *Knee*, *19*(6), 760–765. http://doi.org/10.1016/j.knee.2012.01.006

Stapleton, T. W., Ingram, J., Fisher, J., & Ingham, E. (2011). Investigation of the regenerative capacity of an acellular porcine medial meniscus for tissue engineering applications. *Tissue Engineering. Part A*, *17*(1–2), 231–242. http://doi.org/10.1089/ten.TEA.2009.0807

Sweigart, M. A., & Athanasiou, K. A. (2001). Toward Tissue Engineering of the Knee Meniscus, *7*(2), 111–129.

Sweigart, M. A., & Athanasiou, K. A. (2005). Tensile and compressive properties of the medial rabbit meniscus. *Proc IMech E*, *219*, 337–347. http://doi.org/10.1243/095441105X34329

Sweigart, M. A., Zhu, C. F., Burt, D. M., DeHoll, P. D., Agrawal, C. M., Clanton, T. O., & Athanasiou, K. A. (2004). Intraspecies and Interspecies Comparison of the Compressive Properties of the Medial Meniscus. *Annals of Biomedical Engineering*, *32*(11), 1569–1579.

Szojka, A., Lalh, K., Andrews, S. H. J., Jomha, N. M., Osswald, M., & Adesida, A. B. (2017). Biomimetic 3D printed scaffolds for meniscus tissue engineering. *Bioprinting*, *8*(April), 1–7. http://doi.org/10.1016/j.bprint.2017.08.001

Tamayol, A., Najafabadi, A. H., Aliakbarian, B., Arab-tehrany, E., Akbari, M., Annabi, N., … Khademhosseini, A. (2015). Hydrogel Templates for Rapid Manufacturing of Bioactive Fibers and 3D Constructs, 2146–2153. http://doi.org/10.1002/adhm.201500492

Tanaka, T., Fujii, K., & Kumagae, Y. (1999). Comparison of biochemical characteristics of cultured fibrochondrocytes isolated from the inner and outer regions of human meniscus. *Knee Surgery, Sports Traumatology, Arthroscopy*, *7*(2), 75–80. http://doi.org/10.1007/s001670050125

Taylor, S. A., & Rodeo, S. A. (2013). Augmentation techniques for isolated meniscal tears, 95–101. http://doi.org/10.1007/s12178-013-9165-z

Teberg, A. J., Wu, P. Y., Hodgman, J. E., Mich, C., Garfinkle, J., Azen, S., & Wingert, W. A. (1982). Infants with birth weight under 1500 g: physical, neurological, and developmental outcome. *Critical Care Medicine*, *10*(1), 10–14.

Thie, M., Schlumberger, W., Rauterberg, J., & Robenek, H. (1989). Mechanical confinement inhibits collagen synthesis in gel-cultured fibroblasts. *European Journal of Cell Biology*, *48*(2), 294–302.

Tienen, T. G. Van, Hannink, G., & Buma, P. (2009). Meniscus Replacement Using Synthetic Materials. *Clinics in Sports Medicine*, *28*(1), 143–156. http://doi.org/10.1016/j.csm.2008.08.003

Tissakht, M., & Ahmed, A. M. (1995). Tensile stress-strain characteristics of the human meniscal material. *Journal of Biomechanics*, *28*(4), 411–422. http://doi.org/10.1016/0021-9290(94)00081-E

Tissakht, M., Ahmed, A. M., & Chan, K. C. (1996). Calculated Stress-Shielding in the Distal Femur after Total Knee Replacement Corresponds to the Reported Location of Bone Loss. *Jounral of Orthopaedic Research*, *14*, 778–785.

Tuli, R., Tuli, S., Nandi, S., Huang, X., Manner, P. A., Hozack, W. J., … Tuan, R. S. (2003). Transforming growth factor-beta-mediated chondrogenesis of human mesenchymal progenitor cells involves N-cadherin and mitogen-activated protein kinase and Wnt signaling cross-talk. *The Journal of Biological Chemistry*, *278*(42), 41227–41236. http://doi.org/10.1074/jbc.M305312200

Uchio, Y., Ochi, M., Adachi, N., Kawasaki, K., & Iwasa, J. (2003). Results of rasping of meniscal tears with and without anterior cruciate ligament injury as evaluated by second-look arthroscopy. *Arthroscopy: The Journal of Arthroscopic & Related Surgery*, *19*(5), 463–469. http://doi.org/https://doi.org/10.1053/jars.2003.50109

Van Der Straeten, C., Doyen, B., Dutordoir, C., Goedertier, W., Pirard, S., & Victor, J. (2016). SHORT- AND MEDIUM-TERM RESULTS OF ARTIFICIAL MENISCAL IMPLANTS. *Orthopaedic Proceedings*, *98–B*(SUPP_4), 91. http://doi.org/10.1302/1358-992X.98BSUPP_4.ISTA2014-091

van Trommel, M. F., Simonian, P. T., Potter, H. G., & Wickiewicz, T. L. (1998). Arthroscopic meniscal repair with fibrin clot of complete radial tears of the lateral meniscus in the

avascular zone. *Arthroscopy: The Journal of Arthroscopic & Related Surgery*, *14*(4), 360–365. http://doi.org/https://doi.org/10.1016/S0749-8063(98)70002-7

Vedicherla, S., Romanazzo, S., Kelly, D. J., Buckley, C. T., & Moran, C. J. (2018). Chondrocyte-based intraoperative processing strategies for the biological augmentation of a polyurethane meniscus replacement. *Connective Tissue Research*, *59*(4), 381–392. http://doi.org/10.1080/03008207.2017.1402892

Verdonk, P., Forsyth, R., Wang, J., Almqvist, K., Verdonk, R., Veys, E., & Verbruggen, G. (2005). Characterisation of human knee meniscus cell phenotype. *Osteoarthritis and Cartilage*, *13*, 548–560. http://doi.org/10.1016/j.joca.2005.01.010

Verdonk, R., Verdonk, P., Huysse, W., Forsyth, R., & Heinrichs, E.-L. (2011). Tissue Ingrowth After Implantation of a Novel , Biodegradable Polyurethane Scaffold for Treatment of Partial Meniscal Lesions. *The American Journal of Sports Medicine*, *39*(4), 774–782. http://doi.org/10.1177/0363546511398040

Verdonk, R., Volpi, P., Verdonk, P., Bracht, H. Van Der, Laer, M. Van, Almqvist, K. F., … Quaglia, A. (2013). Indications and limits of meniscal allografts. *Injury*, *44*, S21–S27. http://doi.org/10.1016/S0020-1383(13)70006-8

Videman, T., Eronen, I., Friman, C., & Langenskiold, A. (1979). Glycosaminoglycan metabolism of the medial meniscus, the medial collateral ligament and the hip joint capsule in experimental osteoarthritis caused by immobilization of the rabbit knee. *Acta Orthopaedica Scandinavica*, *50*(4), 465–470. http://doi.org/10.3109/17453677908989791

Visser, J., Levett, P. A., te Moller, N. C. R., Besems, J., Boere, K. W. M., van Rijen, M. H. P., … Malda, J. (2015). Crosslinkable Hydrogels Derived from Cartilage, Meniscus, and Tendon Tissue. *Tissue Engineering Part A*, *21*(7–8), 1195–1206. http://doi.org/10.1089/ten.tea.2014.0362

Visser, J., Melchels, F. P. W., Jeon, J. E., van Bussel, E. M., Kimpton, L. S., Byrne, H. M., … Malda, J. (2015). Reinforcement of hydrogels using three-dimensionally printed microfibres. *Nature Communications*, *6*, 6933. http://doi.org/10.1038/ncomms7933

Vrancken, A. C. T., Hannink, G., Madej, W., Verdonschot, N., Tienen, T. G. Van, & Buma, P. (2017). In Vivo Performance of a Novel , Anatomically Shaped , Total Meniscal Prosthesis Made of Polycarbonate Urethane A 12-Month Evaluation in Goats. *The American Journal of Sports Medicine*, *45*(12), 2824–2834. http://doi.org/10.1177/0363546517713687

Vrancken, A. C. T., Madej, W., Hannink, G., Verdonschot, N., & Tienen, T. G. Van. (2015). Short Term Evaluation of an Anatomically Shaped Polycarbonate Urethane Total Meniscus Replacement in a Goat Model. *PloS One*, *10*(7), 1–16. http://doi.org/10.1371/journal.pone.0133138

Vundelinckx, B., Vanlauwe, J., & Bellemans, J. (2014). Long-term Subjective, Clinical, and

Radiographic Outcome Evaluation of Meniscal Allograft Transplantation in the Knee. *The American Journal of Sports Medicine*, *42*(7), 1592–1599. http://doi.org/10.1177/0363546514530092

Wang, J., Wei, Y., Zhao, S., Zhou, Y., He, W., Zhang, Y., & Deng, W. (2017). The analysis of viability for mammalian cells treated at different temperatures and its application in cell shipment, 1–16.

Wang, Y. J., Griffith, J. F., Ahuja, A. T., Wang, Y. J., Griffith, J. F., & Ahuja, A. T. (2010). Non-invasive MRI assessment of the articular cartilage in clinical studies and experimental settings. *World Journal of Radiology*, *2*(1), 44–54. http://doi.org/10.4329/wjr.v2.i1.44

Warnecke, D., Stein, S., Ha, M., Roy, L. De, Skaer, N., Walker, R., … Dürselen, L. (2018). Biomechanical , structural and biological characterisation of a new silk fi broin sca ff old for meniscal repair. *Journal of the Mechanical Behavior of Biomedical Materials*, *86*(March), 314–324. http://doi.org/10.1016/j.jmbbm.2018.06.041

Wasserstein, D., Dwyer, T., Gandhi, R., Austin, P. C., Mahomed, N., & Ogilvie-harris, D. (2008). A Matched-Cohort Population Study of Reoperation After Meniscal Repair With and Without Concomitant Anterior Cruciate Ligament Reconstruction, 349–356. http://doi.org/10.1177/0363546512471134

Weinand, C., Peretti, Æ. G. M., Adams, S. B., Mark, J. Æ., Savvidis, E., & Gill, Æ. T. J. (2006). Healing potential of transplanted allogeneic chondrocytes of three different sources in lesions of the avascular zone of the meniscus : a pilot study. *Archives of Orthopaedic and Trauma Surgery*, *126*, 599–605. http://doi.org/10.1007/s00402-005-0100-7

Weinand, C., Peretti, G. M., Jr, S. B. A., Bonassar, L. J., Randolph, M. A., & Gill, T. J. (2006). An Allogenic Cell – Based Implant for Meniscal Lesions. *The American Journal of Sports Medicine*, *34*(11), 1779–1789. http://doi.org/10.1177/0363546506290666

Weiss, B. Y. C. B. E., Lundberg, M. N. E. W., Gillquist, J. A. N. P. E. R., & Hospital, M. (1989). Non-Operative Treatment of Meniscal Tears *. *The Journal of Bone and Joint Surgery Incorporated*, *71*(6).

Woodruff, M. A., & Hutmacher, D. W. (2010). The return of a forgotten polymer — Polycaprolactone in the 21st century. *Progress in Polymer Science*, *35*, 1217–1256. http://doi.org/10.1016/j.progpolymsci.2010.04.002

Wu, J., Ding, Q., Dutta, A., Wang, Y., Huang, Y., Weng, H., … Hong, Y. (2015). An injectable extracellular matrix derived hydrogel for meniscus repair and regeneration. *Acta Biomaterialia*, *16*, 49–59. http://doi.org/https://doi.org/10.1016/j.actbio.2015.01.027

Wunner, F. M., Eggert, S., Maartens, J., Bas, O., Dalton, P. D., De-juan-pardo, E. M., & Hutmacher, D. W. (2018). Design and Development of a Three-Dimensional Printing High-Throughput Melt Electrowriting Technology Platform. *3D Printing and Additive*

Manufacturing, *0*(0), 1–9. http://doi.org/10.1089/3dp.2017.0149

Wunner, F. M., Wille, M., Noonan, T. G., Bas, O., Dalton, P. D., De-juan-pardo, E. M., & Hutmacher, D. W. (2018a). Melt Electrospinning Writing of Highly Ordered Large Volume Scaffold Architectures, *1706570*, 1–6. http://doi.org/10.1002/adma.201706570

Wunner, F. M., Wille, M., Noonan, T. G., Bas, O., Dalton, P. D., De-juan-pardo, E. M., & Hutmacher, D. W. (2018b). Melt Electrospinning Writing of Highly Ordered Large Volume Scaffold Architectures. *Advanced Materials*, *1706570*, 1–6. http://doi.org/10.1002/adma.201706570

Xu, C., Dai, G., & Hong, Y. (2019). Acta Biomaterialia Recent advances in high-strength and elastic hydrogels for 3D printing in biomedical applications q. *Acta Biomaterialia*, *95*, 50–59. http://doi.org/10.1016/j.actbio.2019.05.032

Xu, C., & Zhao, J. (2015). A meta-analysis comparing meniscal repair with meniscectomy in the treatment of meniscal tears : the more meniscus , the better outcome ? *Knee Surg Sports Traumatol Arthrosc*, *23*, 164–170. http://doi.org/10.1007/s00167-013-2528-6

Yang, G., Rothrauff, B. B., Lin, H., Gottardi, R., Alexander, P. G., & Tuan, R. S. (2013). Enhancement of tenogenic differentiation of human adipose stem cells by tendon-derived extracellular matrix. *Biomaterials*, *34*(37), 9295–9306. http://doi.org/https://doi.org/10.1016/j.biomaterials.2013.08.054

Zaffagnini, S., & Giordano, Æ. G. (2007). Arthroscopic collagen meniscus implant results at 6 to 8 years follow up. *Knee Surg Sports Traumatol Arthrosc*, *15*, 175–183. http://doi.org/10.1007/s00167-006-0144-4

Zaffagnini, S., Marcheggiani Muccioli, G. M., Lopomo, N., Bruni, D., Giordano, G., Ravazzolo, G., … Marcacci, M. (2011). Prospective Long-Term Outcomes of the Medial Collagen Meniscus Implant Versus Partial Medial Meniscectomy. *The American Journal of Sports Medicine*, *39*(5), 977–985. http://doi.org/10.1177/0363546510391179

Zellner, J., Pattappa, G., Koch, M., Lang, S., Weber, J., Pfeifer, C. G., … Angele, P. (2017). Autologous mesenchymal stem cells or meniscal cells : what is the best cell source for regenerative meniscus treatment in an early osteoarthritis situation ? *Stem Cell Research & Therapy*, *8*(225), 1–12. http://doi.org/10.1186/s13287-017-0678-z

Zhang, Y., He, Y., Bharadwaj, S., Hammam, N., Carnagey, K., Myers, R., … Van Dyke, M. (2009). Tissue-specific extracellular matrix coatings for the promotion of cell proliferation and maintenance of cell phenotype. *Biomaterials*, *30*(23), 4021–4028. http://doi.org/https://doi.org/10.1016/j.biomaterials.2009.04.005

Zhang, Z.-Z., Jiang, D., Ding, J. X., Wang, S. J., Zhang, L., Zhang, J. Y., … Yu, J. K. (2016). Role of scaffold mean pore size in meniscus regeneration. *Acta Biomaterialia*, *43*, 314–326. http://doi.org/10.1016/j.actbio.2016.07.050

Zhang, Z.-Z., Wang, S.-J., Zhang, J.-Y., Jiang, W.-B., Huang, A.-B., Qi, Y.-S., … Yu, J.-K. (2017). 3D-Printed Poly(ε-caprolactone) Scaffold Augmented With Mesenchymal Stem Cells for Total Meniscal Substitution. *The American Journal of Sports Medicine*, 36354651769151. http://doi.org/10.1177/0363546517691513

Zhang, Z., Arnold, J. A., Williams, T., & McCann, B. (1995). Repairs by Trephination and Suturing of Longitudinal Injuries in the Avascular Area of the Meniscus in Goats. *The American Journal of Sports Medicine*, *23*(1), 35–41. http://doi.org/10.1177/036354659502300106

Zhang, Z., Chen, Y., Wang, S., Zhao, F., Wang, X., Yang, F., … Zou, T. (2019). Orchestrated biomechanical , structural , and biochemical stimuli for engineering anisotropic meniscus. *Science Translational Medicine*, *750*(April).

Zhu, K., Chen, N., Liu, X., Mu, X., Zhang, W., & Wang, C. (2018). A General Strategy for Extrusion Bioprinting of Bio-Macromolecular Bioinks through Alginate-Templated Dual-statge Crosslinking, *1800127*, 1–8. http://doi.org/10.1002/mabi.201800127

Zielinska, B., Killian, M., Kadmiel, M., Nelsen, M., & Haut Donahue, T. L. (2009). Meniscal tissue explants response depends on level of dynamic compressive strain. *Osteoarthritis and Cartilage*, *17*(6), 754–760. http://doi.org/10.1016/j.joca.2008.11.018